



**University of  
Leicester**

*In Vitro* Manipulation of Urotensin-II Receptor  
Expression: Implications of  
Receptor Density on Ligand Efficacy.

Thesis submitted in partial fulfilment of the requirements for the degree of  
Doctor of Philosophy, by

**Benjamin D. Hunt**

*Supervisors: Prof. D. G. Lambert*  
*Prof. L. L. Ng*

November 2010

*Funded by a British Heart Foundation Studentship*



## **In Vitro Manipulation of Urotensin-II Receptor Expression: Implications of Receptor Density on Ligand Efficacy**

### **BENJAMIN D. HUNT**

Many urotensin-II (UT) receptor ligands characterised to date exhibit assay-dependent paradoxical agonist / antagonist properties. This activity is likely to be due to differences in UT receptor density between assays, especially between *in vivo* and *in vitro* systems. The present study characterised the effect of UT receptor density on the absolute and relative efficacies of experimental UT ligands (urantide and UFP-803). Two *in vitro* models were produced allowing the density of UT to be controlled in the presence of a fixed cellular background.

1. Ecdysone-inducible Chinese hamster ovary (CHO) cell-line, allowing UT transcription to be induced by a nuclear steroid hormone, (pon-A).
2. UT-targeting siRNAs, allowing UT translation to be inhibited in CHO cells expressing the human recombinant UT receptor (CHO<sub>h</sub>UT).

The production and characterisation of the first of these models was problematic due to significant expression of UT in the absence of pon-A, therefore affording no advantage over classical *in vitro* systems.

Two UT-targeting siRNAs were transfected into CHO<sub>h</sub>UT and were shown to knockdown UT expression by 94 & 73% at the mRNA level and 64 & 40% at the functional level.

This model has allowed us to control UT receptor density in the presence of a fixed cellular background. We have shown that decreasing the density of UT in CHO<sub>h</sub>UT reduces the absolute efficacies of experimental UT ligands (urantide and UFP-803). We attribute this effect to reduced mass of ligand-receptor complexes. Reducing the density of UT in CHO<sub>h</sub>UT does not affect the relative efficacies of the same ligands. We attribute this effect to the absence of a UT receptor reserve over the range of UT densities used.

A better understanding of system-dependent efficacy is crucial for effective use of UT ligands in the clinical setting. The technologies employed in this thesis represent an important avenue for future work.

## **ACKNOWLEDGEMENTS**

I would first and foremost like to thank both of my supervisors, Professors Lambert and Ng, for their continued support and guidance throughout this project. I would especially like to thank Dave for his open door policy (excepting Mr. Grumpy) and down-to-earth approach which has helped the project along enormously! I would also like to acknowledge the influence of Dr. Thelma Lovick (Birmingham) who helped me to appreciate the merits of an academic research career.

My gratitude goes to the British Heart Foundation for their generous funding of this project and for providing me with a stipend with which to live for the duration.

My thanks go to the whole research group and to 'the rest of the corridor' for humorous and entertaining lunchtimes and coffee breaks! To Carmela and Nikos for adding a European flair to the office and for testing my tenuous grasp of linguistics! To John for his technical expertise and unique sense of humour.

Special thanks go to my good friend, ex-housemate, and drinking partner - Emer. For challenging my IT skills at times and for reminding me that one must also 'play hard'! I wish to thank all of my family who have been loving, helpful, and understanding throughout. My thanks go to my parents for supporting me (twice) through university and to my granddad (professor) John for his frequent insights into the project. Finally, extra special thanks to my partner Chris for his loving support and for his understanding of my unique way of doing things!

**“Measure what is measurable, and make measurable what is not so”**

*Galileo Galilei.*

## **LIST OF CONTENTS**

<b>1. INTRODUCTION.....</b>	<b>11</b>
<b>1.1 UROTENSIN II: AN OVERVIEW .....</b>	<b>11</b>
<b>1.2 G-PROTEIN COUPLED RECEPTORS .....</b>	<b>12</b>
1.2.1 THE SEVEN-TRANSMEMBRANE RECEPTOR SUPERFAMILY.....	12
1.2.2 HETEROTRIMERIC G-PROTEINS.....	13
1.2.3 G-PROTEIN ACTIVATION .....	14
1.2.4 G <sub>q</sub> PROTEIN ACTIVATION .....	14
1.2.4.1 Inositol Phosphates and Intracellular Calcium Mobilisation .....	15
1.2.4.2 Diacylglycerol and Protein Kinase C.....	16
<b>1.3 THE UROTENSIN II RECEPTOR SYSTEM .....</b>	<b>17</b>
1.3.1 UROTENSIN-II .....	17
1.3.2 UROTENSIN II-RELATED PEPTIDE .....	18
1.3.3 UT RECEPTOR.....	19
1.3.4 UROTENSIN-II CONVERTING ENZYMES .....	19
<b>1.4 INTRACELLULAR SIGNAL TRANSDUCTION PATHWAYS OF UT .....</b>	<b>21</b>
1.4.1 TYROSINE KINASES.....	21
1.4.2 RHO/RHO-KINASE RELATED PATHWAYS .....	21
1.4.3 EXTRACELLULAR SIGNAL-RELATED PROTEIN KINASES (ERKS).....	21
<b>1.5 EXPRESSION OF UT AND ITS ENDOGENOUS LIGANDS .....</b>	<b>22</b>
1.5.1 UT RECEPTOR .....	22
1.5.2 U-II PEPTIDE.....	22
1.5.3 UROTENSIN-RELATED PEPTIDE.....	23
<b>1.6 FUNCTIONAL STUDIES .....</b>	<b>27</b>
1.6.1 IN VIVO STUDIES .....	27
1.6.2 KNOCKOUT STUDIES.....	28
1.6.3 IN VITRO STUDIES.....	29
<b>1.7 UROTENSIN-II IN PATHOLOGY.....</b>	<b>32</b>
1.7.1 DISORDERS AFFECTING THE CARDIOVASCULAR SYSTEM.....	32
1.7.1.1 Myocardial Hypertrophy.....	32
1.7.1.2 Congestive Heart Failure.....	32
1.7.1.3 Arrhythmogenesis.....	33
1.7.1.4 Essential Hypertension.....	33
1.7.1.5 Atherosclerosis.....	33
1.7.1.6 Pulmonary Hypertension .....	34
1.7.2 THE METABOLIC SYNDROME .....	34
1.7.3 TYPE 2 DIABETES MELLITUS .....	34
1.7.4 RENAL DISEASE .....	35
1.7.5 CIRRHOSIS OF THE LIVER AND PORTAL HYPERTENSION .....	35
1.7.6 ANGIOGENESIS AND TUMOUR GROWTH.....	35
<b>1.8 DRUG DEVELOPMENT AT THE UT RECEPTOR.....</b>	<b>37</b>
1.8.1 PEPTIDIC UT DRUG DEVELOPMENT .....	37
1.8.2 NON-PEPTIDIC UT DRUG DEVELOPMENT.....	39
1.8.2.1 Palosuran .....	39
1.8.2.2 SB-706375 .....	40
1.8.2.3 BIM-23127.....	40
1.8.3 UT DRUG DEVELOPMENT: A SUMMARY.....	41

<b>1.9</b>	<b>THE ECDYSONE-REGULATED GENE SWITCH .....</b>	<b>42</b>
<b>1.10</b>	<b>RNA INTERFERENCE .....</b>	<b>45</b>
<b>1.11</b>	<b>OVERALL AIMS.....</b>	<b>48</b>
<b>2.</b>	<b><u>GENERAL METHODS .....</u></b>	<b><u>51</u></b>
<b>2.1</b>	<b>DATA HANDLING .....</b>	<b>51</b>
2.1.1	DEFINITIONS .....	51
2.1.2	CURVE FITTING AND GRAPHING .....	51
<b>2.2</b>	<b>TISSUE CULTURE .....</b>	<b>52</b>
2.2.1	CELL-LINES .....	52
2.2.2	SUBCULTURE AND PROPAGATION .....	52
2.2.3	FEEDING MONOLAYER CULTURES.....	53
2.2.4	CRYOPRESERVATION AND RESUSCITATION.....	54
2.2.5	CELL QUANTIFICATION .....	55
<b>2.3</b>	<b>PRINCIPLES OF REVERSE TRANSCRIPTION PCR .....</b>	<b>56</b>
<b>2.4</b>	<b>REAL-TIME QUANTITATIVE PCR.....</b>	<b>57</b>
2.4.1	SYBR GREEN I PCR.....	59
2.4.2	TAQMAN™ PCR .....	60
<b>2.5</b>	<b>RNA EXTRACTION METHODS .....</b>	<b>61</b>
2.5.1	PHENOL:CHLOROFORM ORGANIC EXTRACTION.....	61
2.5.2	MIRVANA™ MIRNA ISOLATION KIT.....	62
2.5.3	CELLS-TO-CT™ GENE EXPRESSION KIT.....	63
<b>2.6</b>	<b>DNASE TREATMENT .....</b>	<b>64</b>
<b>2.7</b>	<b>REVERSE TRANSCRIPTION.....</b>	<b>65</b>
<b>2.8</b>	<b>POLYMERASE CHAIN REACTION.....</b>	<b>66</b>
2.8.1	SYBR GREEN I PCR.....	66
2.8.2	TAQMAN™ PCR .....	66
<b>2.9</b>	<b>PRINCIPLES OF [Ca<sup>2+</sup>]<sub>i</sub> MEASUREMENT USING THE RATIOMETRIC FLUOROPHORE, FURA-2.....</b>	<b>68</b>
<b>2.10</b>	<b>CUVETTE-BASED FLUORIMETRY FOR MEASUREMENT OF [Ca<sup>2+</sup>]<sub>i</sub> IN WHOLE CELL SUSPENSIONS.....</b>	<b>70</b>
2.10.1	CALIBRATION OF SINGLE-CUVETTE DATA .....	71
<b>2.11</b>	<b>HIGH-THROUGHPUT FLUORIMETRY FOR MEASUREMENT OF [Ca<sup>2+</sup>]<sub>i</sub> IN ADHERENT CELL MONOLAYERS</b>	<b>72</b>
2.11.1	CALIBRATION OF HIGH-THROUGHPUT FLUORESCENCE DATA .....	73
<b>3.</b>	<b><u>OPTIMISATION AND REFINEMENT OF METHODS.....</u></b>	<b><u>75</u></b>
<b>3.1</b>	<b>OPTIMISATION OF PCR: SYBR GREEN I vs. TAQMAN™ .....</b>	<b>75</b>
3.1.1	METHODS .....	75
3.1.2	RESULTS.....	76
3.1.3	DISCUSSION.....	79
<b>3.2</b>	<b>OPTIMISATION OF A DUPLEX TAQMAN™ PCR ASSAY .....</b>	<b>81</b>
3.2.1	METHODS .....	81
3.2.2	RESULTS.....	82
3.2.3	DISCUSSION.....	83
<b>3.3</b>	<b>OPTIMISATION OF HIGH-THROUGHPUT [Ca<sup>2+</sup>]<sub>i</sub> FLUORIMETRY IN THE NOVOSTAR PLATE READER.....</b>	<b>84</b>
3.3.1	METHODS .....	84
3.3.2	RESULTS.....	85
3.3.3	DISCUSSION.....	87

<b>3.4</b>	<b>OPTIMISATION OF INJECTOR SETTINGS IN THE NOVOSTAR PLATE READER.....</b>	<b>88</b>
3.4.1	METHODS .....	88
3.4.2	RESULTS.....	88
3.4.3	DISCUSSION.....	90
<b>3.5</b>	<b>EVALUATION OF A FINALISED PROTOCOL FOR HIGH-THROUGHPUT [Ca<sup>2+</sup>]<sub>i</sub> FLUORIMETRY IN THE NOVOSTAR PLATE READER .....</b>	<b>91</b>
3.5.1	METHODS .....	91
3.5.2	RESULTS.....	92
3.5.3	DISCUSSION.....	92
<b>4.</b>	<b><u>STUDIES IN A STABLY TRANSFECTED UT CELL-LINE.....</u></b>	<b>95</b>
<b>4.1</b>	<b>PRINCIPLES OF IN VITRO MEASUREMENT OF AGONIST-MEDIATED INOSITOL PHOSPHATE TURNOVER ...</b>	<b>95</b>
<b>4.2</b>	<b>CONCENTRATION-RESPONSE CURVES .....</b>	<b>96</b>
4.2.1	METHODS .....	96
4.2.1.1	Data manipulations.....	97
4.2.2	RESULTS.....	97
4.2.3	DISCUSSION.....	99
<b>4.3</b>	<b>INITIAL ANTAGONISM STUDIES .....</b>	<b>100</b>
4.3.1	METHODS .....	100
4.3.2	RESULTS.....	100
4.3.3	DISCUSSION.....	101
<b>4.4</b>	<b>TIME-COURSE STUDIES .....</b>	<b>101</b>
4.4.1	METHODS .....	101
4.4.2	RESULTS.....	102
4.4.3	DISCUSSION.....	102
<b>4.5</b>	<b>ASSAY DEVELOPMENT .....</b>	<b>103</b>
4.5.1	METHODS .....	103
4.5.2	RESULTS.....	104
4.5.3	DISCUSSION.....	105
<b>4.6</b>	<b>REFINED ANTAGONISM STUDIES .....</b>	<b>106</b>
4.6.1	METHODS .....	106
4.6.2	RESULTS.....	106
4.6.3	DISCUSSION.....	108
<b>5.</b>	<b><u>STUDIES IN AN ECDYSONE-INDUCIBLE UT CELL-LINE .....</u></b>	<b>110</b>
<b>5.1</b>	<b>PRODUCTION OF AN ECDYSONE-INDUCIBLE UT CELL-LINE .....</b>	<b>110</b>
<b>5.2</b>	<b>CLONING OF THE PEGSH-UT VECTOR.....</b>	<b>110</b>
5.2.1	PLASMID DIGESTIONS.....	110
5.2.1.1	Linearisation of Cloning Vector 70981-hUT.....	111
5.2.1.2	Excision of the UT Receptor cDNA Insert from 70981-hUT .....	112
5.2.1.3	Linearisation of the pEGSH Vector.....	112
5.2.1.4	Second Digestion of the pEGSH Vector.....	113
5.2.2	PURIFICATION OF DNA FOLLOWING ENZYMATIC REACTIONS .....	113
5.2.3	AGAROSE GEL ELECTROPHORESIS .....	114
5.2.4	PURIFICATION OF DNA FROM AGAROSE GEL .....	115
5.2.5	DNA LIGATION .....	116

5.2.6	PROKARYOTIC TRANSFORMATION.....	116
5.2.7	EXTRACTION AND PURIFICATION OF PEGSH-UT FROM E.COLI.....	117
5.2.8	RESTRICTION ANALYSIS AND CLONE SELECTION .....	118
5.2.9	DNA SEQUENCING .....	120
5.2.10	MAXIPREP OF CLONE 9.....	121
<b>5.3</b>	<b>MAMMALIAN TRANSFECTION .....</b>	<b>122</b>
5.3.1	DETERMINING THE SENSITIVITY OF ER-CHO TO HYGROMYCIN-B .....	122
5.3.2	OPTIMISATION OF TRANSFECTION CONDITIONS.....	123
5.3.3	TRANSFECTION OF PEGSH-UT INTO ERCHO .....	124
<b>5.4</b>	<b>SUBCLONING TECHNIQUES .....</b>	<b>125</b>
5.4.1	CLONING CYLINDER METHOD .....	125
5.4.2	LIMITING DILUTION METHOD .....	125
<b>5.5</b>	<b>SCREENING OF ERCHO<sub>H</sub>UT SUBCLONES.....</b>	<b>126</b>
5.5.1	SCREENING BY PCR.....	126
5.5.1.1	Methods.....	126
5.5.1.2	Results.....	127
5.5.2	FUNCTIONAL SCREENING.....	128
5.5.2.1	Methods.....	128
5.5.2.2	Results.....	128
5.5.2.3	Discussion.....	129
<b>5.6</b>	<b>TROUBLESHOOTING.....</b>	<b>131</b>
5.6.1	ER-CHO CELL-LINE VALIDATION.....	131
5.6.1.1	Methods.....	131
5.6.1.2	Results.....	132
5.6.1.3	Discussion.....	134
<b>5.7</b>	<b>FINAL PRODUCTION OF AN ERCHO<sub>H</sub>UT CELL-LINE.....</b>	<b>135</b>
5.7.1	METHODS .....	135
5.7.2	RESULTS.....	135
<b>5.8</b>	<b>FUNCTIONAL SCREENING OF ERCHO<sub>H</sub>UT.....</b>	<b>136</b>
5.8.1	METHODS .....	136
5.8.2	RESULTS.....	137
5.8.3	DISCUSSION.....	138
<b>6.</b>	<b><u>SIRNA-MEDIATED RNA INTERFERENCE STUDIES .....</u></b>	<b><u>140</u></b>
<b>6.1</b>	<b>A TRIAL OF THE SUPPLIED TRANSFECTION PROTOCOL.....</b>	<b>140</b>
6.1.1	METHODS .....	140
6.1.2	RESULTS.....	141
6.1.3	DISCUSSION.....	142
<b>6.2</b>	<b>OPTIMISING CELL NUMBER FOR SIRNA STUDIES .....</b>	<b>143</b>
6.2.1	METHODS .....	143
6.2.2	RESULTS.....	143
6.2.3	DISCUSSION.....	144
<b>6.3</b>	<b>GENOMIC CHARACTERISATION OF UT-TARGETING SIRNAS.....</b>	<b>145</b>
6.3.1	METHODS .....	145
6.3.2	RESULTS.....	146
6.3.3	DISCUSSION.....	147
<b>6.4</b>	<b>SIRNA-MEDIATED EFFICACY STUDIES AT THE UT RECEPTOR .....</b>	<b>147</b>
6.4.1	METHODS .....	147
6.4.2	RESULTS.....	148

6.4.3	DISCUSSION.....	151
<b>7.</b>	<b><u>GENERAL DISCUSSION .....</u></b>	<b><u>153</u></b>
7.1	ECDYSONE-INDUCIBLE CHO CELL-LINE.....	156
7.2	UT-TARGETING SIRNA-MEDIATED RNAI.....	159
7.3	CONCLUSIONS.....	162
7.4	FUTURE WORK .....	164
<b>8.</b>	<b><u>APPENDIX I .....</u></b>	<b><u>166</u></b>
8.1	HARVEST BUFFER (X5) .....	166
8.2	KREBS-HEPES BUFFER .....	166
8.3	SOC MEDIUM.....	166
8.4	LB AGAR.....	167
8.5	PHOSPHATE BUFFERED SALINE.....	167
8.6	TISSUE CULTURE MEDIA .....	167
8.6.1	CHO <sub>h</sub> UT GROWTH MEDIUM .....	167
8.6.2	ER-CHO GROWTH MEDIUM.....	168
<b>9.</b>	<b><u>APPENDIX II .....</u></b>	<b><u>169</u></b>
9.1	QIAQUICK PCR PURIFICATION KIT MANUFACTURER'S PROTOCOL.....	169
9.2	70981 RESTRICTION MAP .....	171
9.3	UT RECEPTOR CDNA INSERT SEQUENCE .....	172
9.4	PEGSH-UT CONSENSUS SEQUENCING DATA .....	173
<b>10.</b>	<b><u>APPENDIX III.....</u></b>	<b><u>177</u></b>
<b>11.</b>	<b><u>REFERENCES .....</u></b>	<b><u>210</u></b>

# Chapter One

# **1. INTRODUCTION**

## **1.1 Urotensin II: An Overview**

Urotensin-II (U-II) is a peptide ligand which was isolated from the neurosecretory system of *Gillichthys mirabilis* (Goby fish) over thirty years ago [1]. For much of the time following its discovery, U-II was considered to exclusively belong to lower organisms and was therefore considered to be an inert substance in mammalian systems [2]. However, this view was challenged when it was demonstrated that Goby U-II can produce slow relaxation of mouse anococcygeus muscle [3] and contraction of rat major artery segments [4]. Successful isolation of human U-II cDNA in 1998 suggested a putative role in mammals [5].

Although early experiments inferred that the actions of U-II were produced through specific binding sites [6], a urotensin-II receptor has only recently been identified [7]. In 1995 Marchese et al. cloned an orphan G-protein coupled receptor in rat, designated GPR14, which shares significant homology with somatostatin and opioid receptors [8]. Ames et al. subsequently identified a G-protein coupled receptor in man, homologous to rat GPR14. Furthermore, using a ‘reverse molecular pharmacology’ technique, this group demonstrated that U-II is the endogenous ligand for this receptor and subsequently renamed it the UT receptor [7]. Within two months of initial discovery, three other independent research groups had verified these findings [9-11]. Subsequent characterisation of this peptide has led to it being dubbed as ‘the most potent vasoconstrictor peptide identified so far’ [7].

## **1.2 G-protein Coupled Receptors**

### ***1.2.1 The Seven-Transmembrane Receptor Superfamily***

Seven-transmembrane (7TM) receptors comprise a large, extremely diverse and ubiquitously expressed superfamily of peptidic cell surface receptors [12]. Careful estimation based on the complete human genome, suggests that approximately 865 genes code for a 7TM receptor (equating to 1.6% of the genome), [13].

All 7TM receptors characterised to date are comprised of a single polypeptide with the C and N termini located in the cytosolic and extracellular domains respectively [14]. The polypeptide traverses the plasma membrane 7-times in an anti-clockwise direction, afforded by seven hydrophobic  $\alpha$ -helices along its length [14].

Phylogenetic analysis identifies 5 main groups within the 7TM superfamily, referred to by the GRAFS acronym [14]. Members of the same group typically share around 25% sequence identity within the transmembrane regions in addition to possessing highly conserved residues and motifs [15]. Beyond the predicted seven transmembrane architecture (previously described), inter-group sequence similarity is nominal [15]. The 5 groups are:

- The **g**lutamate receptor family (15 members)
- The **r**hodopsin receptor family (701 members, sub-divided into 4 further sub-groups ( $\alpha/\beta/\gamma/\delta$ ))
- The **a**dhesion receptor family (24 members)
- The **f**rizzled/taste2 receptor family (24 members)
- The **s**ecretin receptor family (15 members)

There is a final group of 23 unrelated receptors which do not belong to any other group based on phylogenetic analysis, this includes UT [14]. This is most likely due to “atypical parts”, which are most commonly “found in the loops rather than the TM regions”, [14]. Furthermore, sequence alignment between UT and bovine rhodopsin suggests “significant sequence similarities and identities [to exist] in the transmembrane regions of the two proteins”, [16]. Collectively, these data suggest that UT possesses atypical elements but belongs to the rhodopsin receptor family.

The entire superfamily of 7TM receptors regulate intracellular signalling through a heterotrimeric guanine nucleotide-binding regulatory protein (G-protein).

### ***1.2.2 Heterotrimeric G-proteins***

7TM receptors associate with heterotrimeric G-proteins, that is they are comprised of three differing subunits; namely  $\alpha$ ,  $\beta$  and  $\gamma$  [17]. Presently, 23  $\alpha$ -subunits, 7  $\beta$ -subunits and 12  $\gamma$ -subunits have been characterised [18].  $\beta\gamma$  complexes are extremely stable and thus regarded as a single functional unit, the number of  $\beta$  and  $\gamma$  subunit variants (detailed above) theoretically allows for the formation of 84 different  $\beta\gamma$  complexes. All  $G_\alpha$  subunits can be divided into four groups on the basis of amino acid similarity, these are  $G_s$ ,  $G_{i/o}$ ,  $G_{q/11}$  and  $G_{12/13}$  [19].

Activation of the  $G_s$  family causes stimulation of adenylyl cyclase and the opening of  $Ca^{2+}$  channels [19]. The  $G_i$  family inhibits adenylyl cyclase, opens  $K^+$  channels and closes  $Ca^{2+}$  channels.  $G_o$  is primarily expressed in neuronal cell types and is involved in the closure of  $Ca^{2+}$  channels and inhibition of PI turnover [19]. The  $G_q$  family includes  $G_q$ ,  $G_{11}$ ,  $G_{14}$ ,  $G_{15}$  and  $G_{16}$ , they predominantly stimulate PI turnover [19]. The  $G_{12/13}$

family act through RhoGEF and increase the activity of both phospholipase D and  $C_{\varepsilon}$  [20].

### ***1.2.3 G-protein Activation***

In the resting state, the heterotrimeric G-protein is not associated with the 7TM receptor and is able to freely diffuse in the plane of the plasma membrane; the  $\alpha$ -subunit is GDP bound [19, 21]. Activation of a 7TM receptor at the cell surface causes a conformational change, significantly increasing the affinity of the receptor for a heterotrimeric G-protein in the cytoplasmic domain [19]. The subsequent binding of a G-protein to the cytoplasmic portion of the receptor results in the exchange of GDP (bound to the  $\alpha$ -subunit) for GTP. This exchange is responsible for the dissociation of the G-protein from the 7TM receptor as well as the  $\alpha$ -subunit from the  $\beta\gamma$ -subunit [19]. The  $\alpha$  and  $\beta\gamma$  subunits are now considered to be in their active states and are freely diffusible in the plane of the plasma membrane to interact with their respective effector molecules [21]. The  $\alpha$ -subunit possesses intrinsic GTPase activity which is responsible for hydrolysis of its bound GTP to GDP, resulting in dissociation from the effector molecule and re-association of the  $\alpha\beta\gamma$ -trimer; thus completing the cycle [19]. Interestingly, some effector molecules are GTPase-activating proteins (GAP) and therefore increase the  $\alpha$ -subunit's GTPase activity [19].

### ***1.2.4 G<sub>q</sub> Protein Activation***

Activated G<sub>q</sub> family  $\alpha$ -subunits specifically interact with the four isoforms of  $\beta$ -phospholipase C (PLC- $\beta$ ), [22]. Once activated, these enzymes catalyse the breakdown

of the minor membrane phospholipid phosphatidylinositol-4, 5-bisphosphate (PIP<sub>2</sub>) into inositol-1, 4, 5-trisphosphate (IP<sub>3</sub>) and diacylglycerol (DAG), [22].

#### *1.2.4.1 Inositol Phosphates and Intracellular Calcium Mobilisation*

IP<sub>3</sub> binds to specific receptors on the endoplasmic reticulum (ER), designated IP<sub>3</sub>R [23]. On binding four IP<sub>3</sub> molecules, the ion channel opens and Ca<sup>2+</sup> moves down its concentration gradient from the ER into the cytosol [23].

IP<sub>3</sub> has a short half life and is serially dephosphorylated by the action of endogenous phosphatases [23], the end product being inositol which can either be excluded from the cell or recycled into PIP<sub>2</sub> [24]. A proportion of IP<sub>3</sub> is metabolised via a different route; phosphorylation of the 3-carbon hydroxyl group produces inositol (1,3,4,5)-tetrakisphosphate (IP<sub>4</sub>), which may itself function as a second messenger by allowing entry of extracellular Ca<sup>2+</sup> into the cell [23]. IP<sub>4</sub> also has a short half life and is dephosphorylated at the 5-carbon position to generate inositol (1,3,4)-trisphosphate, which then rejoins the previously described pathway for serial dephosphorylation [23]. Exogenous lithium specifically inhibits inositol-1-phosphatase, which is responsible for the dephosphorylation of inositol (1)-phosphate into inositol [24]. Lithium can be used both clinically and experimentally to prevent the recycling of inositol phosphates [24, 25]. The inositol phosphate cycle is shown diagrammatically in Figure 1.1.

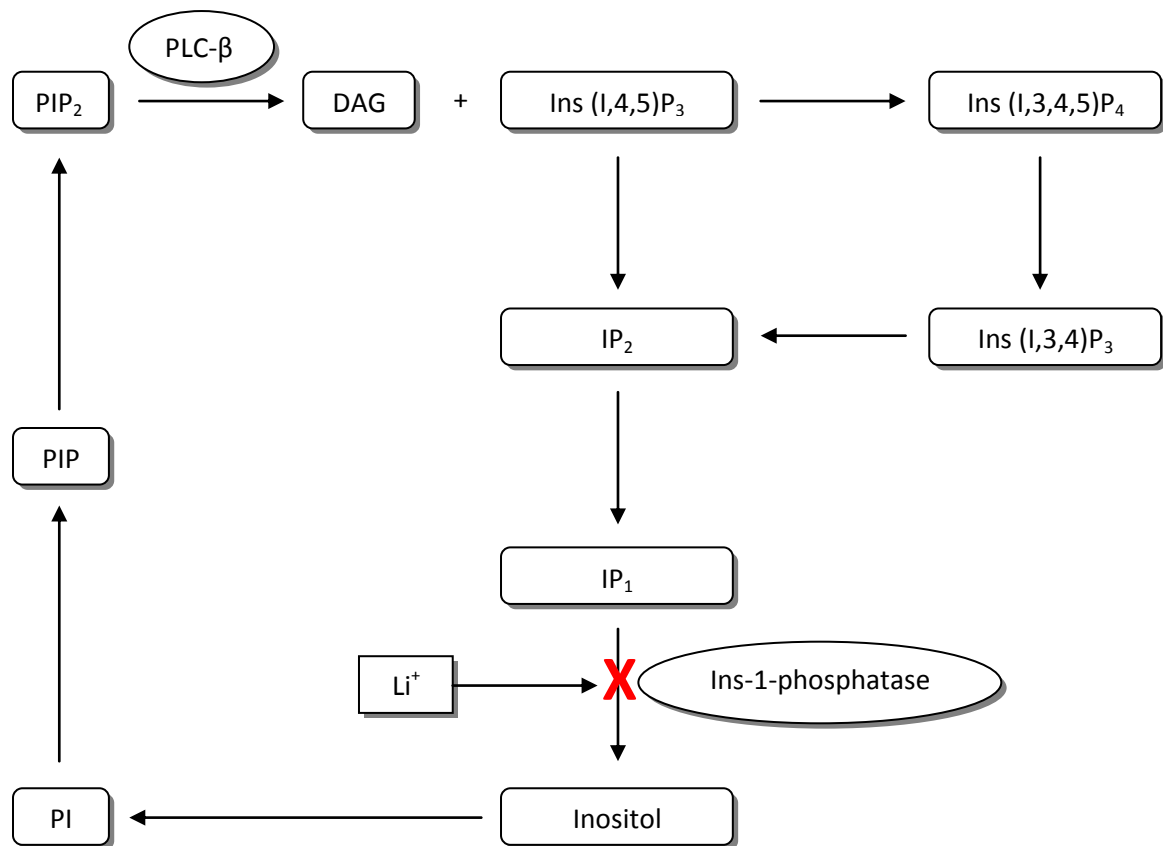


**Figure 1.1.** A schematic representation of the inositol phosphate cycle.

#### *1.2.4.2 Diacylglycerol and Protein Kinase C*

Diacylglycerol is primarily involved with the activation of membrane-bound protein kinase C (PKC), [26]. On activation PKC is liberated from the plasma membrane and is responsible for the phosphorylation of a variety of intracellular proteins [26]. To date, twelve different PKC subtypes have been identified, each with their own subcellular localisation and target proteins [27]. PKC may also be activated in response to any pathway resulting in raised intracellular calcium concentration, including the  $IP_3$  pathway [26].

### 1.3 The Urotensin II Receptor System

#### 1.3.1 *Urotensin-II*

As with other peptides, U-II is synthesised from a larger precursor molecule known as prepro-urotensin II [28]. In humans, two isoforms have been identified (see Figure 1.2) of lengths 124 and 139 residues [5, 7]. Human prepro-urotensin II shares very little amino acid similarity with that of other species (16% similarity to carp, 25% similarity to frog). However, significant amino acid similarity is evident at the C-terminus, which includes the U-II peptide and prohormone convertase cleavage sites [5]. Cleavage of either of the two prohormones in humans, produces identical eleven amino acid peptides (Figure 1.3), [7].

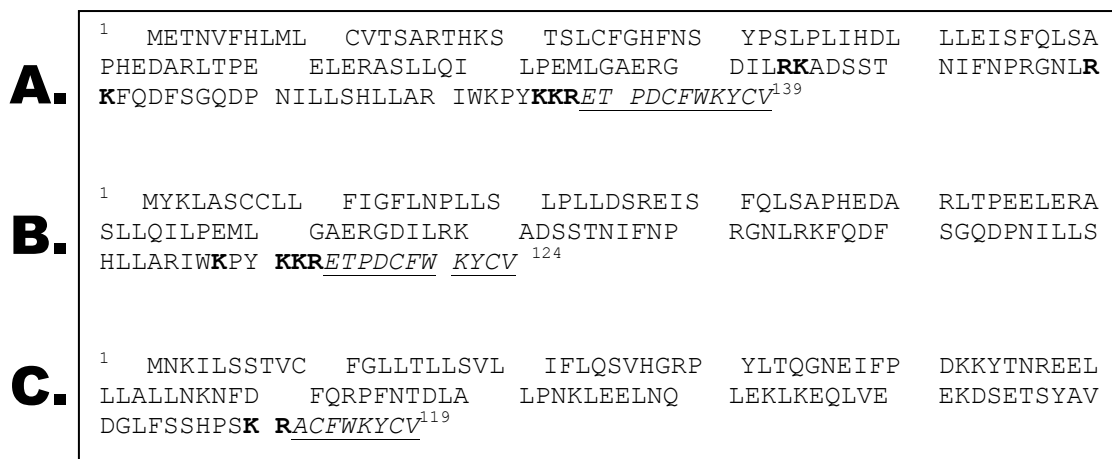


**Figure 1.2. Amino acid sequences of: A. Human Prepro-urotensin II (isoform a) B. Human Prepro-urotensin II (isoforms b) C. Human Prepro-urotensin Related Peptide. Sequence in italics and underlined denotes a mature peptide, sequences in bold denote deduced cleavage sites.**

Despite some inter-species variation of the U-II peptide in both length and sequence [5], the C-terminus includes a cyclic hexapeptide sequence which has been absolutely conserved through evolution from lamprey to human [5]; species which first diverged some 560 million years ago [29]. The fact that such a strong evolutionary pressure has acted to conserve this sequence highlights its physiological importance, indeed this hexapeptide sequence alone confers biological activity [6].

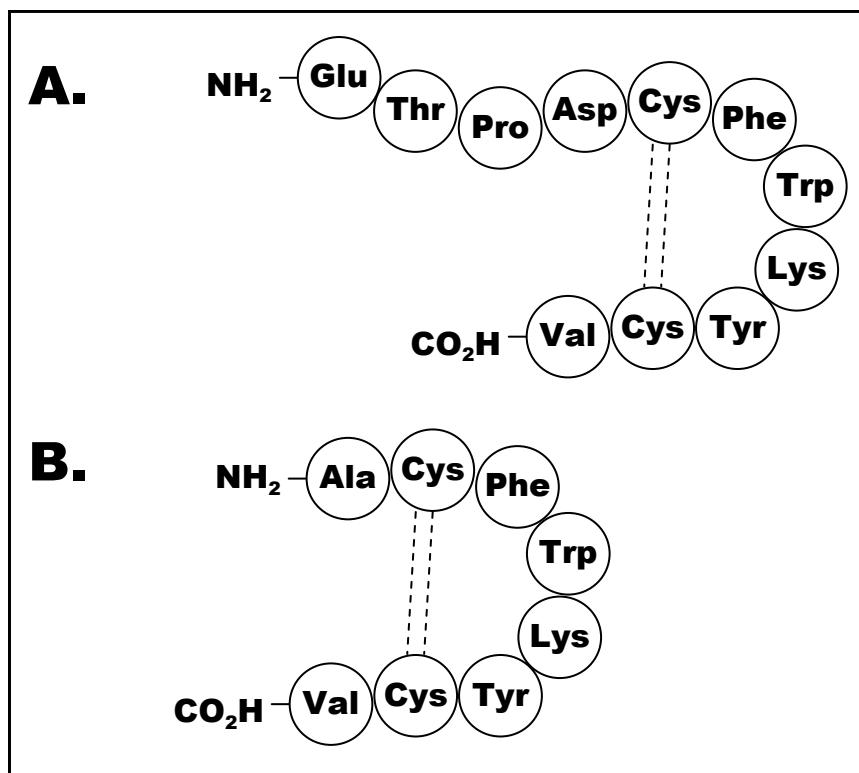


Figure 1.3. Amino acid sequence of: A. Human Urotensin-II B. Human Urotensin-II Related Peptide. Dotted lines illustrate a disulphide bridge.

### 1.3.2 Urotensin II-related Peptide

Urotensin II-related peptide (URP) is an eight amino acid peptide (see Figure 1.3), which was initially isolated in rat brain [30]. In man, the peptide is cleaved from a larger precursor molecule (see Figure 1.2), 119 residues long and named prepro-URP [30]. Although the precursor proteins of URP and U-II share little overall amino acid identity, their respective genes have many comparable structural features, suggesting that they both diverged from a common molecular ancestor through tandem gene duplication [31]. Both U-II and URP share the same conserved carboxy-terminal hexapeptide sequence, which confers biological activity [6, 30].

### 1.3.3 UT Receptor

In common with other G-protein coupled receptors (GPCR), UT (see Figure 1.4) is a seven transmembrane spanning receptor [8] and is coded on human chromosome 17q25.3 [32]. The gene is devoid of introns and encodes a protein comprised of 389 amino acid residues, exhibiting 75% identity with rat GPR14 [7]. The UT receptor is coupled to the G<sub>q/11</sub> class of G-protein [9]. Subsequently, UT receptor activation is associated with increased phospholipase C activity [33], increased turnover of phosphoinositides [33] and elevation of [Ca<sup>2+</sup>]<sub>i</sub> [7].

To date, three single nucleotide polymorphisms (SNPs) of the UT gene have been reported; T21M [34], S89S [35] and S89N [34-36], the latter of which is associated with type two diabetes mellitus (T2DM) and essential hypertension (1.7). A further SNP of the UT promoter region, designated “-605G>A”, has been identified [34].

<p><sup>1</sup> MALTPESSPSS FPGLAATGSS VPEPPGGPNA TLNSSWASPT EPSSLEDLVA TGTIGTLLSA MGVVGVVGNNA YTLVVTCRSL RAVASMYVYV VNLALADLLY LLSIPFIVAT YVTKEWHFGD VGCRVLFGLD FLTMHASIFT LTVMSSERYA AVLRPLDTVQ RPKG<b>Y</b>RKLLA LGTWLLALLL TLPVMLAMRL VRRGPKSLCL PAWGPRAHRA YLTLLFATSI AGPGLLIIGLL YARLARA<b>Y</b>RR SQRASFKRAR RPGARALRLV LGIVLLEWAC FLPFWLWQLL AQYHQAPLAP RTARIVNYLT TCLTYGNSCA NPFLYTLLTR NYRDHLRGRV RGPSSGGGRG PVPSLQPRAR FQRCSGRSLS SCSPQPTDSL VLAPAAPARP APEGPRAPA<sup>389</sup></p>
--

**Figure 1.4. Amino acid sequence of the human UT receptor. Underlined portions denote deduced transmembrane domains, bold portions denote predicted N-linked glycosylation sites and shaded portions indicate PKA/PKC phosphorylation sites.**

### 1.3.4 Urotensin-II Converting Enzymes

The potency of mature hU-II is significantly higher than that of prepro-urotensin II, suggesting that biological activity may be dependent upon the presence of an active urotensin-converting enzyme (UCE), [37]. If true, then pathological over-activation of the urotensin system can potentially be managed by a specific urotensin-converting enzyme inhibitor.

Furin is an enzyme ubiquitously expressed in mammalian cells, primarily localised to the *trans*-golgi network and associated with the cleavage of many precursor molecules [38]. The amino acid sequence of prepro-urotensin II between positions 11 & 17 complies with the somewhat stringent rules governing efficient cleavage with furin. Human U-II immunoreactivity has also been demonstrated in the perinuclear region of mesothelial cells [39]. Intracellular proteolytic conversion of prepro-urotensin II has been demonstrated *in vitro*, however inhibition of furin does not completely abolish cleavage in this setting, suggesting that other intracellular UCEs may exist [39].

Analysis of the sequence of pre-pro URP suggests this precursor cannot be cleaved by furin [40]. Additionally, mass spectrometry results obtained from whole blood and plasma have demonstrated the conversion of prepro-urotensin II to the mature peptide in the absence of furin. This activity is sensitive to the protease inhibitor aprotinin; thus implicating a serine protease such as trypsin [39]. Prepro-urotensin II contains dibasic residues at the convertase site (-R<sup>12</sup>-K<sup>13</sup>-), a recognition motif characteristic of a broad range of peptide convertases, including trypsin [41].

It is therefore possible that cleavage of the individual U-II/URP precursors is site (and subsequently enzyme) specific.

## **1.4 Intracellular Signal Transduction Pathways of UT**

In addition to  $G_{q/11}$ -mediated signal transduction (1.2.4), the following pathways may also be activated in response to UT receptor activation.

### ***1.4.1 Tyrosine Kinases***

UII-induced rat aorta ring contractions can be partially inhibited by the specific tyrosine kinase inhibitors, tyrphostin B42 and genistein [42]. Such data suggest a role of tyrosine kinases in UII-induced  $Ca^{2+}$  sensitisation within arterial smooth muscle.

### ***1.4.2 Rho/Rho-kinase Related Pathways***

Activation of the small GTPase Rho A and its downstream effector Rho-kinase has been demonstrated in response to U-II [42]. Specific downstream effects of this signalling pathway include actin polymerisation, cellular proliferation and phosphorylation of myosin light chain phosphatase leading to vascular smooth muscle contraction [42].

### ***1.4.3 Extracellular Signal-related Protein Kinases (ERKs)***

Phosphorylation of ERK2 (and to a lesser extent ERK1) has been demonstrated in response to UT activation; furthermore, at least part of this response is independent of  $[Ca^{2+}]_i$  elevation [43].  $G_{i/o}$  protein inhibitors effectively attenuate UT-mediated phosphorylation of ERK2, suggesting that the UT receptor may also couple to this class of G-protein [43]. Cell adhesion-mediated integrin signalling has also been demonstrated to be involved in U II-mediated ERK phosphorylation. Although this pathway is poorly characterised at present, it appears to be independent of FAK activation [44].

## **1.5 Expression of UT and its Endogenous Ligands**

The UT receptor and its endogenous ligands, U-II and URP, are expressed in a wide variety of tissues; as summarised in Table 1.1. A diagrammatic brain atlas of UT expression is included in Appendix III.

### **1.5.1 *UT Receptor***

UT is most abundantly expressed in the pancreas, kidney, heart and skeletal muscle [7, 45, 46]. Analysis by RT-PCR reveals weaker, although stable, expression of the mRNA transcript in vascular smooth muscle and endothelium derived mostly from arteries [7]. Radioligand binding experiments demonstrate expression of UT in many discrete regions throughout the CNS from spinal cord to cerebral cortex [46].

### **1.5.2 *U-II Peptide***

The mRNA transcript for pre-pro U-II is most abundant in spinal cord, kidney, adrenal gland and heart [5, 47]; consistent expression is also observed in vascular smooth muscle and endothelium mainly from arterial vessels [45, 47]. Furthermore, U-II is stably expressed in many discrete regions of the CNS; including but not limited to those classically involved with central cardiovascular control, such as the medulla oblongata and nucleus ambiguus [5, 48]. Additionally, U-II peptide is present in plasma [45], cerebrospinal fluid [49] and urine [50]. It should be noted that the type of assay currently used to quantify U-II in plasma, cerebrospinal fluid and urine may lack the specificity required to distinguish between U-II, URP and the respective precursor molecules [51]. It is therefore possible that some or all of these species exist in these bodily fluids, each a component of currently detected “U-II like” immunoreactivity.

The origin of blood-borne U-II is undetermined at present, there are however several suspected sites. The vascular endothelium covers a considerable area and is in direct contact with the blood, furthermore this cell type has been shown to express U-II [45]. However, secretion of U-II from the luminal surface of the vascular endothelium has not been demonstrated. Moreover the consistent expression of UT in vascular smooth muscle cells [47] suggests that secretion from the endothelium to be, at least in part, via the basal surface. Significant arteriovenous gradients of U-II exist across the kidney, heart and liver, suggesting these organs to be the principal sites of U-II production and secretion into the circulation [52]. Importantly, plasma U-II concentrations in anephric patients are largely unchanged from controls, perhaps suggesting that there is no single site of U-II secretion into the circulation [53].

### ***1.5.3 Urotensin-Related Peptide***

The mRNA transcript for pre-pro URP is expressed in a pattern similar to that of U-II [30], there are however some notable exceptions; namely a significantly lower expression in spinal cord and significantly higher expression in the ovary and testis when compared to U-II [30].

**Table 1.1. tissue distribution of the UT receptor, its endogenous ligands and their precursor molecules. Studies identifying the presence of U-II peptide are only cited for tissues where expression of the mRNA transcript or presence of the precursor molecule has not been demonstrated. References are given in the following format - <sup>x</sup>[Y]<sup>z</sup>, where x describes the method of analysis, y gives the reference number and z gives the species.**

**Methods of analysis:** (a) RT-PCR, (b) Radio-ligand binding or radioimmunoassay, (c) Immunohistochemistry, (d) Dot blot analysis, (e) Functional assay, (f) *In situ* hybridisation, (g) RNase protection assay.

**Species:** (H) Human, (P) Non-human primate, (R) Rat, (M) Mouse, (F) Frog.

<u>TISSUE</u>	<u>Pre-pro U-II or mRNA transcript</u>	<u>U-II</u>	<u>Pre-pro URP or mRNA transcript</u>	<u>UT</u>
<b>BRAIN</b>				
Abducens nucleus	<sup>f</sup> [48] <sup>R</sup>	-	-	<sup>b</sup> [46] <sup>R</sup>
Accumbens nucleus	-	-	-	<sup>a</sup> [54] <sup>R</sup>
Amygdala	-	-	<sup>a</sup> [30] <sup>H</sup>	<sup>a</sup> [54] <sup>R</sup>
Anteroventral thalamus	-	-	-	<sup>b</sup> [55] <sup>R</sup>
Bed nucleus	-	-	-	<sup>b</sup> [55] <sup>R</sup>
Cerebellum	<sup>a</sup> [56] <sup>P</sup>	-	<sup>a</sup> [30] <sup>H</sup>	<sup>a</sup> [54] <sup>R</sup>
Cerebral cortex	<sup>a</sup> [57] <sup>H</sup>	-	<sup>a</sup> [30] <sup>H</sup>	<sup>b</sup> [46] <sup>H</sup>
Choroid plexus	-	-	-	<sup>g</sup> [58] <sup>R</sup>
Endopiriform nuclei	-	-	-	<sup>b</sup> [55] <sup>R</sup>
Facial nucleus	<sup>f</sup> [48] <sup>R</sup>	-	-	-
Glossopharyngeal nucleus	<sup>f</sup> [5] <sup>F</sup>	-	-	-
Hippocampus	-	-	<sup>a</sup> [30] <sup>H</sup>	<sup>a</sup> [54] <sup>R</sup>
Hypoglossal nucleus	<sup>f</sup> [48] <sup>R</sup>	-	-	-
Hypothalamus	<sup>a</sup> [57] <sup>H</sup>	-	-	<sup>a</sup> [57] <sup>H</sup>
Interpeduncular nucleus	-	-	-	<sup>b</sup> [55] <sup>R</sup>
Lateral dorsal tegmental area	-	-	-	<sup>b</sup> [55] <sup>R</sup>
Lateral septal nucleus	-	-	-	<sup>b</sup> [55] <sup>R</sup>
Medial habenular nucleus	-	-	-	<sup>b</sup> [55] <sup>R</sup>
Medial pre-optic nucleus	-	-	-	<sup>b</sup> [55] <sup>R</sup>
Medulla oblongata	<sup>d</sup> [5] <sup>H</sup> <i>strong</i>	-	<sup>a</sup> [30] <sup>H</sup>	<sup>a</sup> [57] <sup>H</sup>
Nucleus ambiguus	<sup>f</sup> [48] <sup>R</sup>	-	-	-
Nucleus reticularis inferior	<sup>f</sup> [5] <sup>F</sup>	-	-	-
Parasubiculum	-	-	-	<sup>b</sup> [55] <sup>R</sup>
Pedunculopontine tegmental area	-	-	-	<sup>b</sup> [55] <sup>R</sup>
Pituitary	<sup>d</sup> [5] <sup>H</sup>	-	-	<sup>a</sup> [57] <sup>H</sup>
Pons	<sup>a</sup> [30] <sup>H</sup>	-	<sup>a</sup> [30] <sup>H</sup>	<sup>a</sup> [54] <sup>R</sup>
Pontine nuclei	-	-	-	<sup>b</sup> [55] <sup>R</sup>
Striatum	-	-	-	<sup>a</sup> [54] <sup>R</sup>

<u>TISSUE</u>	<u>Pre-pro U-II or mRNA transcript</u>	<u>U-II</u>	<u>URP</u>	<u>UT</u>
Substantia nigra	-	-	<sup>a</sup> [30] <sup>H</sup>	<sup>a</sup> [7] <sup>H</sup>
Superior occipital gyrus	-	-	-	<sup>a</sup> [7] <sup>H</sup>
Tectum	-	<sup>c</sup> [59] <sup>F</sup>	-	-
Tegmentum	-	<sup>c</sup> [59] <sup>F</sup>	-	-
Thalamus	-	<sup>c</sup> [59] <sup>F</sup>	<sup>a</sup> [30] <sup>H</sup>	<sup>a</sup> [7] <sup>H</sup>
Trigeminal motor nucleus	<sup>f</sup> [48] <sup>R</sup>	-	-	-
Trochlear nucleus	<sup>f</sup> [5] <sup>F</sup>	-	-	-
Vagal dorsal motor nucleus	-	<sup>c</sup> [60] <sup>R</sup>	-	-
Ventral lateral geniculate nuclei	-	-	-	<sup>b</sup> [55] <sup>R</sup>
Ventral tagmental area	-	-	-	<sup>b</sup> [55] <sup>R</sup>
<b><u>SPINAL CORD</u></b>	<sup>d</sup> [5] <sup>H</sup> <i>strong</i>	-	<sup>a</sup> [30] <sup>H</sup> <i>weak</i>	<sup>a</sup> [45] <sup>H</sup>
Caudal motoneurons	<sup>f</sup> [5] <sup>H</sup>	-	-	-
Ventral horn	<sup>f</sup> [48] <sup>R</sup>	-	-	<sup>f</sup> [9] <sup>M</sup>
<b><u>CARDIOVASCULAR</u></b>				
Atrium	<sup>a</sup> [50] <sup>H</sup> <i>moderate</i>	-	-	<sup>a</sup> [50] <sup>H</sup> <i>moderate</i>
Coronary artery	<sup>a</sup> [47] <sup>H</sup>	-	-	<sup>a</sup> [7] <sup>H</sup>
Mammary artery	<sup>a</sup> [61] <sup>H</sup>	-	-	-
Myocardium	<sup>a</sup> [47] <sup>H</sup> <i>moderate</i>	-	<sup>a</sup> [30] <sup>H</sup> ("heart" region unspecified).	<sup>a</sup> [50] <sup>H</sup> <i>moderate</i>
Right auricle	<sup>a</sup> [50] <sup>H</sup>	-	-	<sup>a</sup> [50] <sup>H</sup> <i>moderate</i>
Saphenous vein	<sup>a</sup> [50] <sup>H</sup>	-	-	-
Septum	<sup>a</sup> [50] <sup>H</sup>	-	-	-
Thoracic aorta	<sup>a</sup> [50] <sup>H</sup>	-	-	<sup>a</sup> [50] <sup>H</sup>
Vascular endothelium	<sup>a</sup> [45] <sup>H</sup>	-	-	<sup>a</sup> [45] <sup>H</sup>
Vascular smooth muscle	<sup>a</sup> [47] <sup>H</sup>	-	-	<sup>d</sup> [47] <sup>H</sup>
Ventricle	<sup>a</sup> [45] <sup>H</sup> <i>moderate</i>	-	-	<sup>a</sup> [45] <sup>H</sup> <i>moderate</i>

<b>TISSUE</b>	<b>Pre-pro U-II or mRNA transcript</b>	<b>U-II</b>	<b>Pre-pro URP or mRNA transcript</b>	<b>UT</b>
<b>PERIPHERAL</b>				
Kidney	<sup>a</sup> [45] <sup>H</sup> <i>strong/moderate</i>	-	<sup>a</sup> [30] <sup>H</sup>	<sup>a</sup> [45] <sup>H</sup> <i>strong/moderate</i>
Lung	<sup>a</sup> [56] <sup>M</sup>	-	-	<sup>b</sup> [46] <sup>H</sup> (limited to pulmonary vessels and bronchioles).
Liver	<sup>a</sup> [45] <sup>H</sup>	-	<sup>a</sup> [30] <sup>H</sup>	<sup>a</sup> [45] <sup>H</sup> <i>very weak</i>
<b>ENDOCRINE</b>				
Adrenal gland	<sup>d</sup> [5] <sup>H</sup>	-	-	<sup>a</sup> [57] <sup>H</sup>
Pancreas	<sup>d</sup> [5] <sup>H</sup>	-	<sup>a</sup> [30] <sup>H</sup>	<sup>a</sup> [7] <sup>H</sup> <i>strong</i>
Spleen	<sup>d</sup> [5] <sup>H</sup>	-	<sup>a</sup> [30] <sup>H</sup>	-
Thymus	<sup>d</sup> [5] <sup>H</sup>	-	<sup>a</sup> [30] <sup>H</sup>	-
Thyroid	-	<sup>c</sup> [7] <sup>H</sup> (limited to acinar cells lining the follicles).	-	<sup>a</sup> [56] <sup>P</sup>
<b>GASTROINTESTINAL AND GENITOURINARY</b>				
Bladder	<sup>a</sup> [56] <sup>M</sup>	-	-	<sup>f</sup> [9] <sup>H</sup>
Colonic mucosa	<sup>a</sup> [57] <sup>H</sup>	-	<sup>a</sup> [30] <sup>H</sup>	<sup>a</sup> [57] <sup>H</sup>
Oesophagus	<sup>a</sup> [56] <sup>M</sup>	-	-	<sup>a</sup> [56] <sup>P</sup>
Prostate	<sup>d</sup> [5] <sup>H</sup>	-	<sup>a</sup> [30] <sup>H</sup>	<sup>f</sup> [9] <sup>H</sup>
Small intestine	<sup>d</sup> [5] <sup>H</sup>	-	<sup>a</sup> [30] <sup>H</sup>	<sup>a</sup> [56] <sup>P</sup>
Testes	<sup>a</sup> [30] <sup>H</sup> <i>weak</i>	-	<sup>a</sup> [30] <sup>H</sup> <i>strong</i>	-
Ovary	<sup>d</sup> [5] <sup>H</sup> <i>weak</i>	-	<sup>a</sup> [30] <sup>H</sup> <i>strong</i>	-
Placenta	<sup>a</sup> [57] <sup>H</sup> <i>weak</i>	-	<sup>a</sup> [30] <sup>H</sup> <i>moderate</i>	<sup>a</sup> [57] <sup>H</sup>
Stomach	<sup>d</sup> [5] <sup>H</sup>	-	-	<sup>f</sup> [9] <sup>H</sup>
<b>BODILY FLUIDS AND SECRETIONS</b>				
Plasma	-	<sup>b</sup> [45] <sup>H</sup>	-	-
Urine	-	<sup>b</sup> [50] <sup>H</sup>	-	-
Cerebrospinal fluid	-	<sup>b</sup> [49] <sup>H</sup>	-	-
Macrophages	-	<sup>c</sup> [47] <sup>H</sup>	-	-
Myofibroblasts	-	<sup>c</sup> [47] <sup>H</sup>	-	-

## 1.6 Functional Studies

### 1.6.1 *In Vivo Studies*

Systemic administration of U-II in rat produces large increases in regional vascular conductance, indicative of vasodilatation; a consequential fall in mean arterial blood pressure (MAP) is also observed [62]. A pronounced tachycardia ensues, however the temporal characteristics of this effect suggest that at least part of this response is independent of the changes to MAP and therefore due to direct stimulation of the myocardium [62].

Systemic administration of human U-II in non-human primates (*Cynomolgus* monkey) produces a large increase in calculated total peripheral resistance, indicative of systemic vasoconstriction [7]. Antagonistic reductions in stroke volume and myocardial contractility (dP/dt) accompany this response, resulting in a largely unchanged mean arterial blood pressure [7]. This is a dose-dependent response, culminating in severe myocardial depression and fatal circulatory collapse [7]. A more recent study has confirmed the negative inotropic actions of U-II but also reported decreases in total peripheral resistance, contradicting previous work [63]. The implication of these observations is unclear at present, however they do highlight the variability of U-II-mediated responses; even between individuals of a given species.

In humans, infusion of U-II via the brachial artery produces a potent reduction in forearm blood flow, as assessed by venous occlusion plethysmography; indicative of vasoconstriction [64]. This response is not accompanied by changes to heart rate or to blood flow in the contralateral arm during infusion, suggesting it to be produced locally

[64]. However, another study using comparable techniques was unable to correlate experimentally-raised plasma U-II concentration to vascular tone in man [65]. Furthermore, despite the high plasma concentrations of U-II in subjects during these experiments, no changes to heart rate, cardiac output or mean arterial blood pressure were observed [65]. A follow-up study failed to detect any changes to haemodynamic variables despite a 90-fold increase in plasma U-II immunoreactivity [66]. The implication of these contrasting results is again unclear however, it may be of importance to note that the study carried out by Böhm & Pernow was not a placebo controlled trial [64].

### ***1.6.2 Knockout Studies***

Deletion of the UT gene in murine embryonic stem cells allows the production of developmentally normal mice [67]. There are no alterations to systemic basal haemodynamics on deletion of the UT gene, nor any apparent changes in endothelial modulation by other vascular mediators. As expected, loss of U-II induced vasoconstriction in murine thoracic aorta is observed on deletion of this gene [67]. These data suggest that the UT receptor system does not *independently* modulate any haemodynamic variables in the mouse. The physiological processes modulated by this receptor system are therefore likely to be multivariate. Consequently, *in vivo* siRNA-mediated RNA-interference studies of the UT gene may be more instructive in this instance.

### ***1.6.3 In Vitro Studies***

Radioligand binding experiments performed in isolated rat vascular tissue have failed to detect U-II binding sites in blood vessels distal to the aortic arch [6]. In concordance with these data, vasoconstrictor activity of U-II in rat is confined mainly to the thoracic aorta, carotids and coronary arteries [7]. Data obtained from isolated rat thoracic aorta, demonstrate U-II to produce equiefficacious contractions at 16-fold greater potency when compared with endothelin-1 [68]. Rat left anterior descending coronary artery constricts in the presence of low concentrations of U-II (1-30nM), however dilatation is observed at concentrations between 100 and 1000nM [69]. Rat small mesenteric and basilar arteries do not constrict in response to U-II, however once precontracted, these arteries display U-II-induced endothelium-dependent dilatation [69]. Figure 1.5 demonstrates how the efficacy of U-II vasoconstriction is coupled to UT receptor expression in rat vascular beds. There is a difference in the U-II reactivity of vascular tissues isolated from Cynomolgus (old world) and Marmoset (new world), [68]. Human U-II evokes vasoconstriction in both muscular and elastic arteries isolated from Cynomolgus monkey [7]. These contractions are between 6 and 28-fold more potent than those produced by endothelin-1, depending on the blood vessel [7]. On the whole, U-II is an efficacious and potent vasoconstrictor of arterial vessels isolated from the Cynomolgus monkey [68]. Variable constriction of the pulmonary vein has also been observed in this species of primate [68]. Responses obtained from isolated marmoset vascular tissue are best described as variable, there is much intra-species variation to the responses obtained and the efficacy of those responses is significantly lower when compared to those of the Cynomolgus monkey [68].

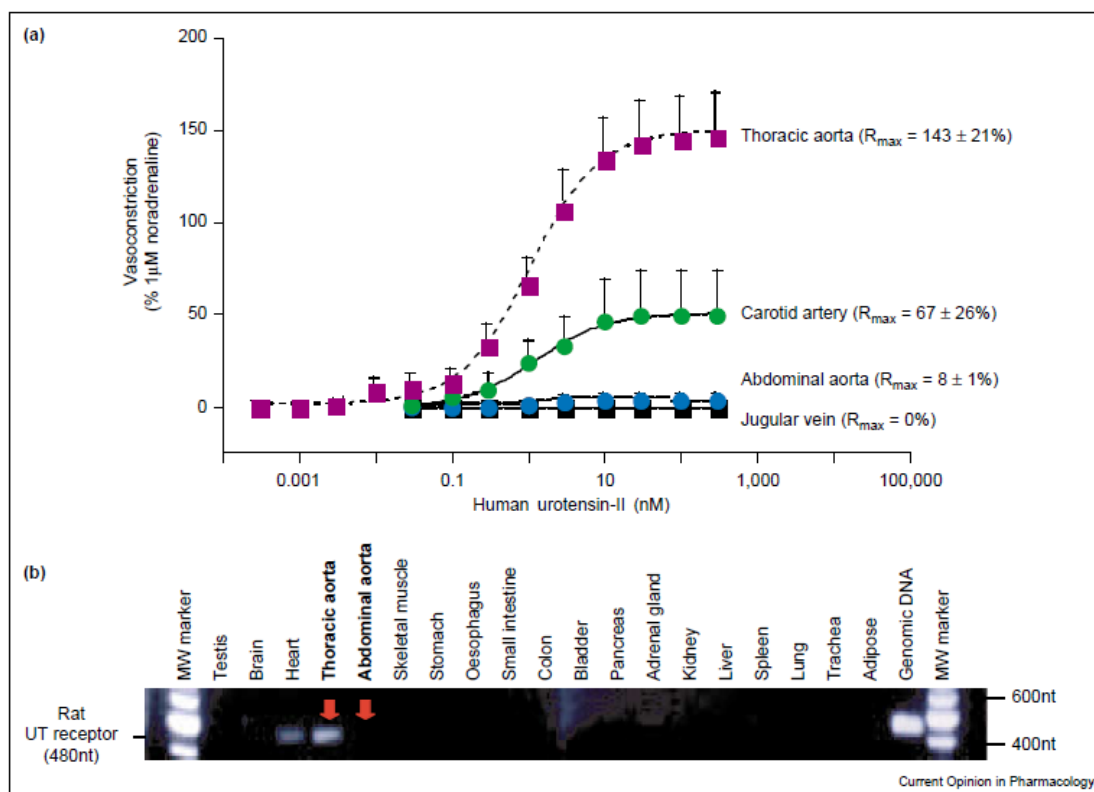


**Figure 1.5. Concentration-response curves to U-II in different vascular beds demonstrating lack of appreciable vasoconstrictor activity in abdominal aorta but not thoracic aorta (a) and, UT mRNA present in thoracic aorta but not abdominal aorta (b). Taken from [70].**

Approximately 30-40% of all isolated human blood vessels tested respond to U-II [70]. However there is considerable variation between these responses, even within a given study (summarised in Table 1.2). If this variation is due to the degree of concomitant endothelial-modulation [70], it may indicate non-pathological plasticity of UT expression in human endothelium and/or vascular smooth muscle. Unlike the majority of other species tested, various human venous tissues also respond to U-II (see Table 1.2). In contrast to *in vivo* data obtained in Cynomolgus monkeys, U-II behaves as a positive inotrope in human isolated atrial and ventricular tissues [71]. The potency of the responses obtained make U-II the most potent inotropic agent identified to date,  $pEC_{50} 9.5 \pm 0.1$ , [71].

**Table 1.2. *Ex vivo* responses to U-II recorded in isolated human tissues; adapted from [70].**

	[46]	[71]	[72]	[73]	[74]	[75]
<b>Coronary artery</b>	67% responders $R_{\max} \leq 15\%$ KCL	0-100% responders $R_{\max} \leq 23\%$ KCL	-	-	-	37% responders
<b>Pulmonary arteriole</b>	-	-	-	30% responders $R_{\max} \leq 220\%$ KCL	-	-
<b>Atrial trabeculae</b>	-	50% responders $R_{\max} \leq 31\%$ KCL	-	-	-	-
<b>Radial artery</b>	100% responders $R_{\max} \leq 20\%$ KCL	-	-	-	-	67% responders $R_{\max} \leq 28\%$ KCL
<b>Umbilical vein</b>	100% responders $R_{\max} \leq 17\%$ KCL	-	89% responders $R_{\max} \leq 4\%$ KCL	-	-	-
<b>Mammary artery</b>	71% responders $R_{\max} \leq 16\%$ KCL	-	-	-	0% responders	-
<b>Facial vein</b>	-	-	40% responders $R_{\max} \leq 13\%$ KCL	-	-	-
<b>Epigastric vein</b>	-	-	29% responders $R_{\max} \leq 11\%$ KCL	-	-	-
<b>Umbilical artery</b>	-	-	50% responders $R_{\max} \leq 6\%$ KCL	-	-	-
<b>Saphenous vein</b>	100% responders $R_{\max} \leq 31\%$ KCL	-	0% responders	-	0% responders	0% responders

## **1.7 Urotensin-II in Pathology**

### ***1.7.1 Disorders Affecting the Cardiovascular System***

#### ***1.7.1.1 Myocardial Hypertrophy***

In cultured cardiac myocytes, U-II induces a dose dependent increase in ERK activation; seen as reporters of the hypertrophic phenotype [76]. This response appears to be dependent upon increased UT receptor density, as is frequently observed in cardiovascular pathology *in vivo* [77, 78]. In a rat model of isoproterenol-induced cardiac fibrosis, cardiac hypertrophy is potentiated by the addition of exogenous U-II [79]. Moreover, endogenous plasma U-II concentration, myocardial U-II content and myocardial UT expression are significantly increased in this model of cardiac fibrosis and hypertrophy [79].

#### ***1.7.1.2 Congestive Heart Failure***

Myocardial expression of UT and U-II is significantly higher in patients with congestive heart failure (CHF), [80]. Moreover, U-II expression is correlated with left ventricular end-diastolic dimension and inversely so with ejection fraction. In these patients, U-II expression is particularly strong in the subendocardial cardiomyocytes [80]. In patients with CHF secondary to ischaemic heart disease (IHD), expression of UT and U-II is elevated in viable cardiomyocytes surrounding ischaemic infarcts. In this same group of patients, U-II expression is evident in inflammatory cells; namely macrophages and myofibroblasts [80]. Plasma U-II concentration is also significantly elevated in heart failure patients [37, 81, 82]. Iontophoresed U-II produces vasoconstriction of the skin microcirculation in CHF patients, however, vasodilatation is observed in healthy controls [83]. Myocardial URP is elevated in a rat model of CHF [84].

### *1.7.1.3 Arrhythmogenesis*

U-II exhibits pro-arrhythmogenic effects in heart tissue (right atrial trabeculae). However the efficacy of U-II in producing spontaneous contractions in heart tissue is significantly lower than that of endothelin-1 [71].

### *1.7.1.4 Essential Hypertension*

Mean arterial blood pressure (MAP) is positively correlated with plasma [85] and cerebrospinal fluid [49] U-II concentrations. Furthermore, plasma U-II concentration is significantly higher in patients with essential hypertension [85]. Iontophoresed U-II produces vasoconstriction of the skin microcirculation in hypertensive patients, compared with vasodilatation observed in normotensive controls [86]. These data may suggest altered UT receptor density in the vascular smooth muscle and/or endothelium of hypertensive patients. A single nucleotide polymorphism (SNP) of the UT receptor gene designated S89N, is prevalent in the Han population of northern China and associated with essential hypertension in males [36].

### *1.7.1.5 Atherosclerosis*

U-II produces a synergistic proliferation of cultured vascular smooth muscle cells when combined with mildly oxidised LDL, a process associated with atheroma formation [87, 88]. U-II is present in atherosclerotic lesions of the carotid and abdominal aorta, with prominent localisation to the hyperplastic intima of the lesion [87]. Prominent UT receptor expression is also noted in atherosclerotic lesions [87], and U-II may be involved in the formation of atherosclerotic foam cells [89].

### ***1.7.1.6 Pulmonary Hypertension***

In models of pulmonary hypertension secondary to left ventricular dysfunction [90, 91] and chronic hypoxia [91], U-II is elevated in the vascular smooth muscle and vascular endothelium of pulmonary arteries isolated from rats and rabbits in the left ventricular dysfunction groups. Furthermore, the pulmonary pressor response to U-II is potentiated in the ventricular dysfunction but not chronic hypoxia group [90, 91].

### ***1.7.2 The Metabolic Syndrome***

The metabolic syndrome (MetS) is a cluster of metabolic disorders, each a cardiovascular risk factor in its own right, including; abdominal obesity, elevated fasting blood glucose concentration, hypertension, raised triglycerides and low HDL cholesterol [92]. MetS is associated with insulin resistance, endothelial dysfunction as well as altered prothrombotic and proinflammatory status [92]. The MetS is considered as an independent risk factor for cardiovascular disease and type II diabetes.

Plasma U-II concentration is correlated with HOMA-IR (a calculated measure of insulin resistance) [93], is elevated in hypertensive patients [49, 86] and correlates positively with body mass [85]. U-II may promote hyperglycaemia [94, 95], increase appetite [96] and stimulate IL-6 release from cardiomyocytes [77]. For these reasons U-II is thought to play a role in the metabolic syndrome, although a statistical link has yet to be proven.

### ***1.7.3 Type 2 Diabetes Mellitus***

Plasma U-II concentration is elevated in patients with type 2 diabetes mellitus [45]. A single nucleotide polymorphism designated S89N, which is associated with essential hypertension in the Han population (see 1.7.1.4), is also associated with type 2 diabetes

mellitus in Japanese subjects [35]. Fasting plasma glucose concentration and HOMA-IR are higher in individuals with the S89N polymorphism [35].

#### ***1.7.4 Renal Disease***

Plasma U-II concentration is significantly elevated in patients with chronic renal failure [57]. Furthermore, plasma U-II concentration correlates with the extent of renal dysfunction in type 2 diabetics as assessed by creatinine clearance and urinary albumin concentration [97]. It is not yet evident whether increased plasma U-II concentration in such patients is due to increased production of U-II as a consequence of this pathology, or more simply secondary to decreased renal function. The UT receptor antagonist, palosuran, improves renal function in macroalbuminuric diabetic patients; thus suggesting an active role of U-II in the development of this condition [98].

#### ***1.7.5 Cirrhosis of the Liver and Portal Hypertension***

Plasma U-II concentration is elevated in patients with cirrhosis of the liver [99]. Plasma U-II concentration also correlates with the degree of portal hypertension, in addition to the severity of the condition as indicated by recurrent bleeding from oesophageal varicies, refractory ascites or hepatorenal syndrome [99]. Iontophoresed U-II produces vasoconstriction of the skin microcirculation in cirrhotic patients, compared with vasodilatation observed in healthy controls [100].

#### ***1.7.6 Angiogenesis and Tumour Growth***

Due to the wide expression of U-II in the body and its proliferative effects in vascular smooth muscle cells [101], U-II is a candidate peptide for the promotion of tumour growth [102]. Furthermore, U-II stimulates angiogenesis [103, 104], a process vital for

tumour growth and maintenance. U-II and UT mRNAs are present in a variety of tumour cell lines and U-II immunoreactivity is present in the culture media of such cells, suggesting active secretion [105]. U-II immunoreactivity is elevated in human adrenal tumours when compared with attached non-neoplastic adrenal tissue [106].

## 1.8 Drug Development at the UT Receptor

In order to fully understand the role(s) of U-II/UT in health and disease, it is necessary to develop a range of potent and specific UT ligands, particularly antagonists.

### 1.8.1 *Peptidic UT Drug Development*

Classical structure-activity relationship studies of the endogenous peptide, U-II, identify Lys<sup>8</sup> as a critical residue for biological activity [107, 108]. Experimental UT ligands which feature a substitution of this critical residue are illustrated in Figure 1.6 and include:

1. **[Orn<sup>8</sup>] U-II** (Lys<sup>8</sup>→ornithine substitution): shortens this critical amino acid side-chain by one carbon (Figure 1.7). Intracellular calcium measurements show **[Orn<sup>8</sup>] U-II** to behave as a full agonist in HEK-293 cells expressing hUT (HEK<sub>hUT</sub>) [109]. In contrast, this same peptide behaves as a competitive antagonist in the rat aorta bioassay, but displays residual agonist activity ( $\alpha \approx 0.25$  relative to that of the endogenous peptide), [109].
2. **[Pen<sup>5</sup>, Orn<sup>8</sup>] U-II (4-11)**: Features the same Lys<sup>8</sup>→ornithine substitution. Furthermore, the peptide is truncated to the shortest biologically active conformation, **U-II (4-11)** [110], and the bioactive conformation is stabilised by substituting Cys<sup>5</sup>→penicillamine ( $\beta$ - $\beta$ -dimethylcysteine). This peptide possesses residual agonist activity of approximately 0.25 in the rat aorta bioassay [110].

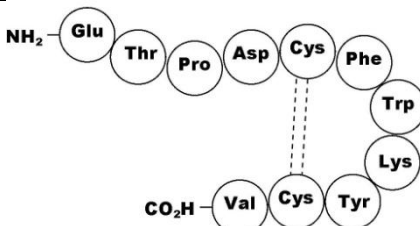
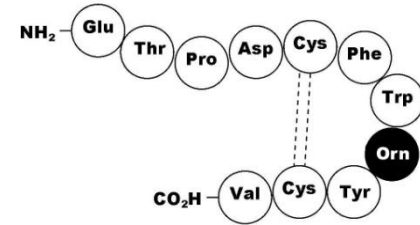
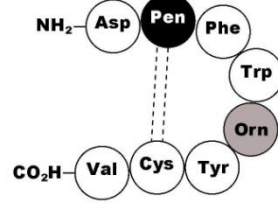
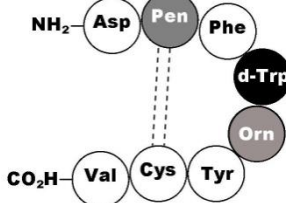
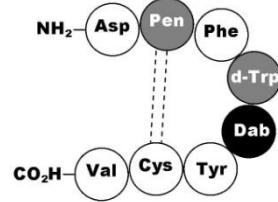
<i>Designation</i>	<i>Details</i>	<i>Diagram</i>	<i>Ref'</i>
Urotensin-II	Full length endogenous peptide.		-
[Orn <sup>8</sup> ] hU-II	Lys <sup>8</sup> → Orn substitution. Behaves as a full agonist in HEK-293 cells expressing the recombinant hUT receptor. Partial agonist in rat aorta, $\alpha \approx 0.25$ .		[109]
[Pen <sup>5</sup> , Orn <sup>8</sup> ] U-II (4-11)	Peptide truncated to the shortest form retaining biological activity. Bioactive conformation stabilised by substituting Cys <sup>5</sup> → Pen.		[110]
Urantide	Substitutions: L-Tryptophan <sup>7</sup> → d-Trp, Lysine <sup>8</sup> → Ornithine. Behaves as an antagonist with partial agonist activity in some assays.		[110]
UFP-803	Substitution: Orn <sup>8</sup> (from previous structure) → diaminobutyric acid. Behaves as an antagonist with partial agonist activity in some assays.		[111]

Figure 1.6. Diagrammatic representations of Urotensin-II and other UT ligands. Modifications made for a specific peptide are shown in black whereas modifications carried forward from other peptides are shown in grey.

3. **[Pen<sup>5</sup>, DTrp<sup>7</sup>, Orn<sup>8</sup>] U-II (4-11), Urantide [112]:** features the same modifications as the previous peptide in addition to an inversion of the Trp<sup>7</sup> residue to the D-isomer. Urantide behaves as a pure antagonist in the rat aorta bioassay [110], but as a low potency partial agonist ( $\alpha \approx 0.8$ ) in Chinese Hamster Ovary cells expressing the recombinant hUT receptor (CHO<sub>hUT</sub>), [112].

4. [Pen<sup>5</sup>, DTrp<sup>7</sup>, Dab<sup>8</sup>] U-II (4-11), UFP-803, [111]: features an Orn<sup>8</sup>→diaminobutyric acid (Dab<sup>8</sup>) substitution, which effectively shortens this critical amino acid side chain by a further carbon residue (Figure 1.7). UFP-803 behaves as a pure and competitive antagonist in the rat aorta bioassay but functional [Ca<sup>2+</sup>]<sub>i</sub> measurements in CHO<sub>hUT</sub> reveal residual agonist activity ( $\alpha \approx 0.21$ ).

The efficacy of peptides 1-4 therefore appears to be tissue and assay dependent.

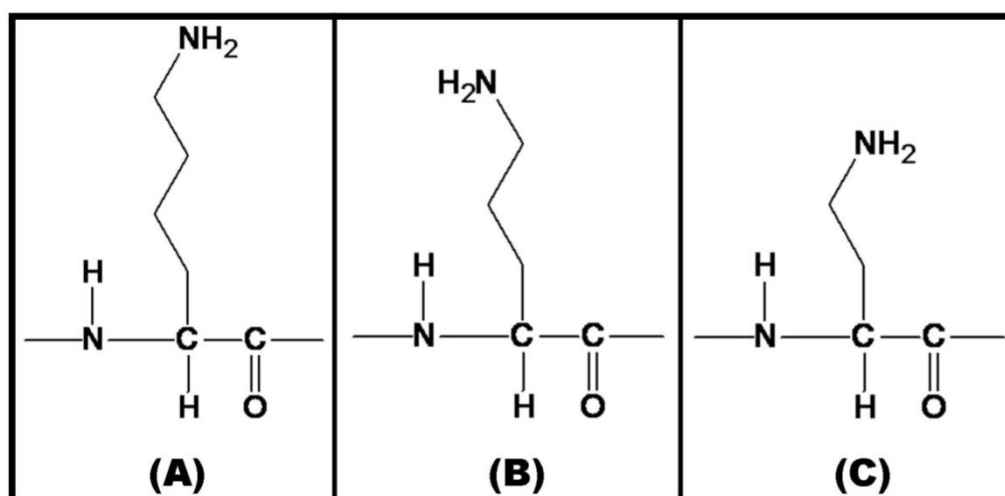


Figure 1.7. Structural formulae of the various modifications made at position 8 of the urotensin-II peptide. (A) Lysine, present in the endogenous peptide (B) Ornithine, present in Urotensin and other precursors (C) Diaminobutyric acid present in UFP-803.

## 1.8.2 Non-peptidic UT Drug Development

### 1.8.2.1 Palosuran

Palosuran (ACT05836) is a non-peptidic UT receptor antagonist (see Figure 1.8 for structure), [113]. This drug exhibits both insurmountable and simple competitive antagonism in the rat aorta bioassay and CHO<sub>hUT</sub> functional assay respectively [113]. This ligand lacks appreciable antagonist potency in numerous functional bioassays across various species ( $pK_b < 6$  calculated from [114]). The drug also behaves as an agonist at somatostatin receptor subtypes sst2 and sst5, demonstrating lack of specificity

of this ligand [115]. Despite the drawbacks detailed above, palosuran is the only UT receptor ligand to have entered clinical trials in humans (see 1.7.4), [98].

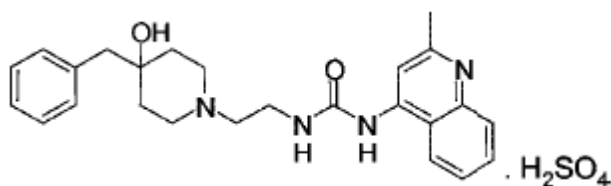


**Figure 1.8. Chemical structure of the non-peptidic antagonist, palosuran (sulphate).**

#### 1.8.2.2 SB-706375

SB-706375 is a non-peptide UT receptor antagonist (see Figure 1.9). SB-706375 potently antagonises UT-mediated  $[Ca^{2+}]_i$  mobilisation in HEK-293 cells stably expressing the recombinant hUT receptor ( $pK_b=8.00$ ), [116].

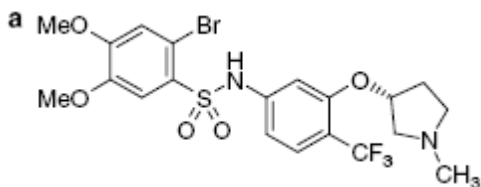


**Figure 1.9. Structural formula of SB-706375.**

#### 1.8.2.3 BIM-23127

BIM-23127, originally characterised as a neuromedin-B receptor antagonist, also behaves as a potent and competitive UT receptor antagonist [117]. The lack of specificity of this ligand makes it an unattractive candidate for further development.

### ***1.8.3 UT Drug Development: A Summary***

The two most attractive pharmacological profiles of all UT ligands characterised to date are those of palosuran and UFP-803. Peptidic candidates further our understanding of how the endogenous peptide interacts with its target(s) natively. They offer advantages such as high selectivity, predictable metabolism and a reduced side effect profile. Furthermore, of these two candidates, UFP-803 is readily available to the scientific community and has greater antagonist potency than palosuran. Although UFP-803 exhibits no residual agonist activity in the rat aorta bioassay, this is not the case *in vitro*.

## 1.9 The Ecdysone-Regulated Gene Switch

Ecdysone is a steroid hormone responsible for the onset of metamorphosis in *Drosophila melanogaster* (common fruitfly) [118]. The endogenous ecdysone receptor (EcR) is related to the mammalian retinoid-X nuclear hormone receptor (RXR). Functional activity of EcR is dependent upon the formation of a heterodimer between itself and the product of the ultraspiracle gene (USP), [119]. The EcR/USP heterodimer interacts with target genes through highly conserved and specific DNA sequences, termed ecdysone response elements (ERE), [120]. Binding of ecdysone to the EcR/USP heterodimer allows recruitment of co-activators, thus affording target gene transcription downstream of the ERE [119]. Conversely, in the absence of ecdysone, the EcR/USP heterodimer recruits co-repressors that actively silence target gene expression (see Figure 1.10), [121]. Interestingly, the presence of ecdysone selectively favours the dimerisation of EcR and USP [119].

In transferring ecdysone inducibility to mammalian cells, No and colleagues have produced a hybrid ecdysone receptor with enhanced transcriptional activity, but which maintains specificity for binding ecdysone and EREs [118]. Additionally, a hormone response element has been constructed with greater binding specificity for the hybrid EcR but reduced reactivity with related mammalian nuclear hormone receptors [118]. The mammalian homologue of USP, the retinoid-X-receptor, functions most effectively with the hybrid EcR in mammalian cells [118].

Studies performed immediately following the development of the above system, led to an unexpected depletion in the stocks of murasterone-A (an ecdysone analogue) [122]. Subsequently a natural plant steroid, ponasterone-A (pon-A), was identified as a potent

ligand for EcR. Due to the availability of pon-A and its benign nature in mammalian systems, this is currently the ligand of choice as an ecdysone-system inducer [122].

The ecdysone mammalian inducible expression system is now widely available in kit form from a number of biotechnology companies. Typically two plasmids are supplied to be co-transfected into the cell-line of choice: one to constitutively express the modified EcR and RXR and another containing a multi-cloning site (MCS), for insertion of the cDNA of interest, downstream of the modified ERE (Stratagene, Invitrogen).

This system has several advantages over traditional tetracycline-based inducible expression systems, specifically: basal expression of the gene of interest is lower and the system possesses a greater range of inducibility with faster induction kinetics [118]. Furthermore, when applied to studies in transgenic mice, ecdysteroids are distributed very quickly throughout the whole organism and are able to penetrate the blood-brain barrier [123]. Ecdysteroids are neither toxic nor teratogenic and are thought not to significantly affect mammalian physiology [124]. However, recent studies have demonstrated both cytokine elevation and anti-apoptotic effects in mammalian cell culture following ecdysteroid incubation [124, 125].

Despite these potential drawbacks, the ecdysone-inducible expression system has been successfully employed by a variety of groups as a precise method for controlling the density of plasma membrane receptors. Specific examples of receptor systems placed under the control of this system are: 5-HT [126],  $\delta$ -opioid [127], somatostatin SST2 [128] and NOP [129].

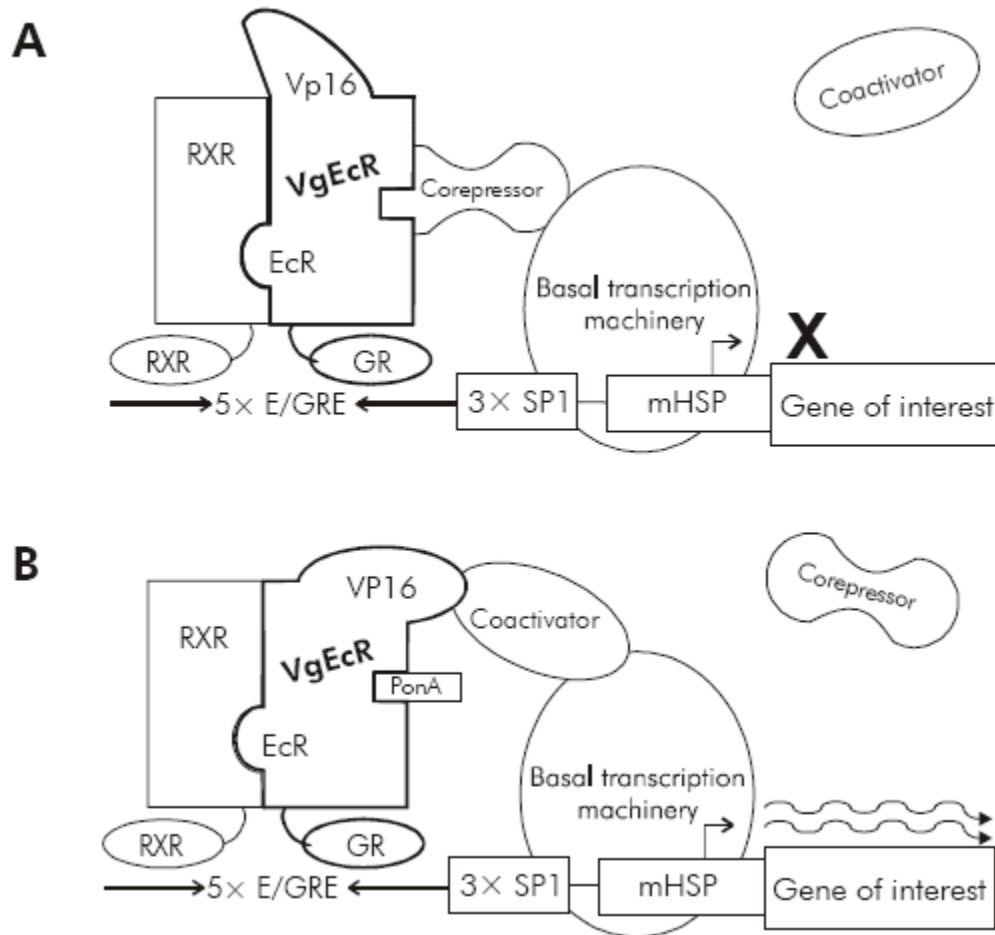


**Figure 1.10. Regulation of transcription in the ecdysone mammalian expression system. In the absence of inducer (A), corepressors bind the modified RXR/EcR heterodimer (VgEcR) and gene transcription is repressed downstream of the modified ERE (E/GRE). In the presence of inducer (B), coactivators bind to the heterodimer and gene transcription is induced downstream of the ERE, under the control of a minimal heat shock promoter (Stratagene).**

### **1.10 RNA Interference**

RNA interference (RNAi) is the process of specific and potent gene silencing, mediated by double-stranded RNA (dsRNA) that is homologous in sequence to the silenced gene [130]. The introduction of viral dsRNA into a mammalian cell triggers an antiviral response, which includes interferon release and degradation of the dsRNA by a specific enzyme named Dicer. Although this process may occur concurrently with RNAi, they are in fact two separate processes [131]. By limiting the length of the exogenous dsRNA to 21bp, it is possible to induce RNAi independently from the interferon response in mammalian cells [132].

Although RNAi can be induced by exogenous dsRNA, it is in fact an innate cellular process [131]. Indeed, a proportion of the “non-coding” DNA identified by the human genome project actually codes for a variety of short-length RNA species [133]. None of these species are translated into proteins, but they do add an additional layer of control to the expression of cellular proteins [133]. Synthetic analogues of these small RNAs are known as short interfering RNAs (siRNAs), which are duplexes of dsRNA with 19 paired nucleotides and 2 overhanging nucleotides at each 3' end [132]. These may be transfected directly into the cell or may be cleaved from larger RNA molecules such as small hairpin RNAs (shRNAs), [134].

siRNAs are able to associate with a protein complex named RISC (RNA-induced silencing complex) [135]. The siRNA is unwound and the sense strand is released for eventual degradation by cellular nucleases [135]. The remaining antisense strand is able to ‘guide’ RISC to the specific mRNA for degradation by RISC endonuclease activity, thus preventing translation of that mRNA to protein (see Figure 1.11), [135].

Two main methods are currently employed to exploit RNAi as a tool for uncovering gene (dys)function:

- 1. Transient transfection of synthetic siRNAs** – this is a potent method employed to study the short term effects of gene product knockdown [136, 137]. Typically mRNA knockdown can be observed just 24 hours after transfection and protein knockdown at between 48 and 72 hours (Applied Biosystems).
- 2. shRNA transcribing plasmids** – this is a method for the longer term study of gene product knockdown [134]. A plasmid coding for a shRNA is transfected into the cell-line of interest and the shRNA will be transcribed by the host cellular machinery [134].

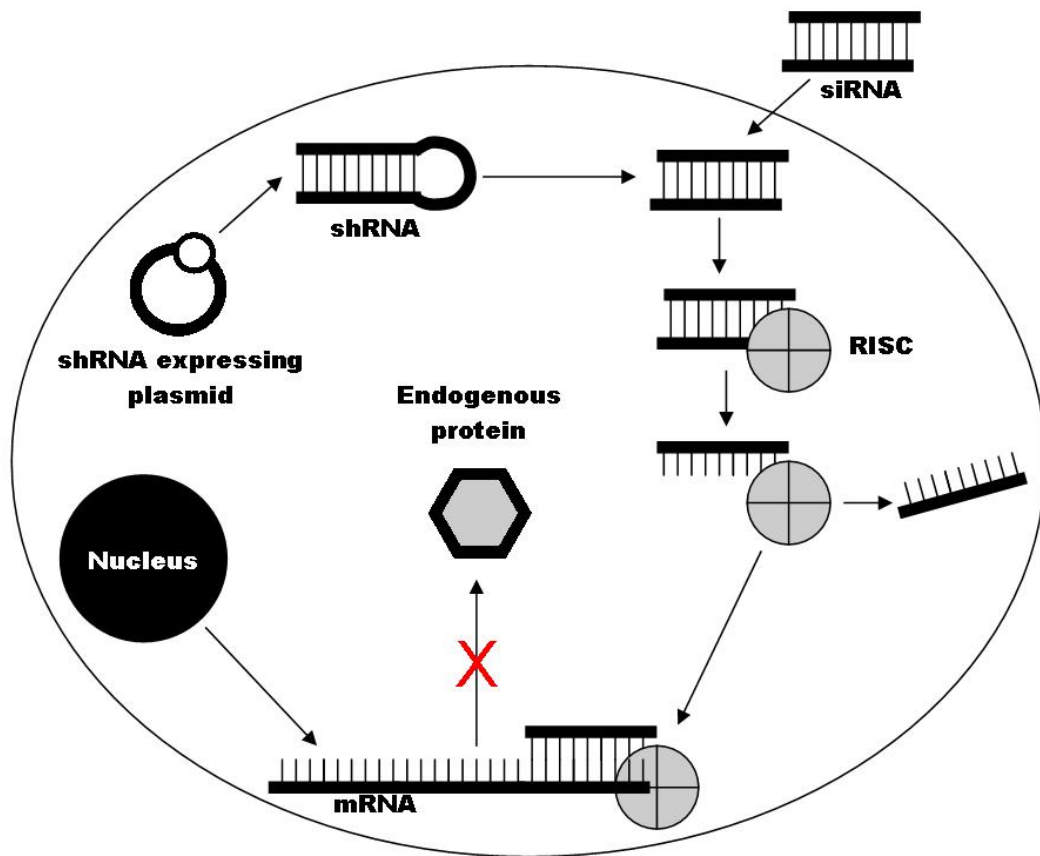


Figure 1.11. RNAi: mechanism of action. Synthetic siRNAs are introduced into the cell or produced from a shRNA expressing plasmid. The siRNA binds RISC and the sense strand is unwound. The remaining anti-sense/RISC complex binds to the endogenous complementary mRNA and degrades it, thus blocking production of endogenous protein.

## 1.11 Overall Aims

There is much controversy surrounding the classification of newly developed UT ligands, particularly with respect to their intrinsic activities. The assay used to characterise a given ligand appears to bias the final classification with the largest disparity apparent between *in vitro* and *in vivo* assays. Considering the sizable difference in UT receptor density between *in vivo* and *in vitro* assays, it is likely that inter-assay differences in UT receptor density are influencing apparent ligand efficacy. Moreover, the point at which the stimulus-response pathway is probed (receptor activation / IP<sub>3</sub> turnover / Ca<sup>2+</sup> mobilisation) also seems to influence the classification of such ligands (Figure 1.12).

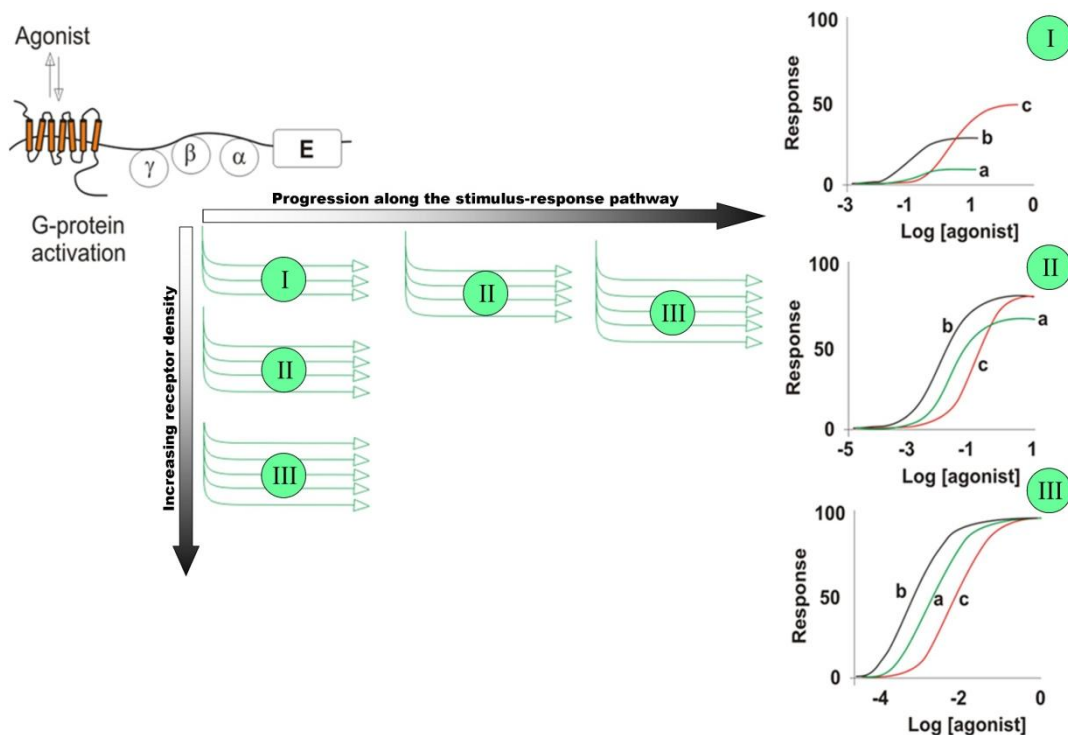


Figure 1.12. Amplification of response observed as receptor density increases or as the stimulus progresses along the stimulus-response pathway. The rank order of efficacy is  $c > b > a$ , however the rank order of potency is  $b > a > c$ . In this example, the rank order of potency is maintained as receptor density increases or the stimulus propagates along the pathway. However, the rank order of efficacy is not apparent at high receptor density or at the end organ response. Adapted from [138].

The aims of this project are centred about the generation and characterisation of the following two models. Both of which should allow UT receptor density to be experimentally controlled:

1. Ecdysone-inducible cell-lines (see 1.9), allowing experimental induction of UT gene transcription in otherwise UT negative cell-lines.
2. Use of UT-specific siRNAs (see 1.10), allowing experimental reduction of UT mRNA translation in stable UT transfects.

The generation of these models will allow the following questions to be addressed:

1. How does UT receptor density influence ligand efficacy and subsequently the classification of UT ligands? (see 1.8)
2. Are there any implications of altered UT receptor density on second messenger coupling (receptor promiscuity)?

Concordance between the data generated by two independent models will strengthen the findings. Moreover, by adapting these models for use in various cell-lines, it will be possible to observe any effects of an altered cellular background.

# Chapter Two

## 2. General methods

### 2.1 Data Handling

#### 2.1.1 *Definitions*

**n** – Data were considered to constitute an individual replication of an experiment (n) if:

- The cells for experimentation came from an individual passage of a stock flask of cells.
- The experiment was conducted with no identical experiments run in parallel.

**$\alpha$**  – was used during this study to give a measure of the relative efficacy of an experimental ligand (expressed as a decimal fraction).  $\alpha$  values were calculated as:

$$\alpha = \frac{(E_{maxA})}{(E_{maxB})}$$

*Where,  $E_{maxA}$  and  $E_{maxB}$  are the baseline-subtracted  $E_{max}$  values for the experimental ligand and full agonist respectively.*

#### 2.1.2 *Curve fitting and graphing*

Curve fitting and graphing of data was achieved by use of Graphpad Prism, version 5. Concentration-response curves were fit according to the non-linear regression ‘sigmoidal dose-response (variable slope)’ algorithm:

$$y = \frac{(top - bottom)}{1 + 10^{((\log EC50 - x) * Hill\ slope)}}$$

## 2.2 Tissue culture

Cells were maintained in sterile T75 culture flasks and were all of the CHO-k1 lineage. This cell-line exhibits fibroblast morphology, was obtained from the adult Chinese Hamster Ovary and is considered to be karyotypically stable [139].

### 2.2.1 *Cell-lines*

**CHO<sub>h</sub>UT:** CHO cells stably transfected with vector 70981-hUT, kindly gifted by Dr G. Calo, University of Ferrara.

**ER-CHO:** CHO cells stably transfected with vector pERV3 (1.9), purchased from Stratagene.

**ER-CHO<sub>h</sub>UT:** Previous cell-line co-transfected with vector ER-CHO<sub>h</sub>UT, produced in-house.

### 2.2.2 *Subculture and propagation*

Once a cell-line is established in culture, its growth follows a standard pattern after which it will require subculturing (Figure 2.1). A lag phase immediately follows seeding of the culture, after which an exponential “log” phase of growth is observed. Once the cell density exceeds the capacity of the medium then growth will cease or be significantly reduced, at which point subculturing will become necessary [140].

Cell medium was removed from the confluent monolayer and rinsed with 2mL of 0.05% trypsin / EDTA (Invitrogen). The monolayer was then incubated in a further 2mL of trypsin at 37°C / 5% CO<sub>2</sub> for approximately 2 min. The monolayer was detached from the culture flask by gently agitating it and 8mL of fresh culture medium

was added to the cell suspension. A 1:10 dilution (typical) was achieved by transferring 1mL of the cell suspension to 19mL of fresh selection medium in a new sterile flask. The new subculture was incubated at 37°C / 5% CO<sub>2</sub> until the next feed (2.2.3) or subculture was required.

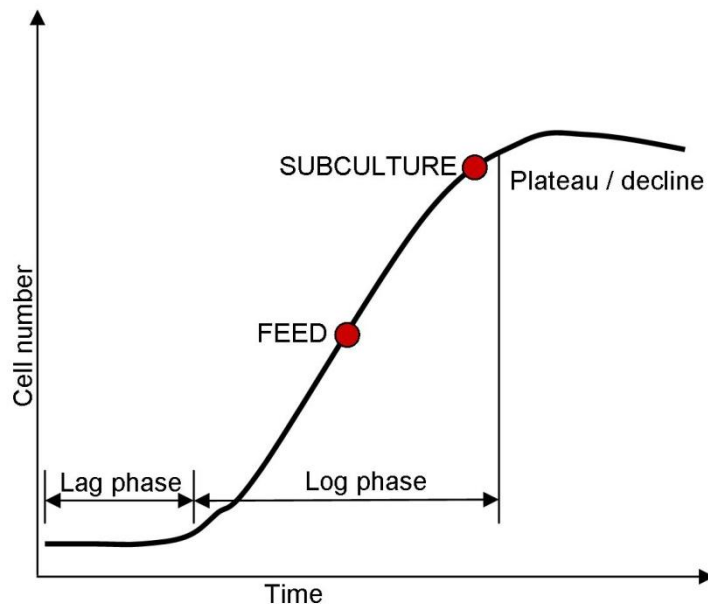


**Figure 2.1. Growth curve and maintenance.** A representative plot of the number of cells in a culture over the age of the culture from last subculture.

### 2.2.3 Feeding monolayer cultures

The replacement of cell media is indicated by 4 factors [140]:

1. **A drop in pH** is observed as the subculture propagates and is crudely monitored by the addition of phenol red in the culture medium. Typically, cell growth will deteriorate as the pH falls below 7.0 and viability will be lost below 6.0.
2. **Cell concentration.** A Culture at a high cell concentration will exhaust the nutrients within the medium more quickly.

3. **Cell type.** ‘Normal’ cells will contact inhibit at high cell concentrations and deteriorate little under these circumstances. Transformed cells and continuous cell-lines deteriorate very quickly at high density.
4. **Morphological deterioration** is often indicative of a poor cell culture and may precede apoptosis.

Cells were fed by removing the spent medium and replacing it with 20mL of fresh selection medium. The culture was then maintained at 37°C / 5% CO<sub>2</sub> until the next subculture.

#### ***2.2.4 Cryopreservation and resuscitation***

Stocks of cell-lines were stored by a process of cryopreservation. Cultures to be cryopreserved were subcultured in T25 flasks and grown to 90% confluence. The culture was then trypsinised and detached from the flask (as previously described). The cell suspension was made to a final volume of 10mL and sedimented in a sterilin tube at 1500xg for 3 min. The supernatant was removed and the pellet was resuspended in 5.5mL of growth medium supplemented with 10% dimethyl sulphoxide (DMSO). Typically 5 x 1mL aliquots were produced in specialised cryotubes (Falcon). Following equilibration on ice, the temperature of the aliquots was reduced in a stepwise manner over a period of 1 hour and ultimately stored in liquid nitrogen (196°C).

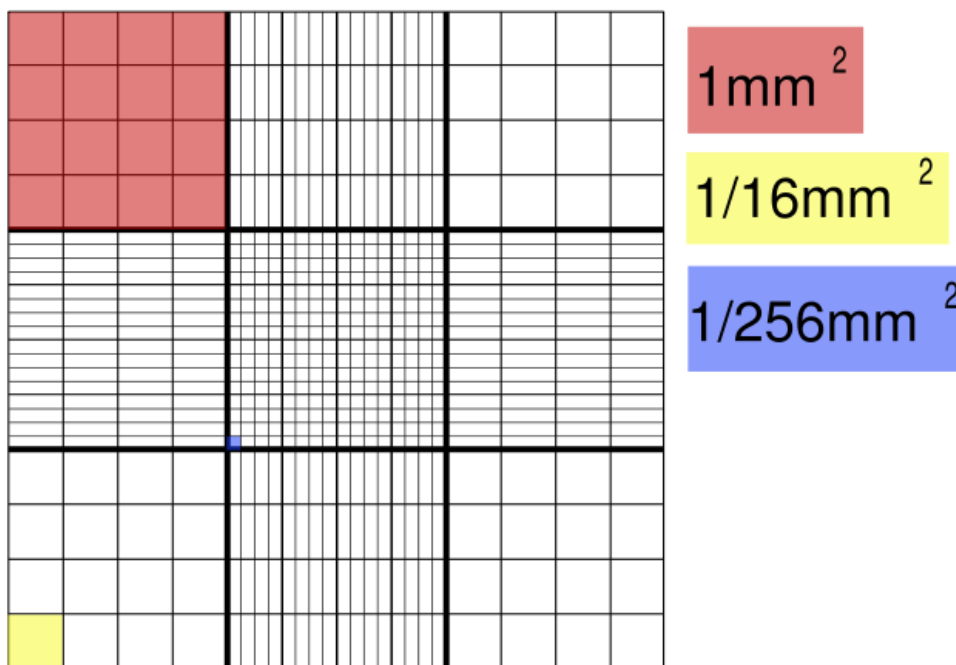
Cells were resuscitated by rapidly thawing the ampoule in warm water, to prevent degradation of the cells due to ice crystal formation [140]. Once thawed, the cell suspension was transferred to a T25 flask containing 10mL of fresh selection medium. The culture was closely monitored until after the first subculture.

### 2.2.5 Cell quantification

The cell concentration of a culture was determined by use of a haemocytometer as per [140]. Briefly, the monolayer was trypsinised as previously described and any aggregates in the subsequent suspension were dispersed by thorough mixing. A small quantity of the suspension was pipetted onto the edge of the haemocytometer cover slip and the chamber was filled by capillarity. The chamber was viewed at 10x objective and the number of cells within the central  $1\text{mm}^2$  area was determined (Figure 2.2). In the case of high cell density, a mean of this area was determined by use of 5 subdivisions. In the case of low cell density, the second chamber was filled and a mean of the two determined. Cell concentration was determined by the following formula:

$$c = \frac{n}{v}$$

Where  $c$  is the cell concentration (cells  $\text{mL}^{-1}$ ),  $n$  is the number of cells counted, and  $v$  is the volume within which the cells were counted (mL).



#### Legend

- $1\text{mm}^2 \sim 0.1\text{mm}^3$
- $1/16\text{mm}^2 \sim 0.00625\text{mm}^3$
- $1/256\text{mm}^2 \sim 0.000390625\text{mm}^3$

Figure 2.2. A haemocytometer chamber showing the areas and volumes of the three main divisions.

### **2.3 Principles of reverse transcription PCR**

Polymerase chain reaction (PCR) is a highly sensitive technique, which allows DNA to be amplified exponentially and the starting quantity to be measured. In this thesis, a variation of the PCR method known as reverse transcription PCR was exclusively utilised. Where traditional PCR may be used to identify the presence or absence of a gene in an organism's genome, reverse transcription PCR allows relative gene expression to be measured.

Following extraction of total RNA from the sample (2.5), the first step is to degrade any contaminating genomic DNA (gDNA) from the sample (2.6). This is necessary to ensure that the subsequent PCR reaction does not amplify gDNA. The 'cleaned' RNA samples are then reverse transcribed, which creates copy DNA (cDNA) from messenger RNA (mRNA). During this stage both RT<sup>+</sup> and RT<sup>-</sup> reactions are incubated, RT<sup>+</sup> contains the reverse transcriptase enzyme and allows gene expression to be quantified during PCR. The RT<sup>-</sup> reaction does not include reverse transcriptase and is included as a negative control sample during PCR. A positive signal gained from a RT<sup>-</sup> sample during PCR may indicate that the DNase treatment was not successful at removing all gDNA.

PCR is facilitated by repeated thermal cycles, each typically consisting of 3 stages (Figure 2.3). The first stage of each cycle is termed 'denaturation' and functions to separate double-stranded DNA. Once separated, specific oligonucleotide primers (designed for both strands of the sequence) are able to bind in the second stage termed 'hybridisation'. During the final stage termed 'extension', complimentary strands are produced in a 5' to 3' direction by the action of a thermo-stable DNA polymerase

enzyme. Owing to the fact that *both* sense and anti-sense strands are copied during each cycle, the amplicon quantity is theoretically doubled per cycle.

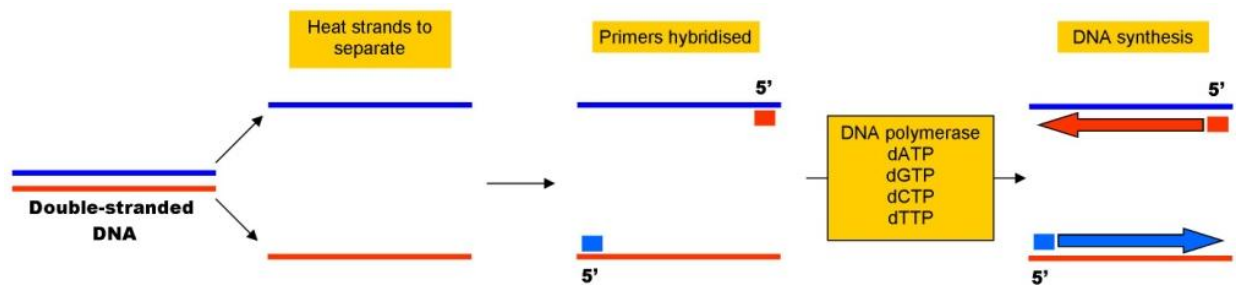


**Figure 2.3. Diagrammatic representation of one cycle of the polymerase chain reaction. Double-stranded template DNA is denatured at high temperature allowing specific oligonucleotide primers to anneal. Complimentary strand DNA synthesis occurs in the presence of a thermo-stable DNA polymerase enzyme.**

## **2.4 Real-time quantitative PCR**

Real-time quantitative PCR is an extension of the above technique, allowing the relative quantity of DNA to be measured at the end of each thermal cycle by a fluorometric probe. During such an experiment, an amplification curve is generated (Figure 2.4). A computer algorithm is able to determine the fractional cycle number at which a threshold quantity of fluorescence is reached (representing a set quantity of DNA and termed cycle threshold ( $C_t$ )). The threshold is set at a point where “amplicon DNA just becomes detectable, but is still within the exponential phase of amplification”, [141]. The  $C_t$  value is inversely proportional to the starting quantity of template cDNA, thus a low  $C_t$  value is indicative of a high starting quantity. Relative quantification of a gene of interest (GOI) is achieved by normalising the  $C_t$  value to that of an endogenous control (EC) gene. Endogenous control genes must be carefully selected in each experimental setting to ensure that its expression does not change as a consequence of the experimental conditions. Typically, so-called ‘housekeeping’ genes are selected as their expression is considered to be largely stable and therefore should not affect measurement of the GOI.

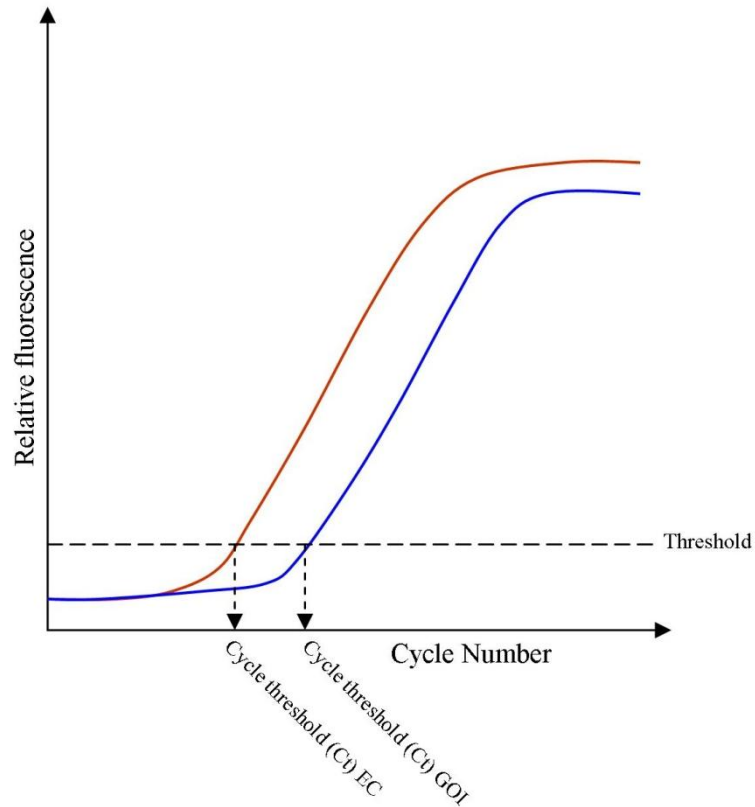


**Figure 2.4.** A representation of a real-time quantitative PCR amplification curve. Cycle threshold (Ct) values are shown for the endogenous control (EC) and gene of interest (GOI), as the cycle number at which the relative fluorescence reaches the threshold.

Normalisation of a GOI to an EC is easily achieved by the following formula:

$$\Delta C_t = C_t^{GOI} - C_t^{EC}$$

Normalisation of  $\Delta C_t$  values between experimental conditions is easily achieved by the following formula:

$$\Delta\Delta C_t = \Delta C_t^{treatment} - \Delta C_t^{control}$$

*Where 'treatment' and 'control' represent two experimental conditions.*

Fold-change of GOI expression may be calculated between two experimental conditions by the following formula:

$$fold\ change = 2^{-\Delta\Delta C_t}$$

*Assuming 100% efficiency of the PCR reaction.*

Two main fluorometric methodologies exist for real-time quantitative PCR as detailed below.

#### **2.4.1 SYBR green I PCR**

SYBR green I is a DNA-specific dye, which binds to the minor groove of double-stranded DNA [142]. On binding double-stranded DNA, the fluorescence of SYBR green I (ex:290nm/em:520nm) is greatly enhanced [142]. For this reason, a real-time PCR amplification curve may be generated by measuring the SYBR green I fluorescence of a PCR reaction at the end of each extension stage. The specificity of the amplified product may be confirmed by analysis of a post-PCR dissociation curve [143]. Such a curve may be generated by repeatedly recording the SYBR green I fluorescence of a post-PCR reaction mixture as its temperature is slowly increased (typically 70-99°C). As double-stranded DNA is denatured, the fluorescence of the SYBR green I dye falls substantially. A single product's melting temperature ( $T_m$ ) is dependent upon its length, complementarity and GC content [144], as such, a dissociation curve featuring a single sharp fall in fluorescence indicates that the PCR reaction was specific at producing only one amplicon. A dissociation curve with stepped falls or a gradual decline in fluorescence may indicate that a number of products have been formed, possibly including primer-dimers [145]. These dissociation data are more frequently presented as 'melting peaks', whereby a software algorithm subtracts background fluorescence and compensates for the effect of temperature on fluorescence. These transformed data are then plotted as "the negative derivative of fluorescence with respect to temperature", ( $\Delta F/\Delta T$  vs.  $T$ ), [144].

### 2.4.2 *TaqMan*<sup>TM</sup> PCR

*TaqMan*<sup>TM</sup> PCR is an example of a 5' nuclease assay and was first described by Heid et al. [146]. The technique relies on the addition of a DNA hybridisation probe to the reaction mixture, which is specific to the target sequence to be amplified. The *TaqMan*<sup>TM</sup> probe features both a fluorophore (FAM or VIC in this study) and a quencher (TAMRA), which are bound in close proximity so as to quench fluorescence of the fluorophore. During complementary strand extension, the probe is hydrolysed; afforded by the 5' nuclease activity of *Taq* polymerase. Thereby fluorophore and quencher are separated and fluorescence of the fluorophore is obtained (Figure 2.5).

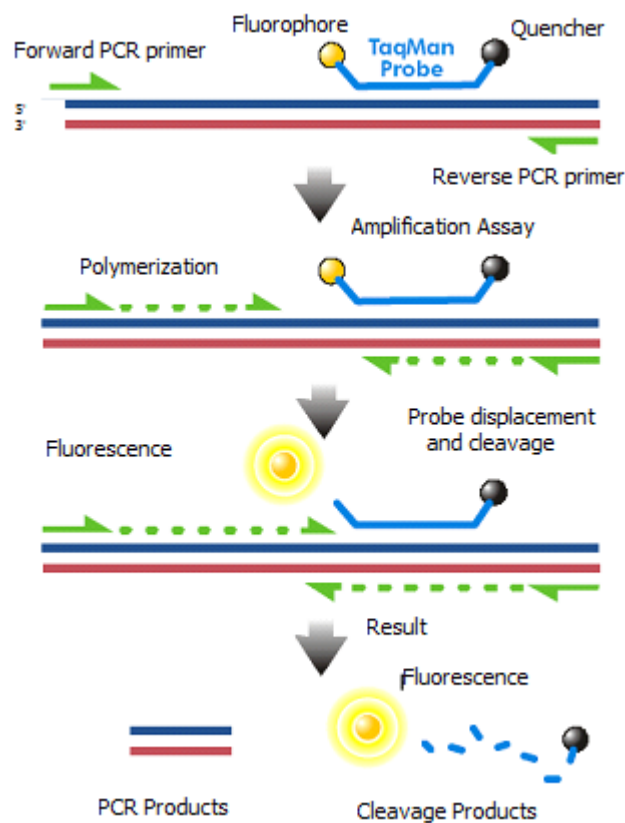


Figure 2.5. A diagrammatic representation demonstrating fluorescence signal generation with the *TaqMan* PCR system. Both primers and probe anneal to the template DNA, fluorescence is low due to the proximity of the quencher to the probe. Extension of the complementary strands occurs in a 5'→3' direction afforded by *Taq* polymerase. The probe is irreversibly cleaved from the quencher by the 5' nuclease activity of the polymerase and a fluorescent signal is generated.

Owing to the specific design of each TaqMan™ probe, fluorescence is only generated by the extension of the target sequence. Therefore, although non-specific sequences may be generated in the reaction mixture (e.g. primer dimmers); these do not contribute to production of the amplification curve. Furthermore, due to the specific nature of each probe, two probes with different fluorophores (and wavelengths) may be included in each reaction. This so-called ‘duplex’ reaction allows both EC and GOI to be measured in the same sample.

## **2.5 RNA extraction methods**

Three methods were used to isolate total RNA from cell cultures. The specific method used in each case was based on the type and quantity of starting material and is detailed below. Two of the methods used, phenol:chloroform organic extraction (2.5.1) and mirVana™ miRNA isolation kit (2.5.2), isolated total RNA which later had to be quantified, DNase treated, and reverse transcribed prior to RT-qPCR. The third method, Cells-to-CT™ gene expression kit (2.5.3), included all of the above stages in a condensed workflow.

### ***2.5.1 Phenol:chloroform organic extraction***

The phenol:chloroform extraction method was used to extract total RNA from flasks of cells, especially where the yield of RNA was expected to be high. The method is similar to that originally described by Chomczynski et al. [147]. Cells were trypsinised, transferred to a sterilin tube in a total suspension volume of 10mL and sedimented at 1500xg for 3min. The supernatant was removed and the pellet was dispersed in 1mL of TRI reagent (Sigma) by thorough pipetting until a homogenous liquid was obtained. The cell lysates were transferred to a PCR-grade eppendorf tube, 200µL of chloroform

was added, and the tube was vortexed until an emulsion was formed. The components of the emulsion were separated under centrifugal force in a desktop centrifuge (10,000xg / 15min / 4°C). The upper aqueous phase was transferred to a fresh PCR-grade eppendorf tube and the RNA was precipitated out of solution by addition of 500µL propan-2-ol and incubation on ice for 10min. The RNA was sedimented at 10,000xg for 10 min at 4°C. The liquid was carefully aspirated and the pellet was allowed to air dry in a class II cabinet for up to 10 min. The pellet was resuspended in 50-100µL of PCR-grade water (depending on the size) and stored at -80°C until DNase treatment (2.6).

### **2.5.2 *mirVana™ miRNA isolation kit***

mirVana™ miRNA isolation kit (Applied Biosystems) was used to isolate total RNA from cell cultures, especially where the yield was expected to be moderate or a high-throughput approach was adopted. “The kit employs an organic extraction followed by immobilisation of RNA on glass-fibre filters to purify either total RNA, or RNA enriched for small species, from cells or tissue samples” (Applied Biosystems).

RNA was extracted as per the manufacturer’s instructions. Media were removed from monolayers of cells in well-plates and rinsed with 1mL of ice-cold phosphate-buffered saline (PBS). 600µL of lysis solution was added and a homogenate lysate was formed by thorough pipetting. 60µL of homogenate additive was added to the lysates which were then incubated on ice for 10 min. The lysates were transferred to PCR-grade eppendorf tubes, 600µL of acid-phenol:chloroform was added, and the components of the emulsion were separated under centrifugal force (10,000xg / 5 min / RT). The upper aqueous phases were transferred to fresh PCR-grade eppendorf tubes and the RNA was

precipitated with 1.25x volume of neat ethanol. Precipitates were transferred to the supplied silica membranes (suspended in eppendorf tubes) and subjected to centrifugal force in a desktop centrifuge (10,000xg / 20 sec / RT). The flow-through was discarded and RNA bound to the silica membranes was subjected to 3 wash steps. RNA was eluted from the membranes in 100µL of PCR-grade water which had been heated to approximately 90°C. RNA samples were stored at -80°C until DNase treatment (2.6).

### 2.5.3 *Cells-to-CT™ gene expression kit*

Cells-to-CT™ gene expression kit (Applied Biosystems) was used to extract total RNA from small quantities of cells, cultured in 96-well plates. The kit employs a simple and condensed workflow to quickly prepare cDNA from whole cells (typically 1.5 hours).

Cell monolayers were rinsed with 200µL of ice-cold PBS before being lysed with 50µL of ‘lysis solution’ containing DNase I enzyme. Cells were incubated for 5 min at room temperature, during which the plasma membranes were lysed and genomic DNA (gDNA) was enzymatically degraded. 5µL of ‘stop solution’ was added to the lysates to inactivate DNase I, which would otherwise affect the subsequent reactions. Reverse transcription reaction mixtures were prepared (Table 2.1). RT<sup>+</sup> included the reverse transcription enzyme, whereas RT<sup>-</sup> was devoid of the enzyme and functioned as a negative control reaction to evaluate the effectiveness of the DNase treatment.

**Table 2.1. Reaction volumes for Cells-to-CT™ gene expression's reverse transcription stage.**

<b>Component</b>	<b>Volume per reaction (RT<sup>+</sup>)</b>	<b>Volume per reaction (RT<sup>-</sup>)</b>
2x RT buffer	25µL	25µL
25x RT enzyme mix	2.5µL	-
PCR-grade water	12.5µL	15µL

40µL of either the RT<sup>+</sup> or RT<sup>-</sup> reaction mixture was incubated with 10µL of the DNase-treated cell lysates in PCR-grade tubes according to the following thermocycler program (Table 2.2). cDNA was stored at -20°C until RT-qPCR was performed (2.8).

**Table 2.2. Thermocycler program for Cells-to-CT<sup>TM</sup> gene expression's reverse transcription stage.**

	<b>Stage</b>	<b>Temperature</b>	<b>Time</b>
<u>Reverse Transcription</u>	1	37°C	60 min
Enzyme inactivation	2	95°C	5 min
Hold	3	4°C	Indefinite

## **2.6 DNase treatment**

TURBO<sup>TM</sup> DNase (Applied Biosystems) was used to enzymatically degrade gDNA present in total RNA extracted from 2.5.1 and 2.5.2. The concentration of total RNA in solution was determined by UV spectrophotometry (absorption 260nm). The concentration of RNA was adjusted so that up a maximum of 10µg was included in each reaction. The reaction mixture was assembled in PCR-grade tubes (Table 2.3) and incubated for 30 min at 37°C.

**Table 2.3. Reaction volumes for TURBO<sup>TM</sup> DNase treatment of total RNA samples.**

<b>Component</b>	<b>Volume per reaction</b>
10x buffer	5µL
DNase I	1µL
≤10µg RNA in PCR-grade water	44µL

5µL of 'inactivation reagent' was added to the reaction mixture, mixed and incubated at room temperature for 3 min. The inactivation substance was then sedimented under centrifugal force (10,000xg / 2 min / RT). The RNA solution was removed from the tube and stored at -20°C.

## 2.7 Reverse transcription

DNase-treated RNA (2.6) was reverse transcribed using the high-capacity cDNA reverse transcription kit (Applied Biosystems). The reverse transcription master mix was prepared according to the manufacturer's instructions (Table 2.4).

**Table 2.4. Components of the high-capacity cDNA reverse transcription kit's master mix.**

<b><u>Component</u></b>	<b><u>Volume per reaction (µL)</u></b>
10x RT buffer	2.0
25x dNTP mix	0.8
10x RT random primers	2.0
Multiscribe™ reverse transcriptase	1.0
RNase inhibitor	1.0
PCR-grade water	3.2

10µL of the RT master mix was mixed with 10µL of DNase-treated RNA in a PCR-grade tube. The reaction mixture was incubated according to the following thermal cycler program (Table 2.5).

**Table 2.5. Thermal cycler program for the high-capacity cDNA reverse transcription kit.**

	<b><u>Stage</u></b>	<b><u>Temperature</u></b>	<b><u>Time</u></b>
Pre-incubation	1	25°C	10 min
Reverse transcription	2	37°C	120 min
Enzyme inactivation	3	85°C	5 sec
Hold	4	4°C	Indefinite

Samples were subsequently stored at -20°C until PCR was performed (2.8).

## 2.8 Polymerase Chain Reaction

### 2.8.1 *SYBR green I PCR*

SYBR green I PCR was conducted according to the following method (Table 2.6):

**Table 2.6. Reaction mixture for SYBR green I PCR.**

<u>Component</u>	<u>Volume (µL)</u>
SYBR green jumpstart Taq readymix (Sigma)	12.5
Quantitect forward and reverse primers (GOI or EC), (Qiagen)	2.5
ROX™ passive reference dye (Sigma)	0.5
PCR-grade water	7.5
Template cDNA	2

Samples were incubated according to the following thermal cycler program (Step-one, Applied biosystems), (Table 2.7):

**Table 2.7. Thermal cycler program for SYBR green I PCR.**

<u>Step</u>	<u>Stage</u>	<u>Description</u>	<u>Temperature (°C)</u>	<u>Time</u>
1	1	Taq polymerase activation	94	5 min
2 (x cycles)	1	Denaturation	94	15 sec
-	2	Annealing	55	30 sec
-	3	Extension*	72	30 sec

\*Fluorescence measured at the end of this stage.

### 2.8.2 *TaqMan™ PCR*

TaqMan™ PCR was conducted according to the following method (Table 2.8):

**Table 2.8. Reaction mixture for singleplex TaqMan™ PCR.**

<u>Component</u>	<u>Volume (µL)</u>
2x Gene expression master mix (Applied biosystems)*	10
20x Assay mix EC (VIC™-labelled), (Applied Biosystems)** <b>OR</b> 20x Assay mix GOI (FAM™-labelled), (Applied Biosystems)**	1
PCR-grade water	7
Template cDNA (2.7)	2

\*Containing AmpliTaq Gold® DNA polymerase, Uracil-DNA glycosylase, dNTPs, dUTP, ROX™ passive reference dye, "optimised buffer components".

\*\*Containing forward and reverse primers at 900nM final concentration (each) and a dye-labelled TaqMan™ probe at 250nM final concentration.

Samples were incubated as per the following thermal cycler program (Step-one, Applied biosystems), (Table 2.9):

**Table 2.9. Thermal cycling program for TaqMan™ PCR.**

<u>Step</u>	<u>Stage</u>	<u>Description</u>	<u>Temperature (°C)</u>	<u>Time</u>
1	1	Uracil-DNA glycosylase incubation	50	2min
2	1	Polymerase activation	95	10min
3 (x cycles)	1	Denaturation	95	15sec
-	2	Annealing/extension*	60	1min

*\*Fluorescence measured at the end of this stage.*

## 2.9 Principles of $[Ca^{2+}]_i$ measurement using the ratiometric fluorophore, fura-2

The control of free ionised intracellular calcium concentration ( $[Ca^{2+}]_i$ ) is an established mechanism of cellular activation.  $[Ca^{2+}]_i$  regulates a diverse range of cellular processes (depending on the cell type) including muscle contraction [148], modulation of gene expression [149], and apoptosis [150].  $[Ca^{2+}]_i$  may be measured experimentally by use of the calcium-sensitive fluorophore, fura-2. Figure 2.6 is a diagrammatic representation illustrating the mechanism of action of fura-2 in  $[Ca^{2+}]_i$  measurement.

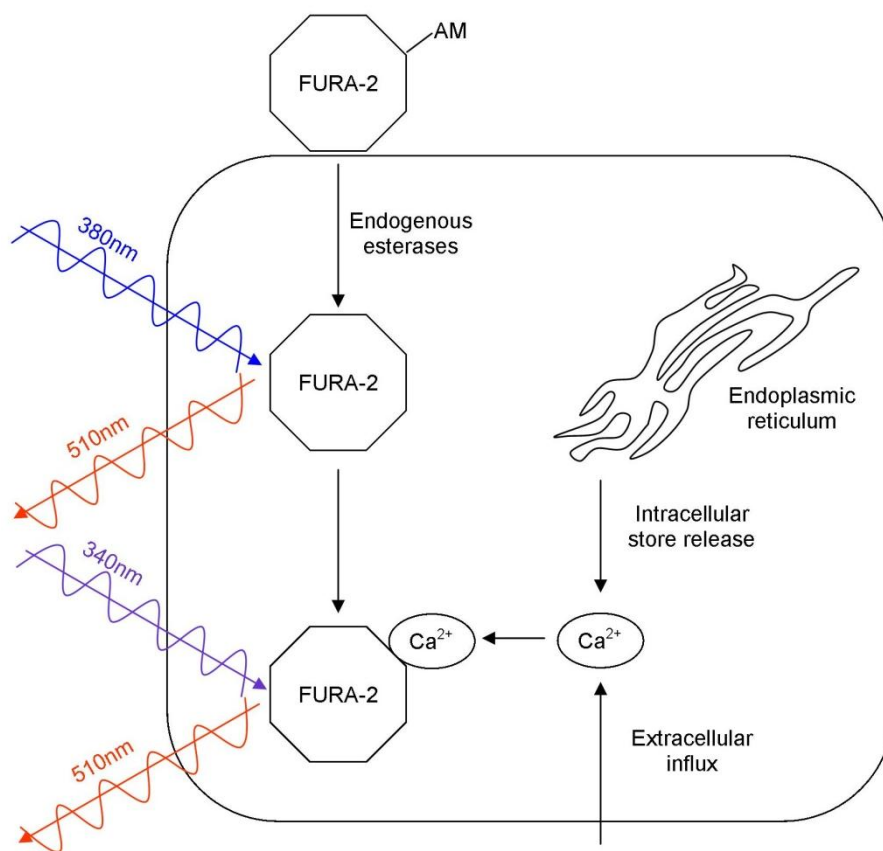


**Figure 2.6. Mechanism of action of fura-2 in intracellular calcium measurement.**

The fura-2 molecule can be purchased featuring acetoxy-methyl ester (AM) modifications which facilitate the species' passage across the cellular membrane. Endogenous esterases within the cytosolic compartment then cleave this chemical group from the molecule, thus largely preventing its leaving the cell. In a resting cell, the proportion of fura-2 which is calcium-unbound is high. In this instance, fluorescence

emission at 510nm is predominantly achieved by excitation at 380nm. In an activated cell, the proportion of fura-2 which is calcium-bound is high. In this instance, fluorescence emission at 510nm is predominantly achieved by excitation at 340nm. In most cellular settings, where fura-2 is neither solely calcium-bound nor unbound, fura-2 fluorescence emission at 510nm will be produced by excitation at both wavelengths. This principle is illustrated in Figure 2.7.

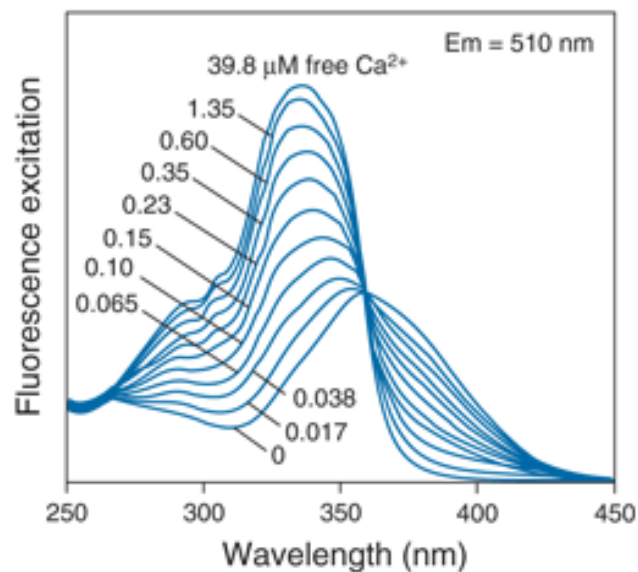


**Figure 2.7. Fluorescence excitation spectra of fura-2 in solutions containing 0-39.8 $\mu$ M free calcium. In a calcium-free solution, fluorescence emission at 510nm is produced with a peak excitation wavelength of 380nm. As the concentration of free calcium in the solution is increased, the peak excitation wavelength gradually decreases towards 340nm (Invitrogen).**

This calcium-dependent excitation spectral shift of fura-2 allows  $[Ca^{2+}]_i$  to be calculated from the ratio of 510nm emission at the two excitation wavelengths.

Absolute  $[Ca^{2+}]_i$  may be calculated according to the Grynkiewicz equation:

$$[Ca^{2+}]_i = K_d \cdot \left[ \frac{(R - R_{min})}{(R_{max} - R)} \right] \cdot \beta$$

Where,  $K_d$  for fura-2/ $Ca^{2+}$  binding at 37°C is 225nM,  $R$  is the 340:380 ratio,  $R_{max}$  is the 340:380 ratio under  $Ca^{2+}$ -saturating conditions,  $R_{min}$  is the 340:380 ratio under zero- $Ca^{2+}$  conditions, and  $\beta$  is the  $Ca^{2+}$ -free: $Ca^{2+}$ -saturating ratio at 380nm.

## **2.10 Cuvette-based fluorimetry for measurement of $[Ca^{2+}]_i$ in whole cell suspensions**

Cuvette-based fluorimetry was performed according to a method similar to Hirst *et al.* [151]. Cells were cultured in T75 flasks as previously described (2.2). At confluence, the cell medium was removed from the monolayer and replaced with 5mL of harvest buffer (Appendix I for composition). The 5mL of harvest buffer was immediately removed and replaced with 5mL of fresh harvest buffer. The cell monolayer was incubated in the harvest buffer for 5 min (37°C / 5% CO<sub>2</sub>). The adherent cell layer was dislodged by gently agitating the flask and the suspension was transferred to a centrifuge tube. Cells were sedimented under centrifugal force (3min / 1500g), the supernatant was removed and the pellet of cells was resuspended in 20mL of Krebs-HEPES buffer (Appendix I for composition). The cell suspension was sedimented and resuspended in Krebs-HEPES buffer twice more, the final suspension volume was 2mL. 10µL of fura-2/AM (1mM stock in DMSO) was added to the cell suspension to give a loading concentration of 5µM. The suspension was incubated in the dark for 30 min at 37°C. The fura-2 was diluted with excess Krebs-HEPES buffer and the suspension was incubated in the dark for 20 min at room temperature. The cells were sedimented and resuspended in Krebs-HEPES buffer a total of three-times (1500xg). The final resuspension volume allowed 2mL per determination plus 1mL overage. The fura-2 loaded cell suspension was maintained at room temperature in the dark.

Fluorometric measurements were made with a Perkin-Elmer LS50B instrument (Beaconsfield, UK). 2mL of the loaded cell suspension was transferred to a quartz cuvette, containing a magnetic stirrer and placed in the instrument's cuvette holder. The cell suspension was equilibrated to 37°C by use of the instrument's water jacket and

excitation at 510nm was determined for both 340nm and 380nm excitation at 1 sec intervals. Data were displayed in real-time and pharmacological challenges were affected once stable 340 and 380 recordings were established (20 $\mu$ L at x100 final concentration).

### ***2.10.1 Calibration of single-cuvette data***

A single calibration was conducted for each batch of cells (typically the final cuvette).  $R_{\max}$  was determined by addition of 0.1% Triton X-100 to the cuvette, producing cell lysis and subsequent saturation of fura-2 with calcium contained within the buffer.  $R_{\min}$  was determined by addition of 4.5mM EGTA (pH>8.0) which chelates  $\text{Ca}^{2+}$  from the suspension. The data were calibrated according to the Grynkiewicz equation (given previously), using the instrument's FLDM software (Beaconsfield, UK).

## **2.11 High-throughput fluorimetry for measurement of $[Ca^{2+}]_i$ in adherent cell monolayers**

High-throughput fluorimetry was performed using the NOVOstar plate reader (BMG labtech, UK). Confluent cell cultures were trypsinised and resuspended in 10mL of fresh medium. Cell density was determined by haemocytometry (2.2.5) and cells were seeded in 96-well plates at a density of 10,000 cells well<sup>-1</sup>/200μL well<sup>-1</sup>. Cells were incubated for 48 hours (37°C / 5% CO<sub>2</sub>) and the media were changed at 24 hours.

The CHO cells used for this assay have been shown to extrude fura-2, afforded by the expression of a multidrug-resistance efflux pump [151]. This process has the unfortunate effect of increasing baseline fluorescence over time. The NOVOstar plate reader was configured in 'well mode', meaning that each experimental well was measured in sequence. To prevent increasing baseline fluorescence in sequential wells, the organic anion transport inhibitor probenecid was included in all experimental buffers during these experiments [151].

Approximately one hour prior to the start of the experiment media were removed from wells using an eight-barrelled pipette and rinsed twice with 50μL of Krebs-HEPES buffer supplemented with 1mM probenecid. The plate was loaded into the NOVOstar plate reader and auto-fluorescence values were obtained for individual wells at 340:380nm emission, 510nm excitation. Buffers were removed and replaced with 100μL of Krebs-HEPES buffer supplemented with 1mM probenecid, 4μM fura-2/AM, and 0.02% pluronic. The plate was incubated in the dark at 37°C / 5% CO<sub>2</sub> for 30 min. Buffers were removed from wells and monolayers were rinsed three-times with 100μL of Krebs-HEPES buffer supplemented with 1mM probenecid. The cells were incubated

for 20 min in the dark at room temperature for de-esterification. Cells were rinsed three-times with Krebs-HEPES buffer supplemented with 1mM probenecid (final volume of 50 $\mu$ L well<sup>-1</sup>). The cells were loaded into the NOVOstar plate reader and maintained at 37°C. Each experimental well was measured in sequence and pharmacological agents were transferred from a separate reagent plate loaded into the machine (25 $\mu$ L / X3 of final concentration). Pharmacological agents were injected at 21 sec and recordings were made at 1.46 sec intervals for a total length of 80 sec.

### ***2.11.1 Calibration of high-throughput fluorescence data***

Three calibrations were performed per plate, at the end of each experiment.  $R_{\max}$  was determined by addition of 10 $\mu$ M of the calcium ionophore, ionomycin (final concentration), [152].  $R_{\min}$  was determined by subsequent addition of 40mM of EGTA [152]. Ionomycin was injected at 15 sec and EGTA was injected at 140 sec. Recordings were made for 210 sec at 1.46 sec intervals. Means of the three  $R_{\min}$  and  $R_{\max}$  values were then calculated.

A Microsoft Excel spreadsheet was used to input the data and calculate absolute  $[Ca^{2+}]_i$ . Auto-fluorescence values were subtracted from the raw fluorescence values in experimental and calibration wells. Ratios were then calculated (340:380) and absolute  $[Ca^{2+}]_i$  were derived according to the Grynkiewicz equation (given previously).

# Chapter Three

### **3. Optimisation and refinement of methods**

#### **3.1 Optimisation of PCR: SYBR green I vs. TaqMan™**

Prior to main PCR experiments, two main methods were tested. This was necessary in order to verify the specificity of the PCR reaction and ultimately the purity of the PCR products formed. The two methodologies tested were (Table 3.1):

**Table 3.1. PCR experience at the beginning of the project.**

<b><u>Method</u></b>	<b><u>Paragraph</u></b>	<b><u>Our group's experience at the start of the project</u></b>
SYBR green I PCR	Theory: 2.4.1 Method: 2.8.1	Routinely used by our research group. This method had also been optimised for use with UT primers. However, dissociation curve analysis indicated non-specific product formation.
Taqman PCR	Theory: 2.4.2 Method: 2.8.2	This method had not previously been used by our group. However, it promised to add an additional layer of specificity to the reaction. Dissociation curve analysis was not possible due to the altered chemistry of the reaction.

##### ***3.1.1 Methods***

The two PCR methods were compared by use of two cell-lines, CHO-wt (UT negative) and CHO<sub>h</sub>UT (UT positive). Both cell-lines were cultured in T75 flasks and RNA was extracted by the phenol:chloroform organic extraction method (2.5.1). RNA was DNase treated (2.6) and reverse transcribed (2.7). PCR amplification curves were then produced (60 cycles) for both cell-lines by both PCR methods and in the case of SYBR green I PCR, dissociation curves were also produced immediately following PCR (60-95°C / 0.3°C increments). The GOI probed was hUT, which was normalised to the EC Glyceraldehyde 3-phosphate dehydrogenase (GAPDH), (routinely used by our group at that time).

Although an amplification curve obtained during a TaqMan™ assay is specific only for the target amplicon, non-specific products may still be formed in the reaction mixture

affecting post-PCR applications. For this reason, the post-PCR products from the above TaqMan™ assays were purified from the reaction mixture using QIAquick® PCR purification kit (Qiagen) as per the manufacturer’s instructions. The kit comprises of a silica membrane suspended in a spin column to fit a standard desktop microcentrifuge. Briefly, the post-PCR amplicons were adsorbed onto the silica membrane under high-salt conditions and unwanted contaminants such as enzymes and salts were removed by use of an ethanol-containing buffer. Purified DNA was then eluted into a fresh tube under low-salt conditions. The manufacturer’s full protocol for this procedure is provided in Appendix II. Dissociation curve analysis (60-95°C / 0.3°C increments) of the purified TaqMan™ post-PCR products was conducted according the following method (Table 3.2).

**Table 3.2. Components of the reaction mixture for dissociation curve analysis of TaqMan™ post-PCR products.**

<u>Component</u>	<u>Volume (µL)</u>
SYBR green jumpstart Taq readymix (Sigma)	12.5
Purified post-PCR products	12.5

### **3.1.2 Results**

GAPDH and UT were amplified in the UT-positive cell-line (CHO<sub>h</sub>UT) sample by both PCR methods ( $\Delta$ CT values = 12.47 and 14.17 for SYBR green I and TaqMan™ methods respectively). The  $\Delta\Delta$ CT value between these two measurements was 1.7, equating to a fold difference of 3.3. GAPDH was amplified in the UT-negative cell-line (CHO-wt) sample by both PCR methods, however, UT was only amplified by the SYBR green I method for this sample ( $\Delta$ CT value = 23.88). Amplification curves are shown in Figure 3.1.

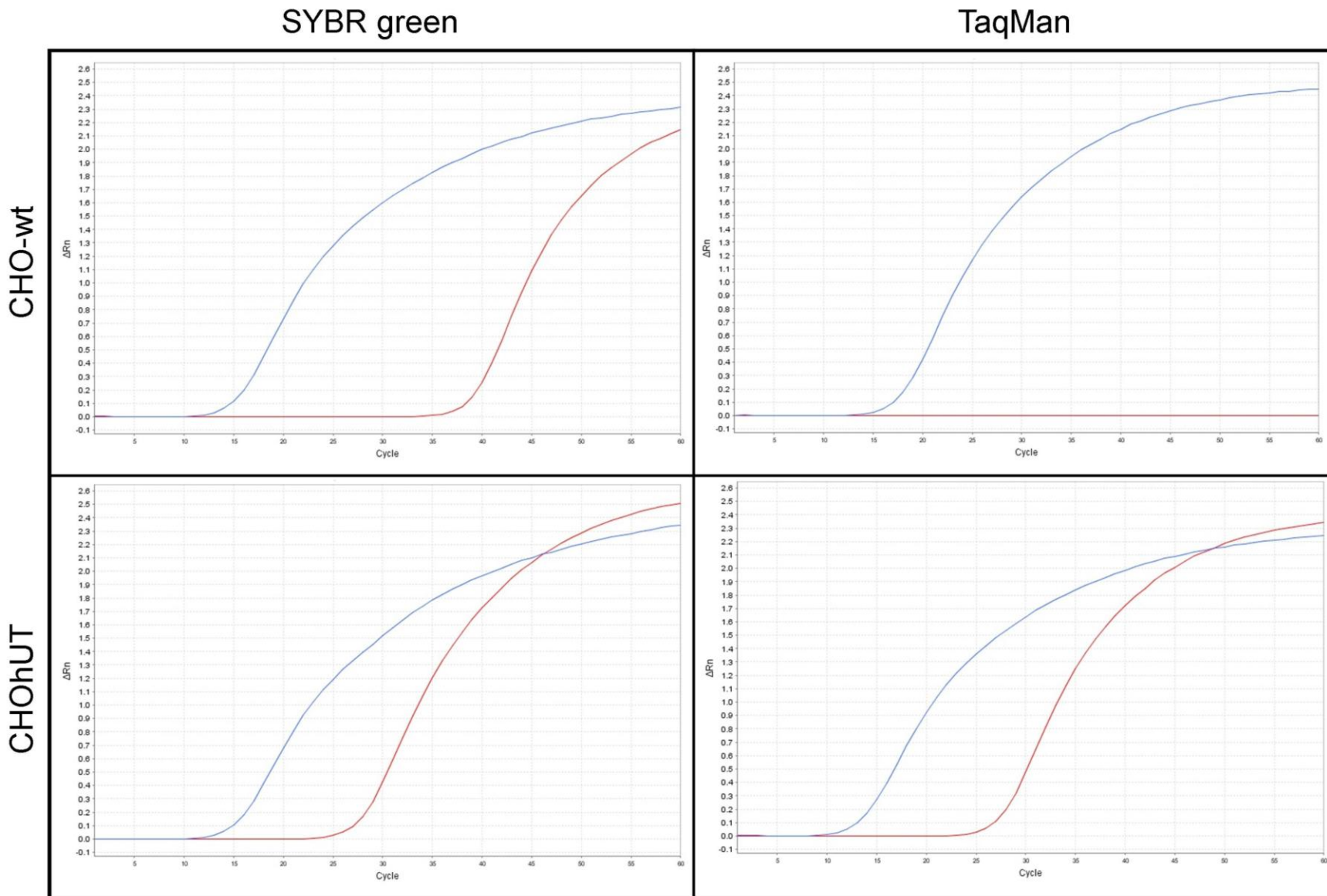


**Figure 3.1.** Amplification curves for GAPDH (blue –EC) and hUT (red – GOI) in CHO-wt and CHOhUT by two methods of PCR (SYBR green I and TaqMan™). All PCR was conducted for 60 cycles and all data are shown on equivocal scales, n=1.

SYBR green

TaqMan

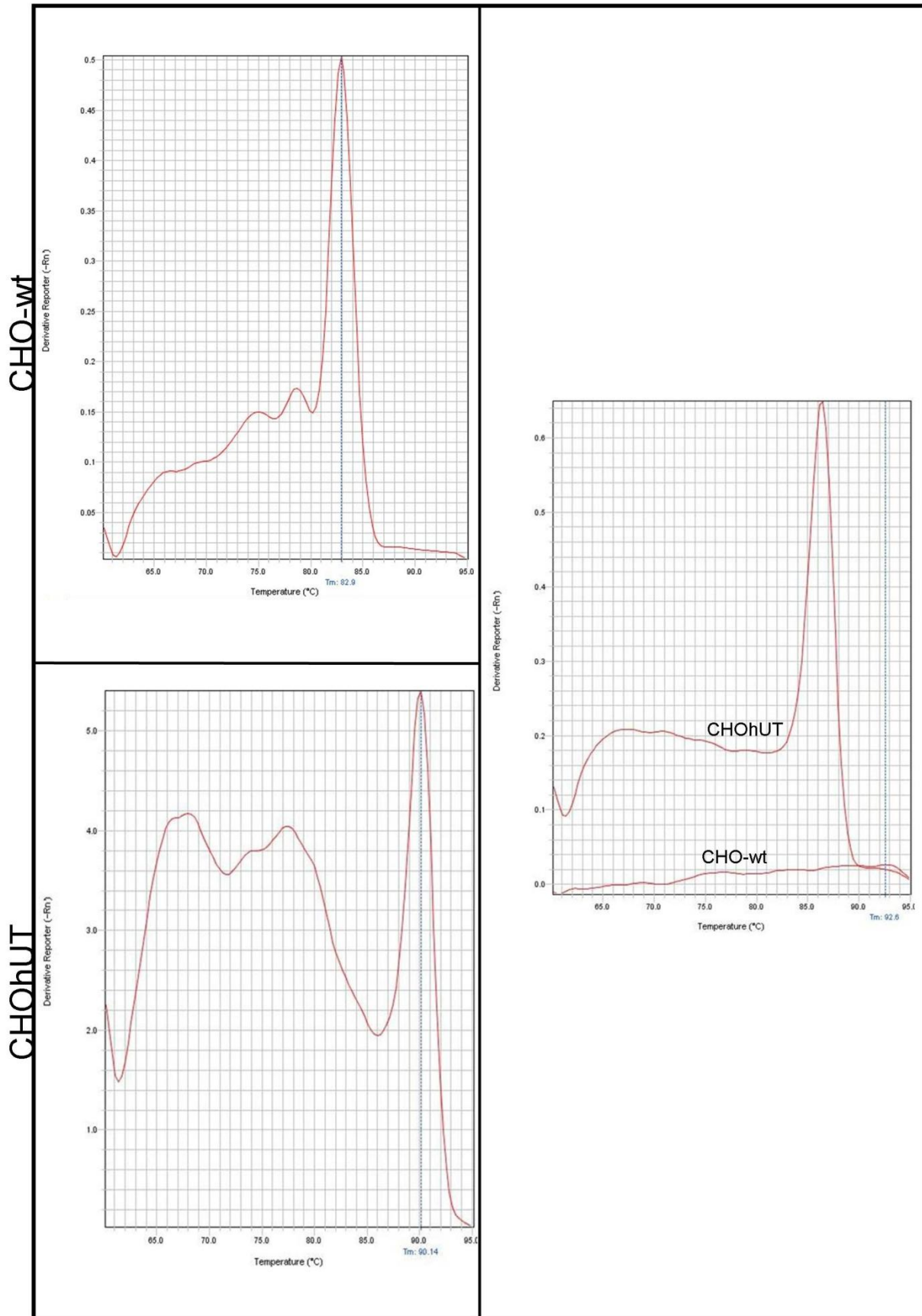


Figure 3.2. Melting peaks of post-PCR products following amplification of hUT in CHO<sub>h</sub>UT and CHO-wt using SYBR green and Taqman™ chemistries.

Melting peaks of post-UT amplification in CHO-wt and CHO<sub>h</sub>UT are shown in Figure 3.2. Analysis of the CHO-wt sample amplified by the SYBR green I method, revealed at least three peaks (dominant peak  $T_m=82.9^\circ\text{C}$ ). The same sample amplified by the TaqMan<sup>TM</sup> method revealed no peaks between 60-95°C. Analysis of the CHO<sub>h</sub>UT sample amplified by the SYBR green I method, revealed at least three peaks. The dominant peak had a  $T_m$  value of 90.14°C; the remaining two peaks had magnitudes of approximately two-thirds of the dominant peak. The same sample amplified by the TaqMan<sup>TM</sup> method revealed one dominant peak with a  $T_m$  of 86.33°C.

### **3.1.3 Discussion**

Both of the PCR methods were successful at measuring hUT expression in the UT-positive cell-line, CHO<sub>h</sub>UT. Dissociation curve analysis of the post-PCR products of these samples, indicated that the primers included in the TaqMan<sup>TM</sup> assay produced considerably fewer non-specific products than those used in the SYBR green I method. Moreover, the relative measurement of hUT expression in these samples (normalised to GAPDH) suggested a 3.3-fold higher expression of hUT in the same sample when quantified by the SYBR green I method rather than the TaqMan<sup>TM</sup> method. It is likely that hUT mRNA expression is over-estimated by the SYBR green I method due to non-specific product formation, confounded by the absence of a specific fluorometric probe in this assay. A false-positive result was obtained for hUT in the UT-negative cell-line (CHO-wt) by the SYBR green I method. Dissociation curve analysis of the post-PCR products from this reaction, again indicated non-specific product formation. No amplification of hUT was obtained in the same sample when the TaqMan<sup>TM</sup> method was utilised (60 cycles). Dissociation curve analysis of the post-PCR products of this sample reveals a nominal level of fluorescence at all temperatures.

These findings suggest that it is inappropriate to use SYBR green I chemistry for amplification of hUT. The lack of specificity of the fluorometric probe results in over-estimation of hUT content and the lack of specificity of the hUT primers is responsible for marked non-specific product formation. Standard procedures for reducing non-specific product formation, such as designing a probe set which spans an exon-exon boundary [153], is not possible here due to the lack of introns of the hUT gene [8].

These preliminary data suggest that TaqMan™ chemistry is better suited to amplification of hUT. The specific fluorometric probe allows unbiased amplification curves to be generated, even in the presence of non-specific product formation. Moreover, by purifying the post-PCR products of these samples, we have demonstrated that non-specific product formation is markedly reduced with these primer sets. Such findings may be attributed to improved primer design algorithms and rigorous validation (Applied biosystems).

## 3.2 Optimisation of a duplex TaqMan™ PCR assay

### 3.2.1 *Methods*

A duplex TaqMan™ assay was optimised to measure both hUT and eukaryotic 18s rRNA (EC) concurrently. Several advantages were conferred by this approach, namely; reduced error due to pipetting accuracy, increased throughput, and increased cost-effectiveness. Prior to utilising a duplex assay, it is necessary to ensure that the efficiency of the PCR reactions are not altered. This can occur if the most abundant transcript (usually the EC) saturates the polymerase enzyme, thus inhibiting amplification of the GOI. In this instance, the EC primers may be diluted (or limited) to prevent polymerase saturation.

10-fold serial dilutions of the CHO<sub>h</sub>UT cDNA library (3.1.1) were produced and standard curves were produced for both 18s and hUT in singleplex and duplex configurations. Singleplex PCR was conducted as previously described (Table 2.8), duplex PCR was conducted as below (Table 3.3):

**Table 3.3. Reaction mixture for duplex TaqMan™ PCR.**

<b>Component</b>	<b>Volume (µL)</b>
2x Gene expression master mix (Applied biosystems)*	10
20x Assay mix EC (VIC™-labelled), (Applied Biosystems)**	1
20x Assay mix GOI (FAM™-labelled), (Applied Biosystems)**	1
PCR-grade water	6
Template cDNA (2.7)	2

\*Containing AmpliTaq Gold® DNA polymerase, Uracil-DNA glycosylase, dNTPs, dUTP, ROX™ passive reference dye, “optimised buffer components”.

\*\*Containing forward and reverse primers at 900nM final concentration (each) and a dye-labelled TaqMan™ probe at 250nM final concentration.

Both singleplex and duplex assays were incubated according to the standardised thermal profile as previously described (Table 2.9).

PCR efficiency was calculated as [154]:

$$E = 10^{(-1/m)} - 1$$

Where  $m$  is the standard curve gradient.

### 3.2.2 Results

Standard curves of the CHO<sub>h</sub>UT cDNA library for 18s and hUT are shown in Figure 3.3, linear regression statistics are given in Table 3.4.

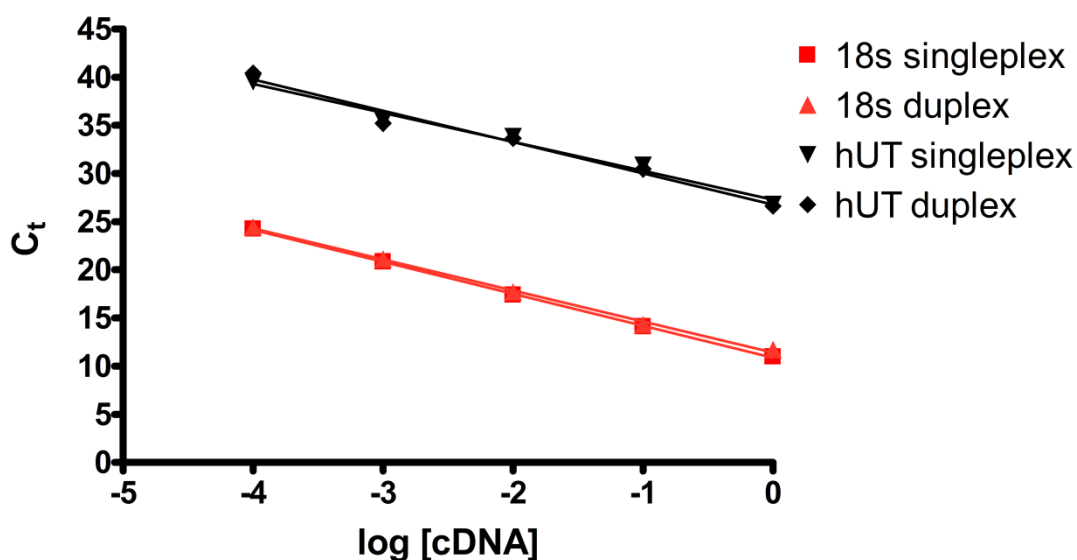


Figure 3.3. PCR standard curves of the CHO<sub>h</sub>UT cDNA library probed for 18s and hUT. Data are expressed as means  $\pm$ S.D. n=3.

Table 3.4. Statistics for standard curves of the CHO<sub>h</sub>UT cDNA library probed for 18s and hUT. Data are expressed as means  $\pm$ S.D. n=3.

Target	Format	Intercept	Gradient	Efficiency	$r^2$
18s	Singleplex	11.1 $\pm$ 0.3	-3.4 $\pm$ 0.1	0.979	0.9882
18s	Duplex	11.8 $\pm$ 0.3	-3.2 $\pm$ 0.1	1.036	0.9825
hUT	Singleplex	26.9 $\pm$ 0.4	-3.1 $\pm$ 0.2	1.092	0.9654
hUT	Duplex	26.3 $\pm$ 0.4	-3.3 $\pm$ 0.2	1.002	0.9660

### **3.2.3 Discussion**

The PCR efficiencies of 18s and hUT were largely unchanged by use of a duplex assay. There was also little difference in the standard curve intercepts between singleplex and duplex methodologies. These data suggest that it is appropriate to amplify 18s and hUT in a duplex assay format. The duplex PCR efficiencies measured are 104% and 100% for 18s and hUT respectively. These are well within the limits for suggested PCR efficiency [154]. Moreover, the efficiencies of the two primers are comparable in magnitude, which is a requirement for co-amplification and normalisation [154].

### **3.3 Optimisation of high-throughput $[Ca^{2+}]_i$ fluorimetry in the NOVOstar plate reader**

#### ***3.3.1 Methods***

Seven wells of a 96-well plate were seeded with CHO<sub>h</sub>UT as previously described (2.11). 48-hours after seeding, auto-fluorescence values were obtained and the cells were loaded with fura-2/AM as per the previously described method (2.11). 10-fold serial dilutions of U-II were prepared in Krebs-HEPES buffer and loaded into corresponding wells of a separate 96-well plate, which was maintained on ice. Both the reagent and experimental plates were loaded into the NOVOstar plate reader, which was set to incubate at 37°C. A concentration-response curve (CRC) was generated by transferring 25µL of each of the seven concentrations of U-II from the reagent plate to the corresponding well of the experimental plate in sequence. The following settings were programmed into the NOVOstar control software (Table 3.5).

**Table 3.5. Settings which were programmed into the NOVOstar control software, concerning the injection and mixing of pharmacological agents during the first test run.**

	<b><u>Description</u></b>	<b><u>Setting value</u></b>
Injection speed	Speed at which the pharmacological agent was injected into the target well of the experimental plate	100µL s <sup>-1</sup>
Dispense depth	Depth at which the automated pipettor dispensed into the target well (measured from the bottom of the well)	0.5mm
Pre-aspirate volume	Volume of buffer aspirated from the target well prior to injection (to enhance mixing)	10µL
Mix volume	Volume of buffer aspirated and then re-injected during a mix cycle (post-initial injection)	10µL
Number of mix cycles	A mix cycle comprises one aspiration and one injection following initial injection into the target well	2
Shake width	Width at which the whole plate was shook following injection and mixing	1.0mm
Shake mode	Pattern of shaking (orbital or linear)	Orbital
Shake time	Length of time during which the plate was shook after injection	1.0s

### 3.3.2 Results

Raw fluorescence data and calculated 340:380 ratios are shown graphically in Figure 3.4 for a single concentration of U-II ( $10^{-6}\text{M}$ ) and a calibration curve. Injection of a single concentration of U-II caused a rapid increase in 340nm fluorescence coupled with a simultaneous decrease in 380nm fluorescence. The calculated 340:380 ratios of these data demonstrated a classic bi-phasic response with a rapid increase of  $[\text{Ca}^{2+}]_i$  (peak fluorescence recorded 2.1 sec after injection) followed by a plateau and slow decline (baseline subtracted fluorescence at approximately 29% of maximum 59 sec after injection).

Injection of  $10\mu\text{M}$  ionomycin caused a rapid increase in 340nm fluorescence with an accompanying anti-parallel 380nm decrease. Subsequent injection of 40mM EGTA produced a rapid decrease in 340nm fluorescence with an accompanying anti-parallel increase in 380nm fluorescence. The calculated 340:380 ratios of these data demonstrated a rapid increase in fluorescence after injection of  $10\mu\text{M}$  ionomycin, followed by a gradually increasing plateau (peak fluorescence observed 86.4 sec after injection). Injection of 40mM EGTA produced a rapid decrease in fluorescence which was stable for the length of recording and which was marginally lower than basal fluorescence ( $0.894\pm 0.013$  and  $0.839\pm 0.007$  for basal and  $R_{\min}$  fluorescence ratios respectively).

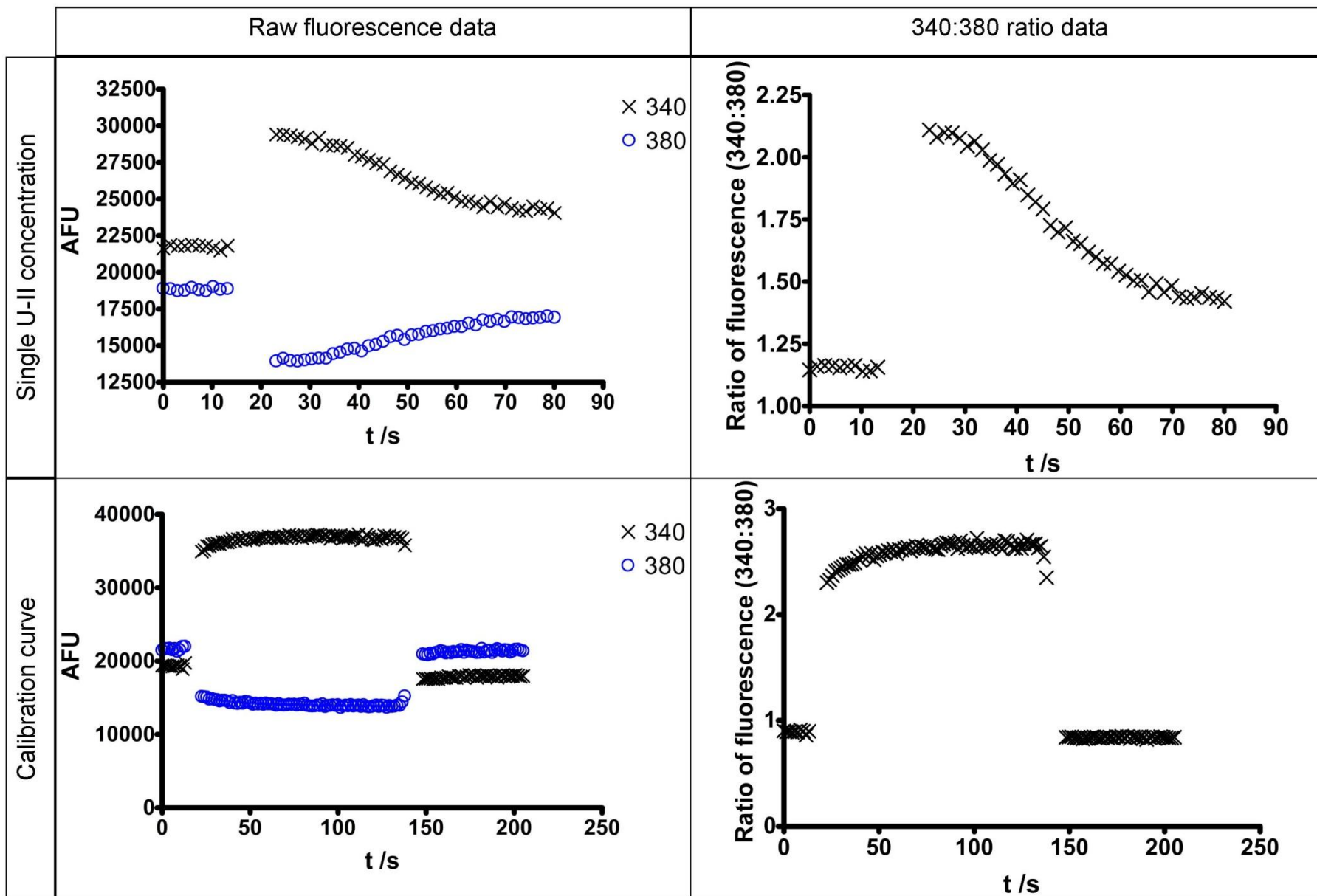


Figure 3.4. Raw fluorescence and raw 340:380 ratio data for a single dose of U-II (-6) and a calibration curve.

The calibrated CRC of U-II in CHO<sub>h</sub>UT is shown in Figure 3.5. The data fitted a sigmoidal relationship with high correlation ( $R^2=0.98$ ). The calculated  $EC_{50}$  was  $4.94 \times 10^{-9}$  and the maximum increase in intracellular calcium concentration ( $\Delta[Ca^{2+}]_i$ ) was 333nM. The CRC was elevated on a baseline of 699nM and the individual traces for the lower U-II concentrations ( $10^{-12}$ - $10^{-10}$ ) clearly indicated that sizable calcium responses were generated immediately following injection.

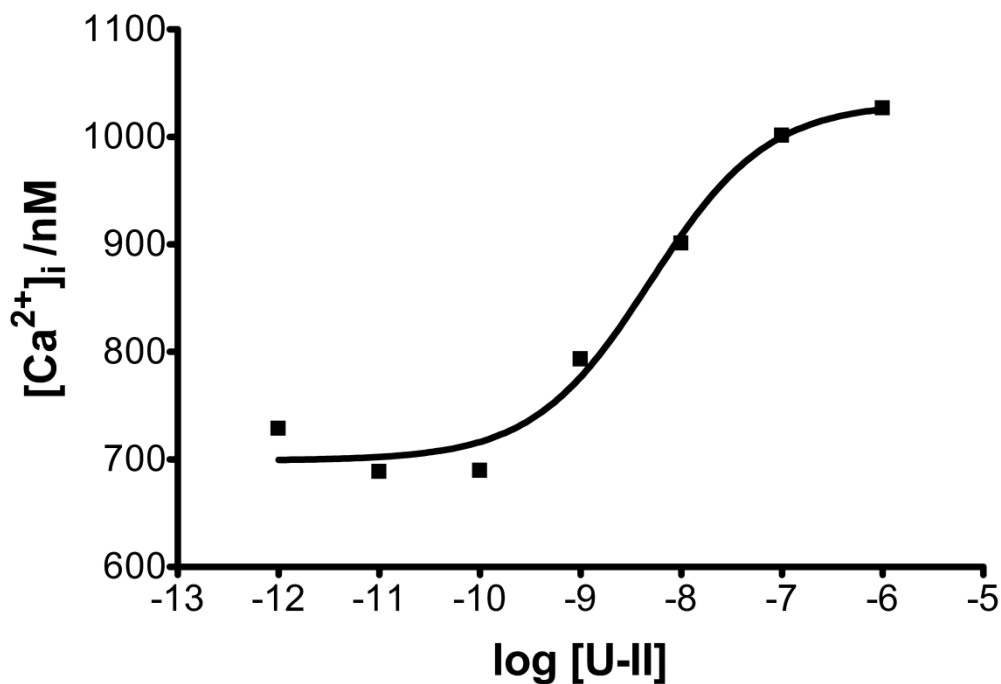


Figure 3.5. A calibrated concentration-response curve showing U-II-mediated elevations in  $[Ca^{2+}]_i$  in CHO<sub>h</sub>UT. n=1.

### 3.3.3 Discussion

The un-optimised  $[Ca^{2+}]_i$  assay in the NOVOstar plate reader produced a CRC of high fit, which was easily calibrated by use of ionomycin and EGTA. The calculated  $EC_{50}$  was in agreement with those previously reported [155]. The CRC was elevated on a baseline which was likely due to injection artefacts as opposed to a calibration error, supported by observable anti-parallel fluorometric responses at the lower U-II concentrations.

### 3.4 Optimisation of injector settings in the NOVOstar plate reader

Following generation of a CRC to U-II in the NOVOstar plate reader, which was elevated on a baseline of approximately 700nM  $[Ca^{2+}]_i$ , the effect of shear stress on  $[Ca^{2+}]_i$  was investigated in CHO<sub>h</sub>UT.

#### 3.4.1 *Methods*

Eleven wells of a 96-well plate were seeded with CHO<sub>h</sub>UT as previously described (2.11). 48-hours after seeding, auto-fluorescence values were obtained and the cells were loaded with fura-2/AM as per the previously described method (2.11). The plate was loaded into the NOVOstar plate reader and fluorimetric measurements were made as 25 $\mu$ L of Krebs-HEPES buffer was injected into each well. The injection speed and the proximity of the pipettor to the cell monolayer was varied in order to control the amount of shear stress the cells were subjected to (Table 3.6).

**Table 3.6. Injection speeds and pipettor depths which were programmed into the NOVOstar plate reader in order to investigate the effect of shear stress on  $[Ca^{2+}]_i$ .**

<u>Well</u>	<u>Injection speed (<math>\mu</math>L s<sup>-1</sup>)</u>	<u>Proximity of the pipettor to the cell monolayer (mm)</u>
1	420	8
2	200	8
3	100	8
4	50	8
5	100	10
6	100	8.6
7	100	7.2
8	100	5.8
9	100	4.4
10	100	3.0
11	100	1.6

#### 3.4.2 *Results*

The effect of injection speed and pipettor depth on the magnitude of the injection artefact is illustrated graphically in Figure 3.6. The magnitude of the injection artefact

was found to be directly proportional to the injection speed ( $m=2.563\pm0.0988$  with y and x intercepts fixed at 0).

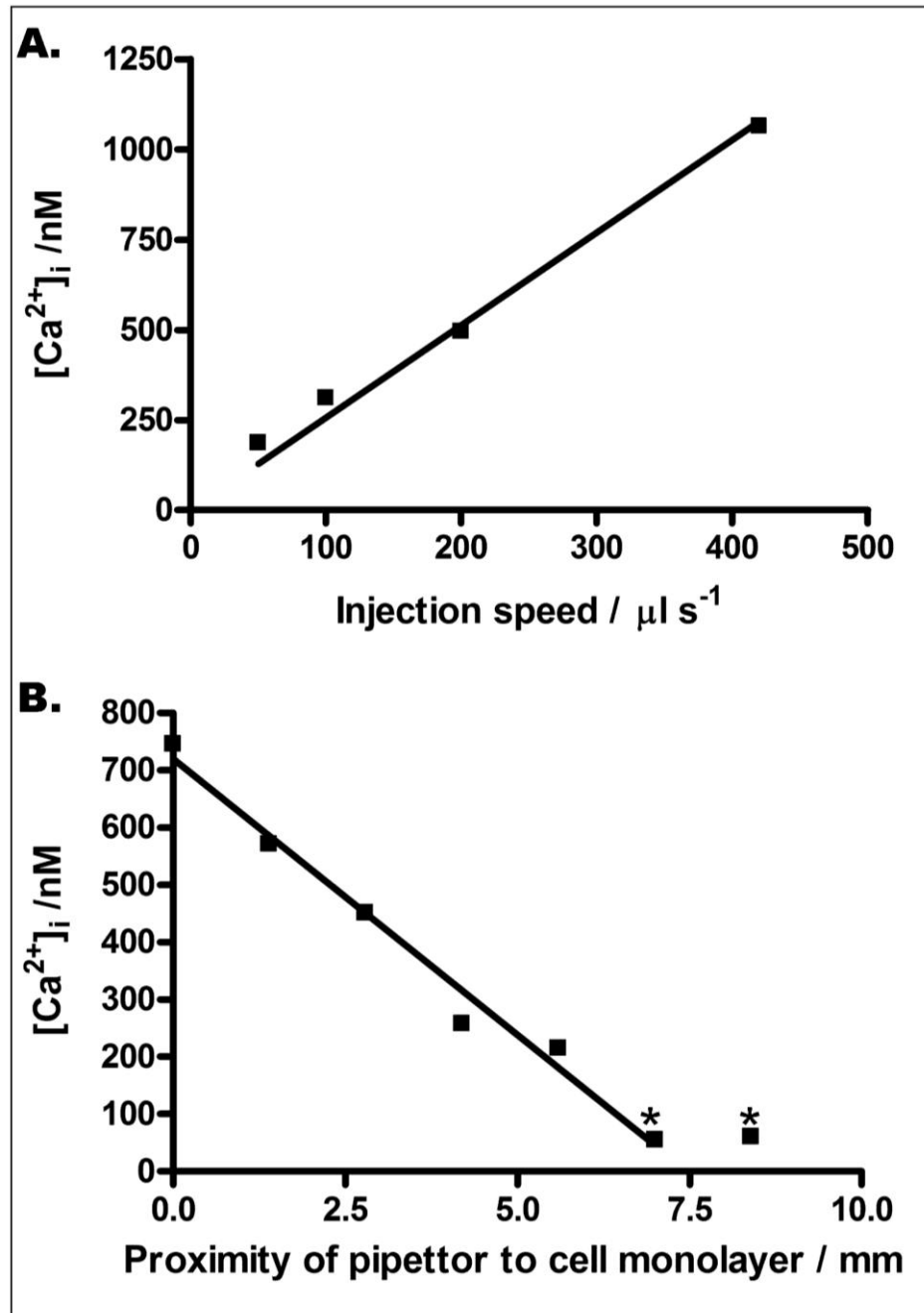


Figure 3.6. Effect of (A) injection speed at a fixed pipettor depth of 2mm (B) pipettor depth at a fixed injection speed of  $100\mu\text{L s}^{-1}$ , on magnitude of injection artefact. Data points marked “\*” indicates that no injection artefact was generated.  $n=1$ .

The magnitude of the injection artefact was found to be inversely proportional to the proximity of the pipettor to the cell monolayer ( $m= -96.18\pm6.298$ ,  $r^2=0.98$ ). No injection

artefact was generated when the distance of the pipettor from the cell monolayer was greater than 7mm (at a fixed injection speed of  $100\mu\text{L s}^{-1}$ ).

### **3.4.3 Discussion**

Shear stress was found to be capable of inducing cellular activation in CHO<sub>h</sub>UT. This phenomenon was demonstrated by varying both injection speed and the distance of the pipettor from the cell monolayer. These observations explain why the previously generated CRC to U-II in CHO<sub>h</sub>UT was elevated on a baseline of approximately 700nM  $[\text{Ca}^{2+}]_i$  (3.3). Previous studies have demonstrated shear stress to induce changes to gene expression [156]. More recently, shear stress has been shown to produce calcium transients in CHO which mimic agonist-induced calcium fluxes [157]. These findings highlight the importance of evaluating the effects of the fluidic force of injection and mixing on signal generation in cellular assays. It is important that agonist-induced cellular activation be evaluated from the resting state, to that end the assay must be optimised so that shear stress is below the threshold for cellular activation.

### **3.5 Evaluation of a finalised protocol for high-throughput $[Ca^{2+}]_i$ fluorimetry in the NOVOstar plate reader**

The previous optimisations (3.3 & 3.4) were further refined (data not shown), a finalised protocol was produced, and it was evaluated for accurate determination of  $[Ca^{2+}]_i$  in CHO<sub>h</sub>UT.

#### **3.5.1 Methods**

Six wells of a 96-well plate were seeded with CHO<sub>h</sub>UT as previously described (2.11). 48-hours after seeding, auto-fluorescence values were obtained and the cells were loaded with fura-2/AM as per the previously described method (2.11). Experimental and reagent plates were loaded into the NOVOstar plate reader which was set to incubate at 37°C. Fluorometric measurements were made of each well in sequence while either 10<sup>-6</sup>M U-II (final) or Krebs-HEPES buffer (25µL) was injected. The following parameters were programmed (Table 3.7).

**Table 3.7. Settings which were programmed into the NOVOstar control software, concerning the injection and mixing of pharmacological agents for the finalised protocol.**

	<b>Description</b>	<b>Setting value</b>
Injection speed	Speed at which the pharmacological agent was injected into the target well of the experimental plate	10µL s <sup>-1</sup>
Dispense depth	Depth at which the automated pipettor dispensed into the target well (measured from the bottom of the well)	10mm
Pre-aspirate volume	Volume of buffer aspirated from the target well prior to injection (to enhance mixing)	0µL
Mix volume	Volume of buffer aspirated and then re-injected during a mix cycle (post-initial injection)	0µL
Number of mix cycles	A mix cycle comprises one aspiration and one injection following initial injection into the target well	0
Shake width	Width at which the whole plate was shook following injection and mixing	2.0mm
Shake mode	Pattern of shaking (orbital or linear)	Orbital
Shake time	Length of time during which the plate was shook after injection	2.0s

### 3.5.2 Results

Fluorescence ratio (340:380) data are presented in Figure 3.7. Injection of  $10^{-6}$ M U-II produced a rapid increase in fluorescence (peak fluorescence reached 6.3 sec after injection, 197% of basal). A slow decline phase was observed (baseline subtracted fluorescence at 39.6% of maximum at 48 sec after injection). Injection of equivolumetric Krebs-HEPES buffer produced no obvious calcium transient during the 48 sec after injection. However, linear regression analysis indicated a significant departure from zero ( $m=3.5 \times 10^{-4}$  /  $P=0.035$ ).

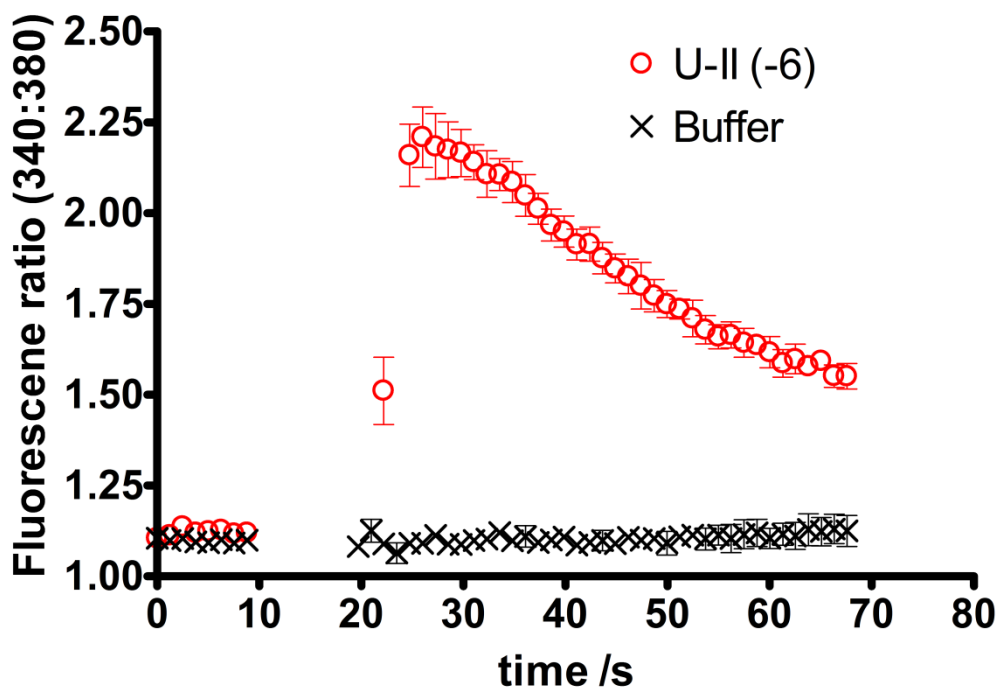


Figure 3.7. Fluorescence ratios over time in CHO<sub>h</sub>UT for injections of  $10^{-6}$ M U-II or Krebs-HEPES buffer. Mean  $\pm$ S.E.M n=3.

### 3.5.3 Discussion

These data demonstrate that agonist-induced changes to  $[Ca^{2+}]_i$  can be measured in CHO<sub>h</sub>UT. Moreover, the finalised protocol allows these measurements to be unbiased

due to absence of shear stress-induced cellular activation. There was a gradual but significant increase in baseline fluorescence observed over time in the absence of agonist. The temporal characteristics of this effect suggest that this is most likely due to nominal extrusion of fura-2 from the cell as opposed to cellular activation.

# Chapter Four

#### **4. Studies in a Stably Transfected UT Cell-line**

Studies were performed with the CHO<sub>h</sub>UT cell-line in order to observe the effects of putative UT receptor antagonists at a high UT receptor density ( $B_{\max} = 1,110 \pm 70$  fmol mg protein<sup>-1</sup>, [155]). Full CRCs of total inositol phosphate turnover (IP<sub>x</sub>) were produced for U-II, urantide, and UFP-803. Moreover, antagonism studies were performed in order to assess the antagonist potency of the two putative antagonists. Details of these ligands' effects in the rat aorta bioassay and standard *in vitro* systems are given in 1.8.1, along with details of their development.

##### **4.1 Principles of in vitro measurement of agonist-mediated inositol phosphate turnover**

Total inositol phosphate (IP<sub>x</sub>) turnover was measured in intact cells using methods comparable to those of Skippen et al. [158]. Prior to experimentation, the inositol lipids were labelled by culturing the cells in [<sup>3</sup>H]myo-inositol for 2-3 days. "This ensures that the inositol-containing lipids are pre-labelled to near equilibrium prior to the experiment" [158]. Immediately prior to experimentation, the cells were equilibrated with LiCl. This served to amplify inositol phosphate responses through inhibition of inositol 1-phosphatase resulting in an accumulation of agonist-induced inositol phosphates [159]. Following pharmacological challenges for a fixed period of time, inositol phosphates were isolated by anion exchange chromatography. The method and solutions used are based on those described by Ellis et al. [160].

## **4.2 Concentration-response curves**

### ***4.2.1 Methods***

CHO<sub>h</sub>UT cells were cultured in T175 flasks in medium supplemented with 1 $\mu$ Ci mL<sup>-1</sup> [<sup>3</sup>H]myo-inositol for 48 hrs [158], as previously described (2.2). On the day of the experiment, cells were rinsed twice and harvested into suspension with 15mL of harvest buffer (Appendix I for composition). Cells were sedimented under centrifugal force (1500xg) and re-suspended in Krebs-HEPES buffer a total of three-times. The final re-suspension volume depended on the size of the cell pellet and the number of determinations required; the buffer was supplemented with 10mM lithium chloride (4.1 for rationale). The cell suspension was distributed into test tubes (400 $\mu$ L tube<sup>-1</sup>) and incubated in a shaking water bath for 15 min (37°C). Pharmacological agents (100 $\mu$ L at X5 final concentration in Krebs-HEPES buffer/ LiCl) were added to each of the test tubes in turn and incubated for a further 15min. The reactions were terminated in the same order that they were started by addition of 500 $\mu$ L of 1M tri-chloroacetic acid (TCA). Following incubation on ice for 30 min, the cell debris was sedimented under centrifugal force (1700xg / 3min). 800 $\mu$ L of the supernatant was recovered and transferred to a polypropylene tube. 160 $\mu$ L of 10mM EDTA and 800 $\mu$ L of a freshly-prepared 1:1 (volumetric) mixture of tri-n-octylamine and Freon were added to each tube. The tubes were mixed intermittently for 15 min prior to the phases being separated under centrifugal force (1700xg / 3 min). 700 $\mu$ L of the upper phase (containing the inositol phosphates) was recovered to a fresh tube and 175 $\mu$ L of 60mM NaHCO<sub>3</sub> was added to neutralise the solution. Dowex 1X7 (200-400 mesh) resin was prepared and transferred to glass Pasteur pipettes plugged with glass-wool (1mL per pipette, referred to as columns). Resins were converted to the formate form by adding 10mL of regeneration buffer (2M ammonium formate / 0.1M formic acid) followed by 20mL of

de-ionised water after the column had voided due to gravity. Samples were added to columns and allowed to void before rinsing with 10mL of de-ionised water, which washed-out free-inositol from the samples [158]. 10mL of buffer A (60mM ammonium formate / 5mM borate) was added to each column which eluted glycerophosphoinositol from the resin [158]. Once the columns had completely voided, the bottoms were dried and 8mL of buffer B (0.75M ammonium formate / 0.1M formic acid) was added and collected into vials placed underneath the columns. 4mL of each of the eluates (containing the inositol phosphates) were transferred to scintillation vials containing 4mL of scintillation fluid and mixed. Beta radiation was quantified in each of the samples following a 1 hr delay.

#### *4.2.1.1 Data manipulations*

Basal [<sup>3</sup>H]-IP<sub>x</sub> turnover was determined as a mean of three test tubes into which pharmacological agents were substituted for equivalent Krebs-HEPES buffer. Percentage response was calculated as:

$$100 \cdot \left( \frac{\text{test} - \text{basal}}{\text{max} - \text{basal}} \right)$$

*Where: 'test' is any given data point, 'basal' is the mean basal IP<sub>x</sub> turnover, and 'max' is the E<sub>max</sub> to U-II.*

Typical disintegration per minute (DPM) values for basal and max, as defined above, were 377 and 5473 respectively.

#### *4.2.2 Results*

Concentration-response curves of inositol phosphate turnover to urantide and UFP-803 are shown in Figure 4.1 and Figure 4.2 respectively.

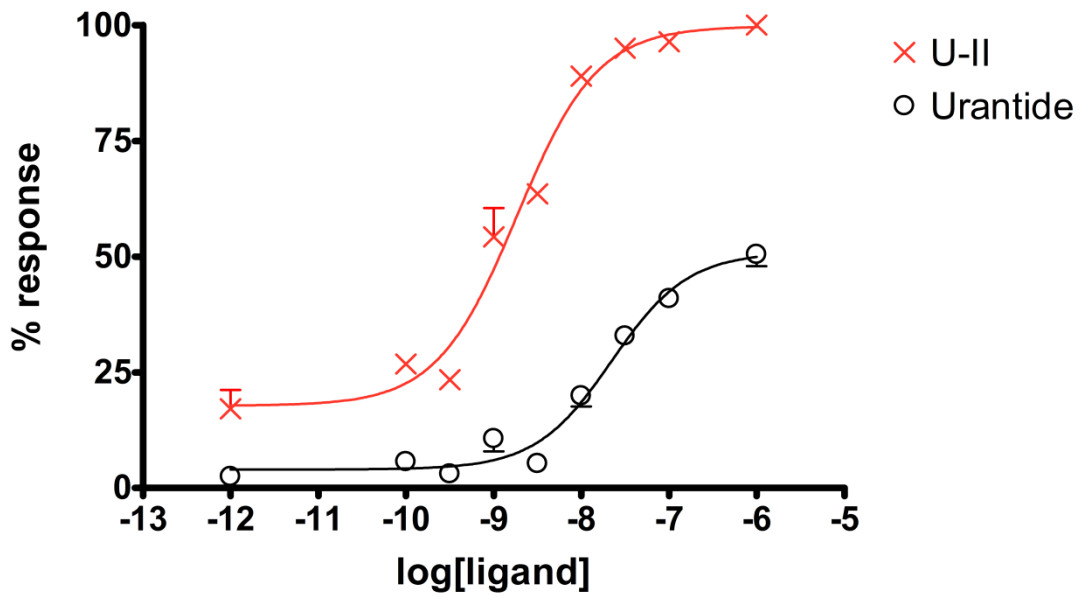


Figure 4.1. Concentration-response curves of inositol phosphate turnover to U-II and urantide in CHO<sub>h</sub>UT. Data are normalised to the fitted  $E_{max}$  of U-II, means  $\pm$ S.E.M, n=3.

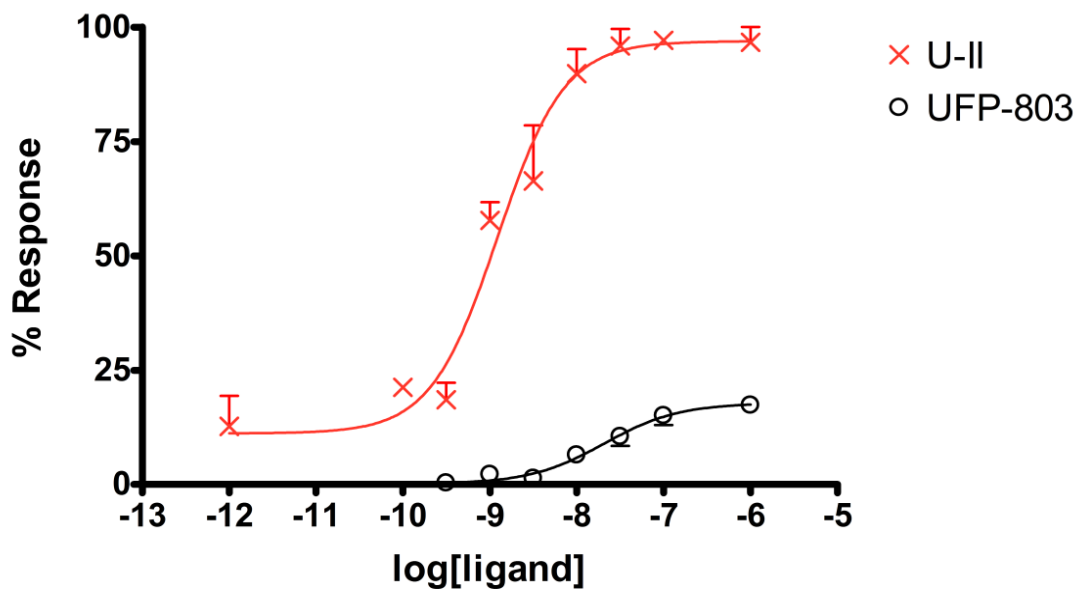


Figure 4.2. Concentration-response curves of inositol phosphate turnover to U-II and UFP-803 in CHO<sub>h</sub>UT. Data are normalised to the fitted  $E_{max}$  of U-II, means  $\pm$ S.E.M, n=3.

Calculated  $pEC_{50}$  and  $\alpha E_{max}$  values for U-II, urantide, and UFP-803 are given in Table 4.1.

**Table 4.1. pEC<sub>50</sub> and  $\alpha E_{\max}$  values for U-II, urantide, and UFP-803 as determined by inositol phosphate turnover studies in CHO<sub>h</sub>UT.**

<b>Ligand</b>	<b>pEC<sub>50</sub></b>	<b><math>\alpha E_{\max}</math></b>
U-II	8.81 ±0.10	1.0
Urantide	7.56 ±0.09	0.51
UFP-803	7.65 ±0.14	0.18

#### **4.2.3 Discussion**

U-II, urantide, and UFP-803 produced a concentration-dependent increase in [<sup>3</sup>H]IP<sub>x</sub> formation in CHO<sub>h</sub>UT. The pEC<sub>50</sub> of U-II in CHO<sub>h</sub>UT is in agreement with that already reported [112]. The pEC<sub>50</sub> of urantide in CHO<sub>h</sub>UT is higher than that previously reported (7.76x10<sup>-9</sup> reported by Camarda et al. [112]) however; this value was calculated from a calcium mobilisation assay in the same cell-line. The pEC<sub>50</sub> of UFP-803 in CHO<sub>h</sub>UT is approximately equal to that of urantide in this study. The  $\alpha E_{\max}$  values obtained for urantide and UFP-803 in this study are both lower than those previously reported (calculated from calcium mobilisation assays in the same cell-line [111, 112]).

In this assay (featuring a high UT receptor density), both urantide and UFP-803 behave as low potency partial agonists ( $\alpha E_{\max}$  of 0.51 and 0.18 respectively). The relative efficacies of these ligands are lower than those previously reported from calcium mobilisation assays in the same cell-line. This may be explained by the upstream vantage point of the inositol phosphate turnover assay used in this study.

### 4.3 Initial Antagonism studies

#### 4.3.1 *Methods*

CHO<sub>h</sub>UT cells were cultured for 48hrs in [<sup>3</sup>H]myo-inositol and then harvested as previously described (4.2.1). Once the cell suspensions had been equilibrated with LiCl, UFP-803 (1x10<sup>-6</sup>M final concentration) or equivolumetric buffer was added and the tubes were incubated for 15 min (37°C in a shaking water bath). CRCs were generated by adding U-II to each of the tubes (1x10<sup>-12</sup>M-1x10<sup>-5</sup>M final concentrations) and incubating for a further 15 min. The reactions were terminated in the same order that they were started by addition of 500µL of 1M tri-chloroacetic acid (TCA). Inositol phosphates were extracted and quantified as previously described (4.2.1).

#### 4.3.2 *Results*

CRCs to U-II in the absence and presence of 1x10<sup>-6</sup>M UFP-803 are shown in Figure 4.3.

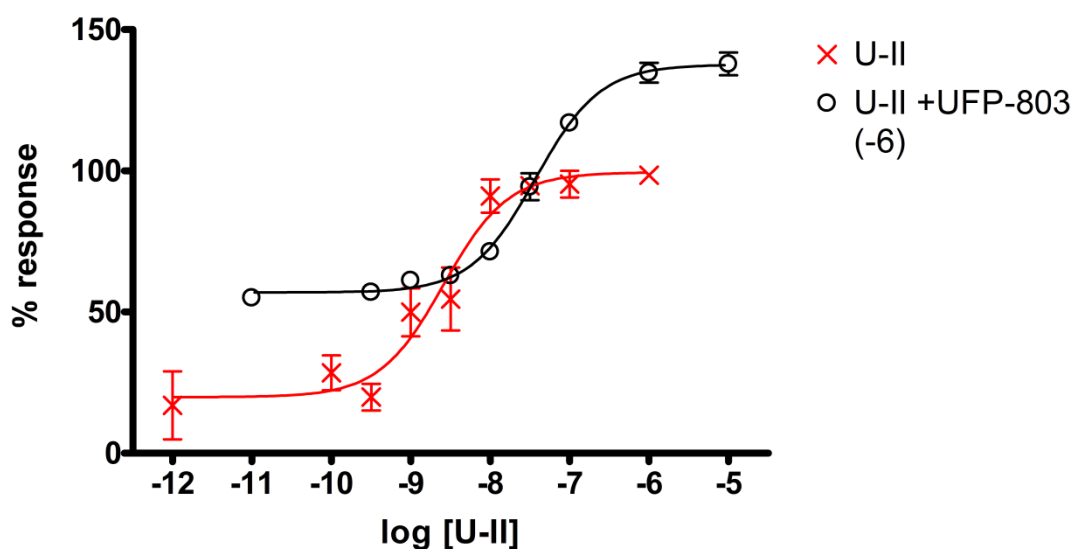


Figure 4.3. Concentration-response curves to U-II following pre-incubation for 15 min with 10<sup>-6</sup>M UFP-803 and equivolumetric buffer. Data are normalised to the maximum response generated by U-II, means ± S.E.M. n=3.

Calculated  $pEC_{50}$  and  $\alpha E_{max}$  values for U-II in the presence and absence of  $1 \times 10^{-6} M$  UFP-803 are given in Table 4.2.

**Table 4.2.  $pEC_{50}$  and  $\alpha E_{max}$  values for U-II in the presence and absence of  $1 \times 10^{-6} M$  UFP-803.**

<u>Condition</u>	<u><math>pEC_{50}</math></u>	<u><math>\alpha E_{max}</math></u>
Control	$8.59 \pm 0.15$	1.0
+UFP-803 (-6)	$7.43 \pm 0.05$	1.38

### 4.3.3 Discussion

U-II produced a concentration-dependent increase in  $[^3H]IP_x$  formation in  $CHO_hUT$ . Prior incubation of  $CHO_hUT$  with  $10^{-6} M$  UFP-803 for 15 min produced a rightward shift of the CRC to U-II by approximately one order of magnitude. Unexpectedly, the CRC which was produced in the presence of  $10^{-6} M$  UFP-803 was elevated on a baseline of over 50%  $E_{max}$  of U-II alone. Consequentially,  $\alpha E_{max}$  of U-II in the presence of  $10^{-6} M$  UFP-803 was determined to be 1.38 in this experimental setting. Considering the previously determined partial agonist activity of UFP-803 (4.2.2), it is likely that the elevated baseline in this study is produced by simple summation of successive responses to UFP-803 and U-II.

## 4.4 Time-course studies

### 4.4.1 Methods

In order to assess the effects of serial incubations (UFP-803/U-II) on  $[^3H]IP_x$  turnover in  $CHO_hUT$ , time-course studies were conducted.  $CHO_hUT$  cells were cultured for 48hrs in  $[^3H]$ myo-inositol and then harvested as previously described (4.2.1). Once the cell suspensions had been equilibrated with LiCl, U-II or UFP-803 ( $1 \times 10^{-6} M$  final concentration) was added and the tubes were incubated for between 5 and 45 min ( $37^\circ C$  in a shaking water bath).

#### 4.4.2 Results

Time-courses of [ $^3\text{H}$ ]IP $_x$  accumulation in response to  $10^{-6}\text{M}$  U-II or UFP-803 are shown in Figure 4.4. U-II and UFP-803 ( $10^{-6}\text{M}$ ) produced a time-dependent increase in [ $^3\text{H}$ ]IP $_x$  accumulation in CHO $_h$ UT. The association was linear for UFP-803 (runs departure from linearity test  $p>0.05$ ) and non-linear in the case of U-II (fit according to a hyperbolic equation), runs departure from model test  $p>0.05$ . Although somewhat ambiguous, the U-II-induced turnover of [ $^3\text{H}$ ]IP $_x$  appears to follow a linear relationship between 0-20 min, after which the curve quickly saturates.

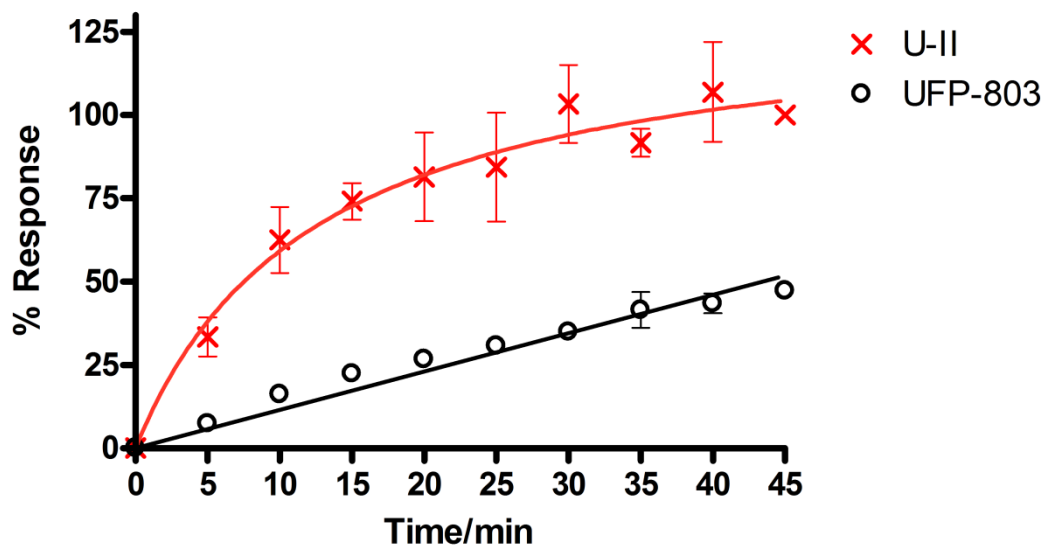


Figure 4.4. Time-course of [ $^3\text{H}$ ]IP $_x$  accumulation in response to  $10^{-6}\text{M}$  U-II or UFP-803. Data are expressed as means  $\pm$ S.E.M,  $n=3$ .

#### 4.4.3 Discussion

The linear UFP-803-induced turnover of [ $^3\text{H}$ ]IP $_x$  was approaching 25% at 15 min. This accounts for the elevated baseline of CRCs to U-II which include 15 min pre-incubation with  $10^{-6}\text{M}$  UFP-803 (4.3.2). The reason for saturation of U-II-induced [ $^3\text{H}$ ]IP $_x$  turnover is unclear. However, the lack of observable saturation in response to UFP-803 suggests that the phenomenon is not time-dependent *per se*. It is therefore likely that the

effect is dependent upon the size of the response generated (a product of the efficacy of the stimulus and the time of incubation). Making this assumption, a number of possible explanations can be proposed, including: depletion of intracellular [<sup>3</sup>H]-inositol species, feedback inhibition of the inositol phosphatases or receptor desensitisation. Regardless of the cause, the previous length of agonist incubation appears to be within the linear phase of [<sup>3</sup>H]IP<sub>x</sub> turnover and therefore remains experimentally valid. The use of a 15 min pre-incubation phase with experimental compounds exhibiting partial agonist activity is experimentally flawed.

## **4.5 Assay development**

### **4.5.1 *Methods***

In an attempt to address the issue of baseline elevation of CRCs in antagonism studies (4.3.2), a new ‘concurrent addition’ method was trialled against the existing ‘pre-incubation’ method. In the case of both methods, CHO<sub>h</sub>UT cells were cultured for 48hrs in [<sup>3</sup>H]myo-inositol and then harvested as previously described (4.2.1). Once the cell suspensions had been equilibrated with LiCl for 15 min, the two methods diverged with respect to their timings. The original method included addition of UFP-803, which was equilibrated for 15 min before addition of U-II. The new method involved adding a single solution, which contained both UFP-803 and U-II, and incubating for 15 min. The lysis of cells and extraction of the inositol phosphates remained unchanged in both methods (4.1). The timings of both methods are illustrated diagrammatically in Figure 4.5. In both methods, UFP-803 was included at a fixed concentration of 10<sup>-6</sup>M.

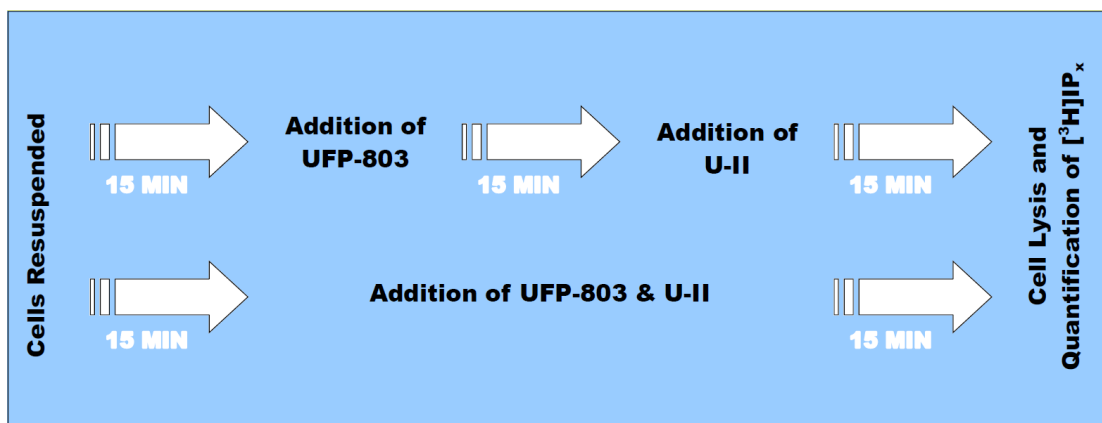


Figure 4.5. A diagrammatic representation illustrating the timings of the original 'pre-incubation' and new 'concurrent addition' methods.

#### 4.5.2 Results

Antagonism data acquired according to the two methods are shown in Figure 4.6. Addition of  $10^{-6}$ M UFP-803 produced a rightward parallel shift in the CRC to U-II in both methods. Raw  $E_{\max}$  (DPM) values for the control, concurrent, and pre-incubation methods were  $2074 \pm 116$ ,  $2014 \pm 119$ , and  $2759 \pm 45$  respectively.  $E_{\max}$  was significantly higher than control in the pre-incubated ( $p=0.043$ ) but not concurrent addition group. Application of the Gaddum-Schild equation yielded  $pK_B$  values of  $7.17 \pm 0.17$  and  $6.94 \pm 0.19$  for the pre-incubated and concurrent addition groups respectively ( $p > 0.05$ ).

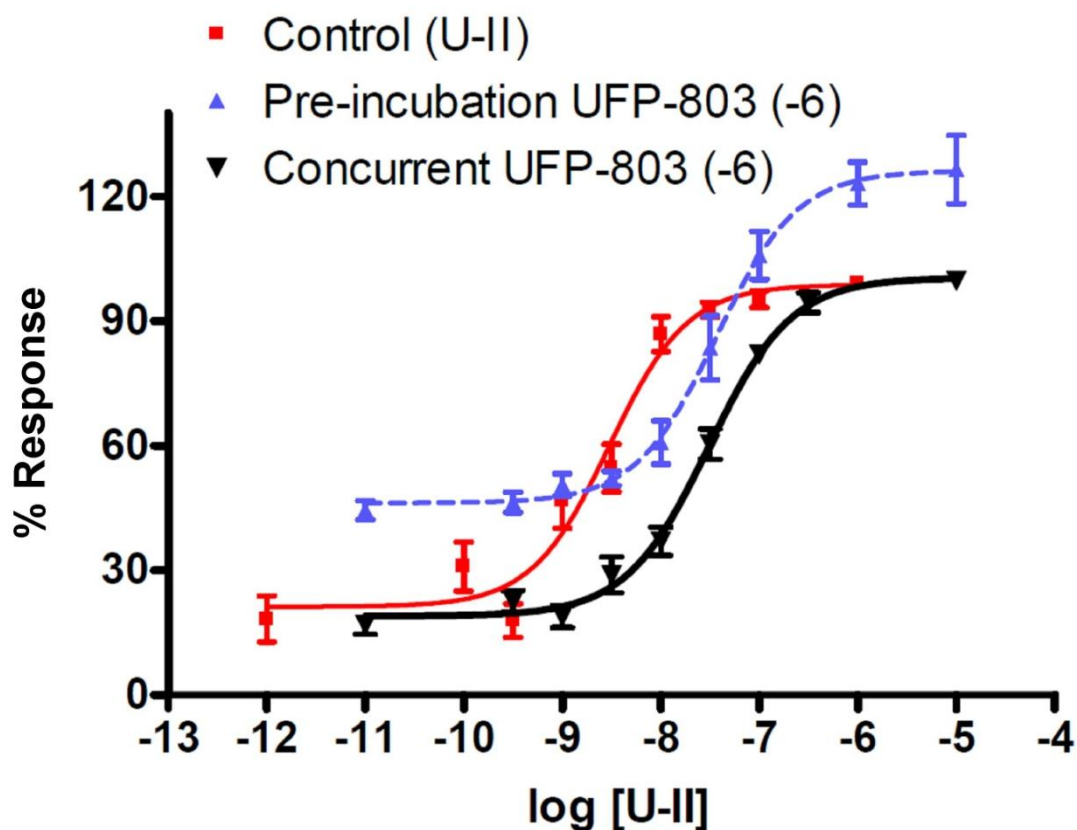


Figure 4.6. Concentration-response curves to U-II in the presence and absence of  $10^{-6}$ M UFP-803, added according to the pre-incubation and concurrent addition methods. Data are expressed as means $\pm$ S.E.M, n=3.

### 4.5.3 Discussion

These data clearly demonstrate that  $E_{max}$  is significantly over-estimated in antagonism studies which utilise the pre-incubation method. Moreover, this error can be removed by conducting such experiments according to the concurrent addition method. Estimated  $pK_B$  values obtained by application of the Gaddum-Schild equation, indicate that antagonist potency is not significantly affected by use of the concurrent addition method.

## **4.6 Refined antagonism studies**

### **4.6.1 *Methods***

CHO<sub>h</sub>UT cells were cultured for 48hrs in [<sup>3</sup>H]myo-inositol and then harvested as previously described (4.2.1). Once the cell suspensions had been equilibrated with LiCl, solutions were added which contained:

1. UFP-803, urantide ( $1 \times 10^{-6}$ M final concentration), or equivolumetric buffer
2. U-II ( $1 \times 10^{-12}$ M- $1 \times 10^{-5}$ M final concentrations)

In accordance with the 'concurrent addition' method (4.5.1) and the tubes were incubated for 15 min (37°C in a shaking water bath). The reactions were terminated in the same order that they were started by addition of 500µL of 1M tri-chloroacetic acid (TCA). Inositol phosphates were extracted and quantified as previously described (4.2.1).

### **4.6.2 *Results***

Antagonism studies data for urantide and UFP-803 are shown in Figure 4.7 and Figure 4.8 respectively.

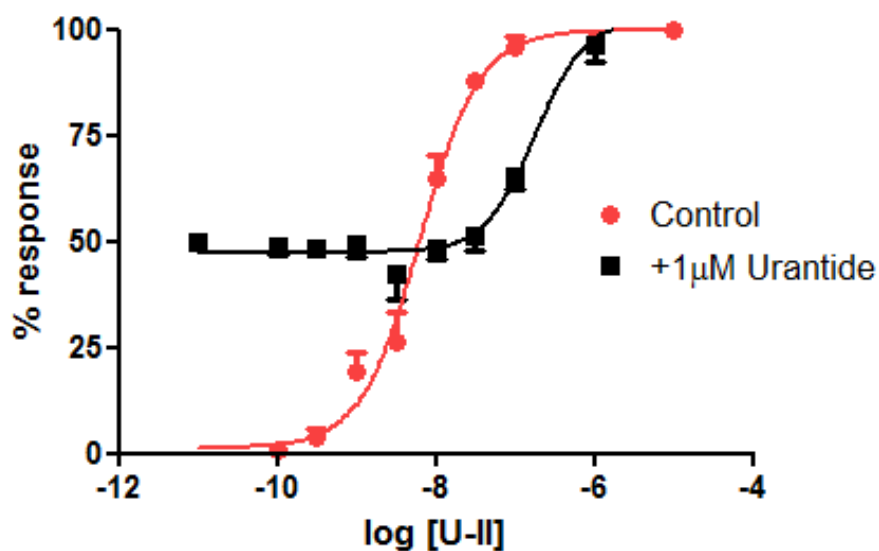


Figure 4.7. Concentration-response curves to U-II in the presence and absence of 1µM urantide. Data are expressed as means  $\pm$  S.E.M, n=3.

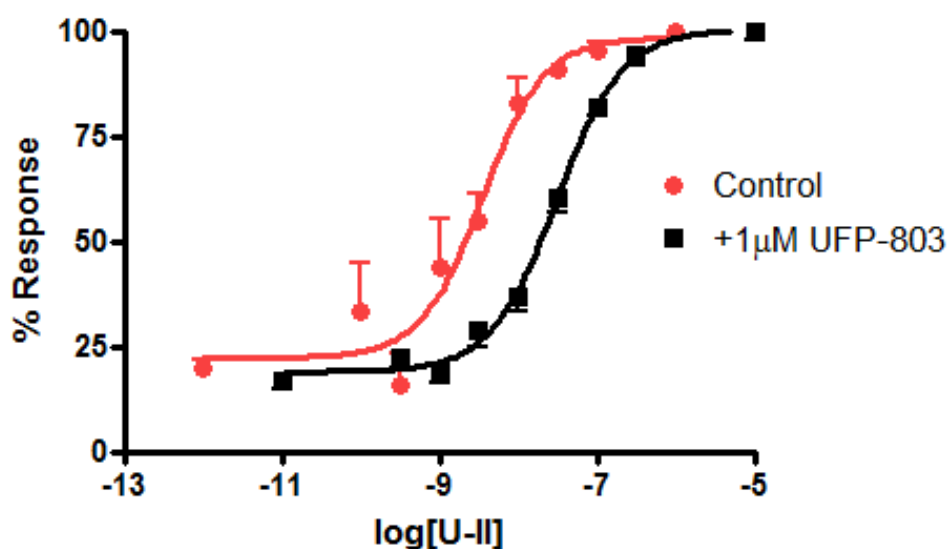


Figure 4.8. Concentration-response curves to U-II in the presence and absence of 1µM UFP-803. Data are expressed as means  $\pm$  S.E.M, n=3.

Both urantide and UFP-803 produced rightward parallel shifts in the CRC to U-II at  $10^{-6}$ M. Application of the Gaddum-Schild equation yielded  $pK_B$  values of  $7.45 \pm 0.08$  and  $6.93 \pm 0.19$  for urantide and UFP-803 respectively. The CRC to U-II produced in the

presence of  $10^{-6}$ M urantide was elevated on a baseline in accordance with its residual agonist activity. However the  $E_{\max}$  values for urantide and UFP-803 were not over-estimated in this optimised assay.

#### **4.6.3 Discussion**

Both urantide and UFP-803 produced rightward parallel shifts in the CRC to U-II at  $10^{-6}$ M, indicating that were both active as antagonists at the UT receptor in this assay. Estimated  $pK_B$  values suggest UFP-803 to be 3.3-fold less active as an antagonist at the UT receptor when compared with urantide. Despite this, UFP-803 remains a more attractive target over urantide due to its significantly reduced residual agonist activity (4.2.2).

# Chapter Five

## 5. Studies in an Ecdysone-inducible UT Cell-line

### 5.1 Production of an Ecdysone-inducible UT Cell-line

An ecdysone-inducible UT cell-line was produced using the ‘complete control mammalian expression system’ (Stratagene), comprising of:

1. **pEGSH vector**: a plasmid containing a multi cloning site, for insertion of the gene of interest, located downstream of a minimal heat shock promoter and ecdysone response element (see 1.9).
2. **ER-CHO cell-line**: Chinese Hamster Ovary cells stably transfected with the pERV3 vector, encoding the modified ecdysone and retinoid x receptors (see 1.9).

The human UT receptor cDNA insert was excised from cloning vector 70981-hUT (gifted by Dr. S. Douglas, GlaxoSmithKline) and ligated into pEGSH. The newly produced pEGSH-hUT vector was then transfected into ER-CHO, thus conferring ecdysone inducibility of the human UT receptor. Details of these methods and their development are included below. A restriction map for vector 70981 as well as the UT insert sequence are included in Appendix II.

### 5.2 Cloning of the pEGSH-UT Vector

#### 5.2.1 *Plasmid Digestions*

The UT receptor cDNA insert was excised from cloning vector 70981 by a two-stage digestion with EcoRI and EcoRV restriction endonucleases. The resultant 1190bp DNA sequence, consisting of the UT insert, possessed a single-stranded 5’ overhang produced by EcoRI digestion and a 3’ blunt end produced by EcoRV digestion (see Figure 5.1). A

6363bp linear sequence consisting of the remainder of the 70981 vector was also produced.

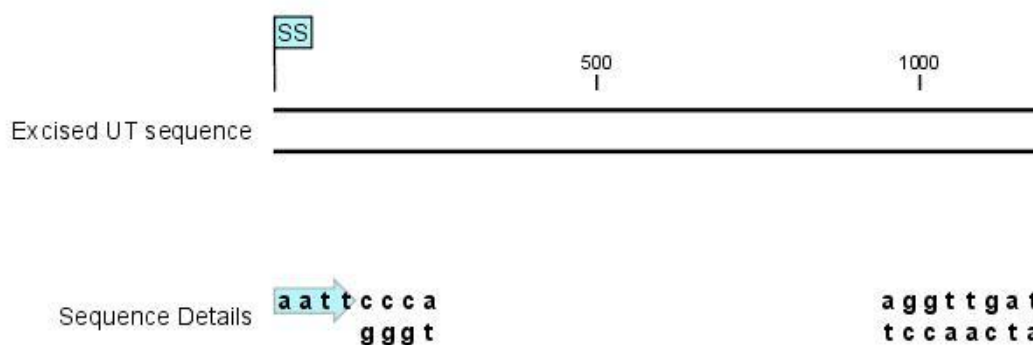


**Figure 5.1. Diagrammatic representation of the UT receptor cDNA insert which was excised from cloning vector 70981. The 5' single-stranded cohesive end (marked 'SS') and the 3' blunt end are illustrated.**

The pEGSH expression vector, into which the UT receptor insert was to be ligated, was subjected to a two-stage digestion with MunI and EcoRV restriction endonucleases. Digestion with EcoRV resulted in the production of a 5' blunt end, and digestion with MunI produced a 3' single-stranded cohesive end; complementary to that on the 5' end of the UT receptor insert. The two-stage digestion produced two linear DNA fragments of lengths 19bp and 4814bp.

### 5.2.1.1 Linearisation of Cloning Vector 70981-hUT

Cloning vector 70981 containing the UT receptor gene insert was diluted in distilled H<sub>2</sub>O to a concentration of 1µg µL<sup>-1</sup> and digested using EcoRI restriction endonuclease (Roche Applied Sciences), for 60min at 37°C as per Table 5.1.

**Table 5.1. Reaction setup for digestion of cloning vector 70981-hUT with EcoRI.**

<b>Reagent</b>	<b>Supplied By</b>	<b>Volume Added</b>
<b>70981 cloning vector (1µg µL<sup>-1</sup>)</b>	Gifted by S. Douglas of GlaxoSmithKline, USA	3µL
<b>EcoRI restriction endonuclease (10 units µL<sup>-1</sup>)</b>	Roche	2µL
<b>10X enzyme buffer H</b>	Roche	2µL
<b>dH<sub>2</sub>O</b>	-	13µL

Following digestion, the DNA was purified (5.2.2).

### 5.2.1.2 Excision of the UT Receptor cDNA Insert from 70981-hUT

DNA purified from 5.2.1.1 was digested using EcoRV restriction endonuclease (Roche Applied Sciences), for 60min at 37°C as per Table 5.2.

**Table 5.2. Reaction setup for digestion of cloning vector 70981-hUT with EcoRV**

<b>Reagent</b>	<b>Supplied By</b>	<b>Volume Added</b>
<b>Purified DNA from previous stage</b>	-	36 $\mu$ L (all recovered)
<b>EcoRV restriction endonuclease (10 units <math>\mu</math>L<sup>-1</sup>)</b>	Roche	2 $\mu$ L
<b>10X enzyme buffer B</b>	Roche	5 $\mu$ L
<b>dH<sub>2</sub>O</b>	-	7 $\mu$ L

Following digestion, the required DNA fragment was isolated by gel electrophoresis (5.2.3).

### 5.2.1.3 Linearisation of the pEGSH Vector

The pEGSH vector (Stratagene) was diluted in distilled H<sub>2</sub>O to a concentration of 1 $\mu$ g  $\mu$ L<sup>-1</sup> and digested using MunI restriction endonuclease (Fermentas), for 60min at 37°C as per Table 5.3.

**Table 5.3. Reaction setup for digestion of pEGSH with MunI**

<b>Reagent</b>	<b>Supplied By</b>	<b>Volume Added</b>
<b>pEGSH vector (1<math>\mu</math>g <math>\mu</math>L<sup>-1</sup>)</b>	Stratagene	3 $\mu$ L
<b>MunI restriction endonuclease (10 units <math>\mu</math>L<sup>-1</sup>)</b>	Fermentas	2 $\mu$ L
<b>10X enzyme buffer G</b>	Fermentas	2 $\mu$ L
<b>dH<sub>2</sub>O</b>	-	13 $\mu$ L

Following digestion, the DNA was purified (5.2.2).

#### 5.2.1.4 Second Digestion of the pEGSH Vector

DNA purified from 5.2.1.3 was digested using EcoRV restriction endonuclease (Roche), for 60min at 37°C as per Table 5.4.

**Table 5.4. Reaction setup for digestion of pEGSH with EcoRV**

<b>Reagent</b>	<b>Supplied By</b>	<b>Volume Added</b>
<b>Purified DNA from previous stage</b>	-	36µL (all recovered)
<b>EcoRV restriction endonuclease (10 units µL<sup>-1</sup>)</b>	Roche	2µL
<b>10X enzyme buffer B</b>	Roche	5µL
<b>dH<sub>2</sub>O</b>	-	7µL

Following digestion, the desired DNA fragment was isolated by gel electrophoresis (5.2.3).

#### 5.2.2 Purification of DNA Following Enzymatic Reactions

Between enzymatic reactions, it was necessary to purify the DNA in order to remove reactants, such as enzyme and buffer, which may have affected subsequent reactions. QIAquick PCR purification spin columns (Qiagen) were used for this purpose. This product comprises of a DNA adsorbing silica-membrane, suspended in a spin-column to fit a standard desktop microcentrifuge. Products from previous enzymatic stages were diluted in a high-salt buffer (Qiagen) to facilitate optimal binding of the DNA to the silica-membrane, while contaminants passed through the membrane during centrifugation. DNA bound to the silica-membrane was then washed in an ethanol containing buffer to remove any residual contaminants. DNA was eluted from the silica-membrane in a low-salt environment, achieved by incubating the membrane in a small volume of warm distilled water for 1 min, prior to centrifugation into a fresh Eppendorf tube (Figure 5.2).

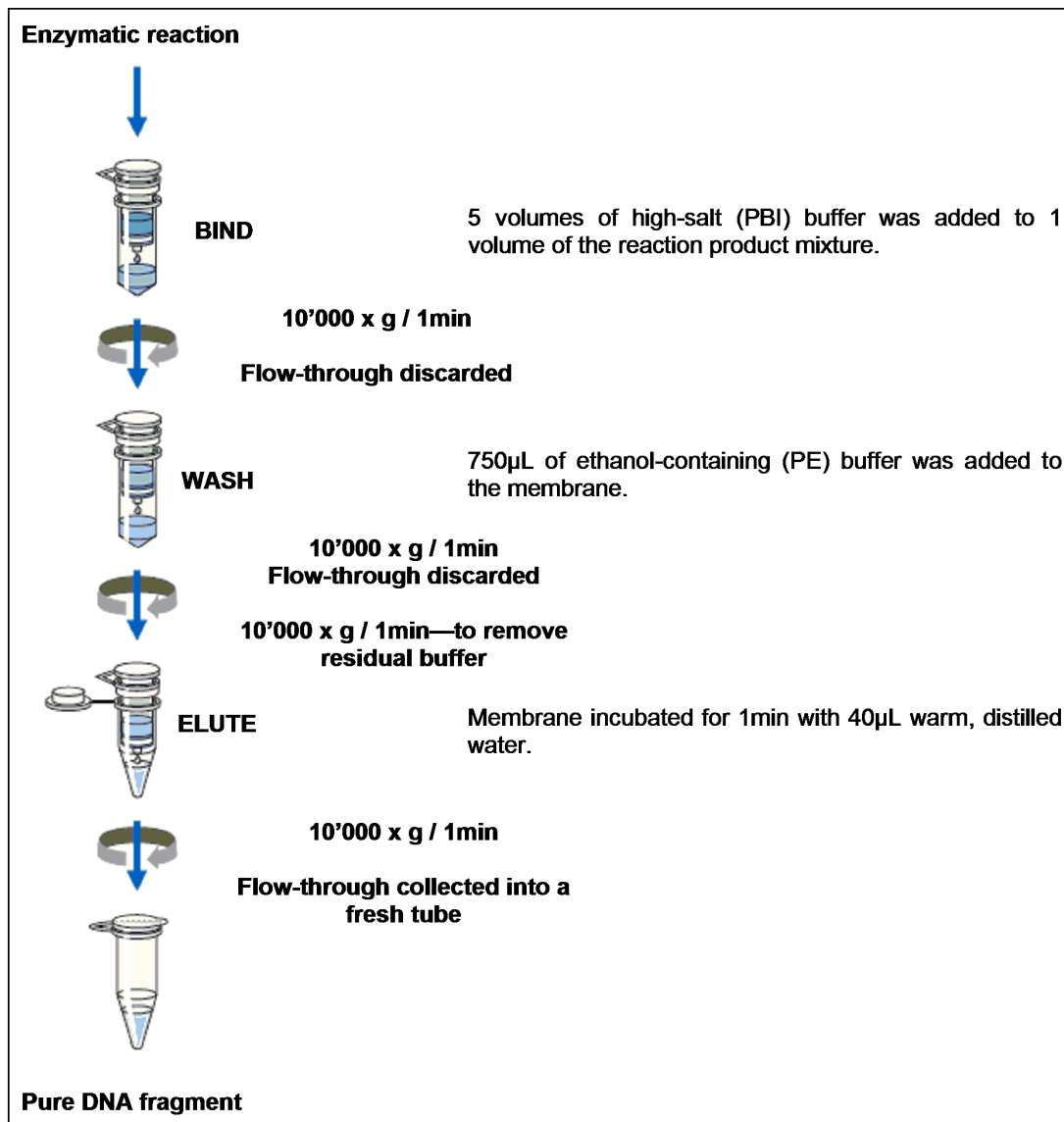


Figure 5.2. Diagrammatic overview of the procedure for purifying DNA following enzymatic reactions (as per manufacturer's instructions).

### 5.2.3 Agarose Gel Electrophoresis

Following digestion with two restriction endonucleases (5.2.1), the required fragments from both the 70981 and pEGSH cloning vectors were separated according to their molecular weight, by agarose gel electrophoresis. A 1% agarose gel was made by dissolving 1g of agarose powder (Sigma) in 100mL of hot 1x TE buffer (X50

concentrate, purchased from Sigma). The gel was placed in an electrophoresis tank and immersed in 1x TE buffer. Samples were mixed with loading dye (1 $\mu$ L per 5 $\mu$ L of sample) and carefully loaded into the wells. A potential difference of 100V/400mA was placed across the tank for approximately 60 min, until the loading dye had travelled half the length of the gel, towards the cathode. The gel was removed from the tank and immersed in a 0.5 $\mu$ g mL<sup>-1</sup> ethidium bromide solution (Sigma) for 10 min. DNA bands were visualised by brief exposure of the gel to long-wavelength UV light from a desktop UV lamp. The approximate molecular weight of visualised bands were determined by comparison to a 0.07-12.2kbp DNA ladder (Roche applied sciences), which had been run in a well adjacent to the samples. This allowed the correct identification of the DNA bands containing the UT receptor insert and linearised pEGSH vector. These were physically cut and removed from the gel using a scalpel blade and placed in separate Eppendorf tubes.

#### ***5.2.4 Purification of DNA from Agarose Gel***

DNA was isolated from the agarose gel by use of Ultrafree-DA spin tubes (Millipore), the physical arrangement of this product is illustrated in Figure 5.3.

The agarose gel slice containing the DNA of interest was finely chopped with a scalpel blade, loaded into the gel nebuliser and centrifuged at 5'000 x g for 10 min. Centrifugal force denatured the gel and forced the resultant slurry through the gel nebuliser. The agarose was retained by the microporous membrane, while the DNA passed freely through it and was collected in the vial below. The purified DNA was present in a large volume of buffer, and was therefore concentrated by use of a QIAquick spin tube (5.2.2).

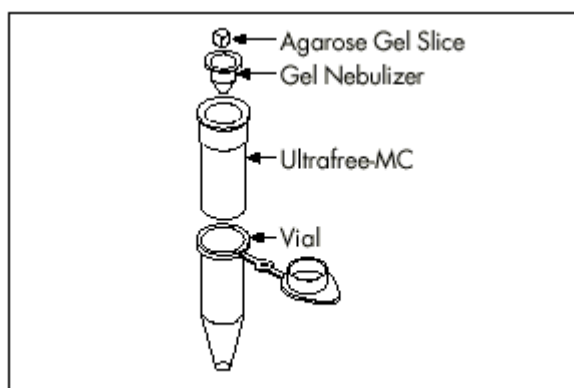


Figure 5.3. The Ultrafree-DA spin tube

### 5.2.5 DNA Ligation

DNA ligase catalyses the formation of covalent phosphodiester bonds in DNA with double-strand breaks [161], and was used to ligate the UT receptor insert to the linearised pEGSH cloning vector and then re-circularise it. T4 bacteriophage DNA ligase was used (Roche applied sciences), for 24 hrs at room temperature as per Table 5.5.

Table 5.5. Reaction setup for ligation of the UT receptor insert into linearised pEGSH.

<u>Reagent</u>	<u>Supplied By</u>	<u>Volume Added</u>
Linearised pEGSH vector	See 5.2.1	4 $\mu$ L
UT receptor insert	See 5.2.1	12 $\mu$ L
10X ATP-containing ligase buffer	Roche	2 $\mu$ L
T4 DNA ligase (10 units $\mu$ L <sup>-1</sup> )	Roche	2 $\mu$ L
dH <sub>2</sub> O	-	-

### 5.2.6 Prokaryotic Transformation

Competent prokaryotic cells such as *E.Coli* preferentially accept small pieces of circular, exogenous DNA [162]. Therefore, a prokaryotic transformation of the ligation products was performed. Competent *E.Coli* cells (Bioline) were removed from -80°C storage and thawed on wet ice, 70 $\mu$ L were pipetted into a Falcon 2059 tube with 5 $\mu$ L of

the ligation product and incubated on ice for 30 min to afford binding of the exogenous DNA to specific membrane proteins [162]. Tubes were placed in a preheated water bath set at 42°C for 45 sec, then replaced on ice for 2 min to induce internalisation of specific membrane proteins including those which had previously bound exogenous DNA [162]. 500µL SOC medium (Appendix I for composition) was added to the cells, which were incubated at 37°C for 60 min. This incubation allowed time for the ampicillin resistance gene (present within the pEGSH-UT construct) to be expressed. 200µL of the transformation products were spread onto LB agar plates (Appendix I for composition) containing ampicillin at 20µg mL<sup>-1</sup>. Colonies expressing the ampicillin resistance gene were grown overnight at 37°C / 5% CO<sub>2</sub>.

Twelve individual colonies from the LB agar plate were picked using sterile pipette tips and dropped into separate falcon tubes containing 1mL LB medium + ampicillin at 20µg mL<sup>-1</sup>. Tubes were placed in a shaking incubator overnight at 37°C.

### **5.2.7 Extraction and Purification of pEGSH-UT from *E.Coli***

DNA was extracted from the twelve *E.Coli* colonies by use of a ‘High Pure Plasmid Isolation Kit’ (Roche applied Science). *E.Coli* cells in suspension were transferred to Eppendorf tubes and sedimented at 13’000 x g for 1 min. The supernatant was discarded and the pellet was resuspended in 250µL suspension buffer + RNase. 250µL (alkaline) lysis buffer was added and the samples were incubated for 5 min during which time, cells were lysed and RNA was degraded. 350µL chilled binding buffer was added, which produced a flocculent precipitate consisting of ‘cell debris’, which was sedimented at 13’000 x g for 10 min. The supernatant was transferred to the membrane

of supplied High Pure filter tubes, which bind nucleic acids under high-salt conditions. Tubes were centrifuged at 13'000 x g for 1 min, the flow-through was discarded and the membrane was washed by addition of 700µL wash buffer II and centrifuging at 13'000 x g for 1 min. The DNA was eluted from the membrane in a low-salt environment by addition of 40µL warm dH<sub>2</sub>O and centrifuging into fresh Eppendorf tubes at 13'000 x g for 1 min.

### ***5.2.8 Restriction Analysis and Clone Selection***

The twelve DNA samples previously extracted (5.2.7) were screened for the presence of the pEGSH-UT vector. The pEGSH-UT sequence was entered into CLC combined workbench software and putative endonuclease restriction sites were analysed. Not-I was identified as an appropriate endonuclease with which to perform restriction analysis. A Not-I restriction map of the pEGSH-UT vector is given in Figure 5.5, illustrating the presence of two such sites within the UT insert and a further one within the pEGSH construct. A 'virtual gel' is given in Figure 5.4 which illustrates the expected number and molecular weight of bands on digestion of pEGSH-UT with Not-I.

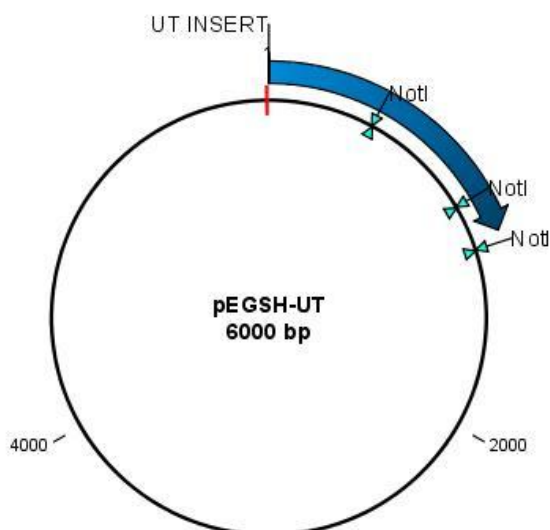


Figure 5.5. Diagrammatic representation of the pEGSH-UT vector. The hUT cDNA insert is illustrated with a blue arrow. NotI restriction sites are illustrated (three in total).

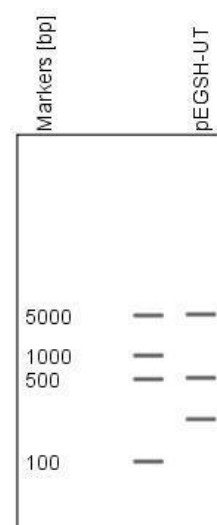


Figure 5.4. A 'virtual gel' produced by CLC combined workshop software illustrating the predicted digestion profile of pEGSH-UT by Not-I. Predicted fragments are of lengths 5263, 517 and 203 base pairs.

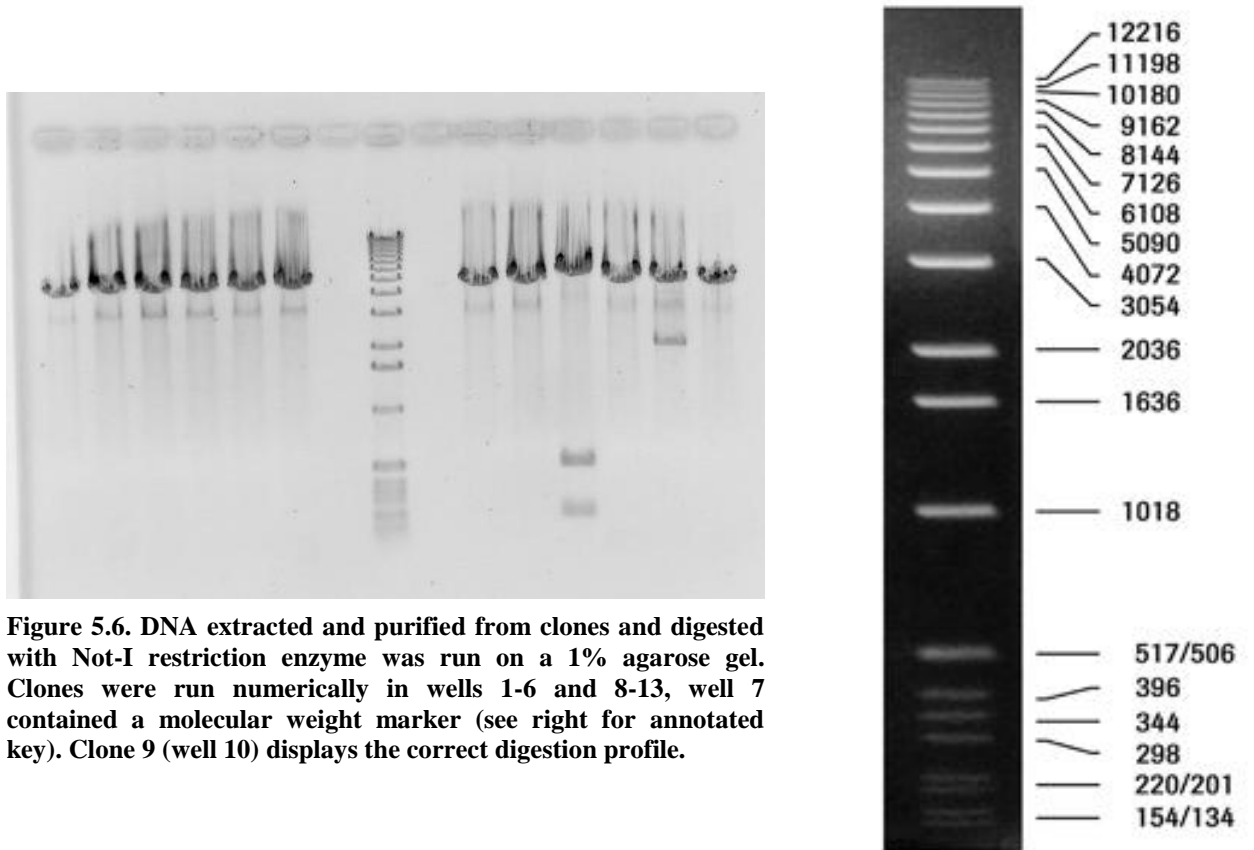
A sample of the purified DNA from the previous stage was digested with Not-I restriction endonuclease (New England Biolabs inc.) for 60 min at 37°C as per Table 5.6.

Table 5.6. Experimental arrangement for digestion of pEGSH-UT with Not-I restriction endonuclease.

Reagent	Supplied By	Volume Added
Purified DNA from previous stage	-	3µL
Not-I restriction endonuclease (10 units µL <sup>-1</sup> )	Biolabs	2µL
10X NE buffer 3	Biolabs	2µL
dH <sub>2</sub> O	-	13µL

Digested samples were electrophoresed on a 1% agarose gel and visualised by UV light in the presence of ethidium bromide (see 5.2.3). DNA from clones adopting the expected digestion profile and therefore inferring uptake of the pEGSH-UT vector were

identified. A photograph of the agarose gel was taken in a UV trans-illuminator (Figure 5.6).



**Figure 5.6.** DNA extracted and purified from clones and digested with Not-I restriction enzyme was run on a 1% agarose gel. Clones were run numerically in wells 1-6 and 8-13, well 7 contained a molecular weight marker (see right for annotated key). Clone 9 (well 10) displays the correct digestion profile.

### 5.2.9 DNA Sequencing

A 10 $\mu$ L sample of DNA purified from clone 9 (see 5.2.7) was submitted for DNA sequencing (PNAACL, University of Leicester) with forward and reverse primers designed to flank the multi-cloning site of pEGSH (Stratagene). The consensus sequence is included in Appendix II with comparison to the UT receptor gene insert. These data confirm clone 9 to express the engineered pEGSH-UT vector.

### ***5.2.10 Maxiprep of Clone 9***

200mL of LB broth was prepared and transferred to a large sterile conical flask. 5 $\mu$ L of the bacterial culture of clone 9 was added and placed in a shaking incubator overnight at 37 $^{\circ}$ C. The expanded bacterial culture was transferred to a polypropylene vial and sedimented at 6000 x g for 15 min at 4 $^{\circ}$ C. The supernatant was removed and the pellet was resuspended in 10mL buffer P1 (suspension buffer + RNase), to which 10mL of buffer P2 (alkaline lysis buffer) was added and incubated at room temperature for 5 min, affording cell lysis and degradation of cellular RNA. 10mL of chilled buffer P3 was added allowing the formation of a flocculent precipitate consisting of 'cell debris', which was sedimented at 20'000 x g for 30 min. The supernatant was transferred to the membrane of a supplied Qiagen-tip 500 tube (previously equilibrated with 10mL buffer QBT), which binds nucleic acids under high-salt conditions. The tube was allowed to void by gravity flow and the flow-through was discarded. The membrane was washed by addition of 2x30mL wash buffer QC and allowed to void by gravity flow. Bound DNA was eluted from the membrane in a low-salt environment by addition of 15mL buffer QF and was collected into a Falcon tube. Eluted DNA was precipitated in 10.5mL isopropanol and immediately sedimented at 15'000 x g for 30 min at 4 $^{\circ}$ C. The supernatant was removed and the pellet was washed in 5mL 70% ethanol, and sedimented for a further 10 min at 10'000 x g. The supernatant was decanted and the pellet was allowed to air-dry for 10 min, before resuspending it in 100 $\mu$ L of TE buffer. The DNA concentration was determined by UV spectrophotometry at 260nm, and the final concentration was adjusted to 1 $\mu$ g  $\mu$ L $^{-1}$ .

### **5.3 Mammalian Transfection**

#### **5.3.1 *Determining the sensitivity of ER-CHO to hygromycin-B***

The pEGSH-UT vector contains the hygromycin-B resistance gene to confirm eukaryotic transfection (see Appendix II), therefore it was necessary to determine the optimum concentration of Hygromycin-B to be included in the selection medium after transfection. This allows efficient removal of non-resistant clones from the cell culture without excessive use of the antibiotic. The optimum concentration is frequently defined as the minimum concentration required to produce 100% death of non-resistant clones after 8 and 14 days for initial selection and maintenance respectively (Stratagene).

6-well plates were seeded with ER-CHO cells and grown to 70% confluence overnight. Hygromycin-B was added to the wells at various concentrations (Table 5.7). Every 3-4 days a blinded observer, who was unaware of the concentration of hygromycin-B in each well, changed the media in the wells and estimated the percentage confluence of each well. The optimum concentration of hygromycin-B in ER-CHO was determined to be  $500\mu\text{g mL}^{-1}$  for initial selection and  $400\mu\text{g mL}^{-1}$  for maintenance. See Table 5.7 for summarised data of this experiment.

**Table 5.7. Time taken for increasing concentrations of hygromycin-B to completely kill cultures of ER-CHO cell-line**

<u>Hygromycin-B Concentration (<math>\mu\text{g mL}^{-1}</math>)</u>	<u>Estimated time of 100% Death (days)</u>
0	<i>Undetermined</i>
50	<i>Undetermined</i>
100	<i>Undetermined</i>
200	16
300	15
<b>400</b>	<b>12</b>
<b>500</b>	<b>8</b>
600	8
700	8
800	8
900	6
1000	4

### 5.3.2 Optimisation of transfection conditions

Fugene HD reagent was used for transfection of the pEGSH vector into ER-CHO. Prior to transfection, it was necessary to determine the optimum ratio of Fugene:DNA allowing the maximum possible number of transfects could be formed.

A twelve-well plate was seeded with ER-CHO cells and allowed to reach 70% confluence overnight. For determination of the optimum ratio for transfection, the pEGSH-luc vector (Stratagene) was used (gene of interest, luciferase). DNA/Fugene complexes were allowed to form at room temperature in serum-free cell medium (ratios 3:2-9:2). After 15 min, the transfection mixtures were added to the cell monolayers and incubated for 24 hours. Media were removed from the wells and replaced with medium supplemented with 10 $\mu\text{M}$  ponasterone-A in order to induce transcription of the luciferase gene in successful transfects.

After 20 hrs incubation, media were removed and the cell monolayers were washed three times in ice-cold PBS. Cells were layered in cell lysis buffer (Sigma) and incubated for 15 min on ice. Cells were scraped and collected into Eppendorf tubes

before sedimentation of the cell debris. The supernatants were transferred to a 96-well plate. Relative luciferase content was determined by fluorescence measurements made in a 96-well plate fluorescence reader on addition of luciferin to supernatants. Peak fluorescence values for each Fugene:DNA ratio are given in Figure 5.7. The optimum ratio was determined to be 8:2 (Fugene:DNA).

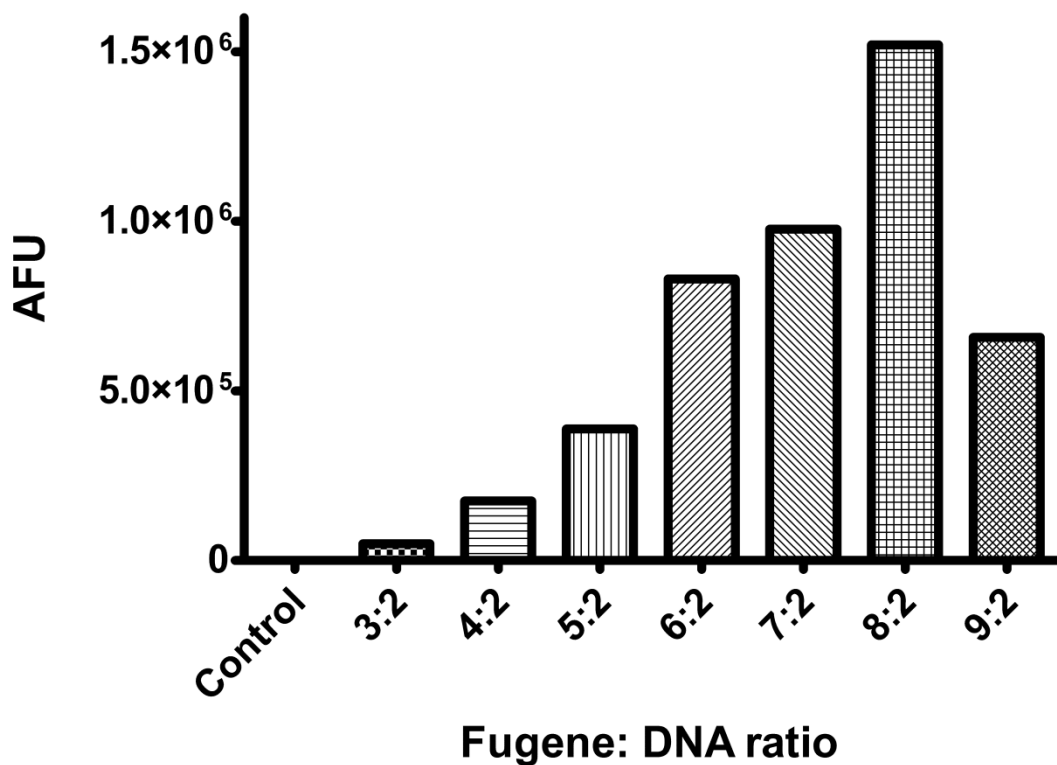


Figure 5.7. Peak fluorescence measurements made in ERCHO-luc transfects produced with varying Fugene:DNA ratios.

### 5.3.3 Transfection of pEGSH-UT into ERCHO

6-well plates were seeded with ER-CHO cells and grown to 70% confluence overnight. Fugene HD/pEGSH-UT complexes were formed for 15 min in serum-free medium at the predetermined ratio of 8:2. The complexes were added to cell monolayers and

incubated for 24 hours. Selection pressure was applied to the transfects by addition of  $500\mu\text{g mL}^{-1}$  hygromycin-B to each of the media. Selection pressure was maintained throughout regular media changes while the cultures were expanded to confluence.

## **5.4 Subcloning Techniques**

### **5.4.1 *Cloning cylinder method***

Polyclonal ER-CHO<sub>h</sub>UT cell populations were trypsinised and serially diluted into 10cm petri dishes. Colonies were allowed to form for between 14-21 days. Media were changed regularly and replaced with 50% conditioned medium from healthy ER-CHO cells in mid-log-phase. Individual colonies were isolated in the sparsest petri dishes, cell media were removed and the colonies isolated with a cloning cylinder held in place with sterile silicone grease. Colonies were subsequently trypsinised and transferred to single wells of a 24-well plate for expansion.

### **5.4.2 *Limiting dilution method***

Polyclonal ER-CHO<sub>h</sub>UT cell populations were trypsinised to a homogenous solution and quantified by use of a haemocytometer (2.2.5). Cells were diluted in suspension and transferred to 96-well plates at a calculated frequency of 0.1 cells well<sup>-1</sup>. Colonies were allowed to form for between 14-21 days. Wells were monitored twice-weekly for colony formation, the emergence of more than one colony per well led to the abandonment of that well. When large enough, suspected monoclonal colonies were expanded into 12-well plates before the procedure was repeated in order to increase the probability of monoclonality.

## **5.5 Screening of ERCHOhUT subclones**

Expression of the gene of interest is insertion site specific and it was therefore necessary to screen candidates in order to identify a monoclonal with the following characteristics:

- nominal expression of the gene of interest when un-induced
- high expression of the gene of interest when induced and;
- appropriate sensitivity of induction of the gene expression to both concentration of ponasterone-A and time of induction.

### **5.5.1 *Screening by PCR***

#### **5.5.1.1 *Methods***

Following adequate expansion, suspected monoclonal cells were seeded in 12-well plates and grown to 70% confluence overnight. The following day, media were removed from wells and replaced with medium supplemented with 5 $\mu$ M ponasterone-A or equivalent vehicle (ethanol). Monoclonal cells were induced for a total of 20 hrs prior to extraction of RNA with the mirVana™ miRNA isolation kit (Applied Biosystems), as previously described (2.5.2). RNA was quantified, DNase treated, and reverse transcribed as previously described (2.3). Taqman™ PCR was performed for hUT (GOI) and 18s (EC) in a duplex assay as previously described (2.8.2). Fold-increases in expression between the vehicle and ponasterone-treated monoclonal cells were calculated according to the  $\Delta\Delta C_t$  method, as a measure of genomic inducibility.

### 5.5.1.2 Results

Tabulated data acquired from PCR screening of 24 ERCHO<sub>h</sub>UT monoclones are given in Table 5.8. Of the 24 monoclones screened; 11 were UT negative after induction with ponasterone-A, 6 fell below the arbitrary threshold of 1.5-fold increase in UT expression following ponasterone treatment, thus leaving 7 candidates for functional characterisation (5.5.2).

**Table 5.8. Tabulated data acquired from PCR screening of ERCHO<sub>h</sub>UT monoclones.  $\Delta$ Ct values (hUT-18s) for each monoclonal are given in the induced state along with the fold change in UT expression after induction with 5 $\mu$ M ponasterone-A. 'Nd' indicates that UT mRNA was unamplified after 60 cycles of PCR. Highlighted entries are selected candidates for functional characterisation.**

<u>Monoclonal</u>	<u><math>\Delta</math>Ct (induced)</u>	<u>Fold change in UT expression</u>
1	Nd	-
2	Nd	-
3	Nd	-
4	17.49	3.01
5	15.82	1.56
6	Nd	-
7	13.69	4.41
8	Nd	-
9	Nd	-
10	11.64	2.01
11	Nd	-
12	20.69	0.60
13	Nd	-
14	Nd	-
15	16.7	7.47
16	Nd	-
17	12.16	0.25
18	15.85	0.44
19	16.79	0.67
20	16.08	1.58
21	26.00	0.29
22	15.73	0.46
23	17.26	2.49
24	Nd	-

## 5.5.2 *Functional screening*

### 5.5.2.1 *Methods*

Following screening by PCR (5.5.1), candidate monoclonal antibodies were seeded in 96-well plates and grown to near confluence over a 20 hr period in the presence of 5  $\mu$ M ponasterone-A or equivalent vehicle. The following day, media were removed from wells and cells were loaded with fura-2 as previously described. Fluorometric measurements were made in the NOVOstar plate-reader on injection of 1  $\mu$ M U-II as previously described (3.5.1). Injections of equivolumetric buffer and 10<sup>-3</sup>M ATP were included as negative and positive controls respectively. The difference in peak U-II-mediated fluorescence was evaluated between vehicle and ponasterone-treated monoclonal antibodies.

### 5.5.2.2 *Results*

A typical set of data, demonstrating the injection timing and intracellular calcium responses are given in Figure 5.8. Tabulated data for the seven candidate subclones are given in Table 5.9.

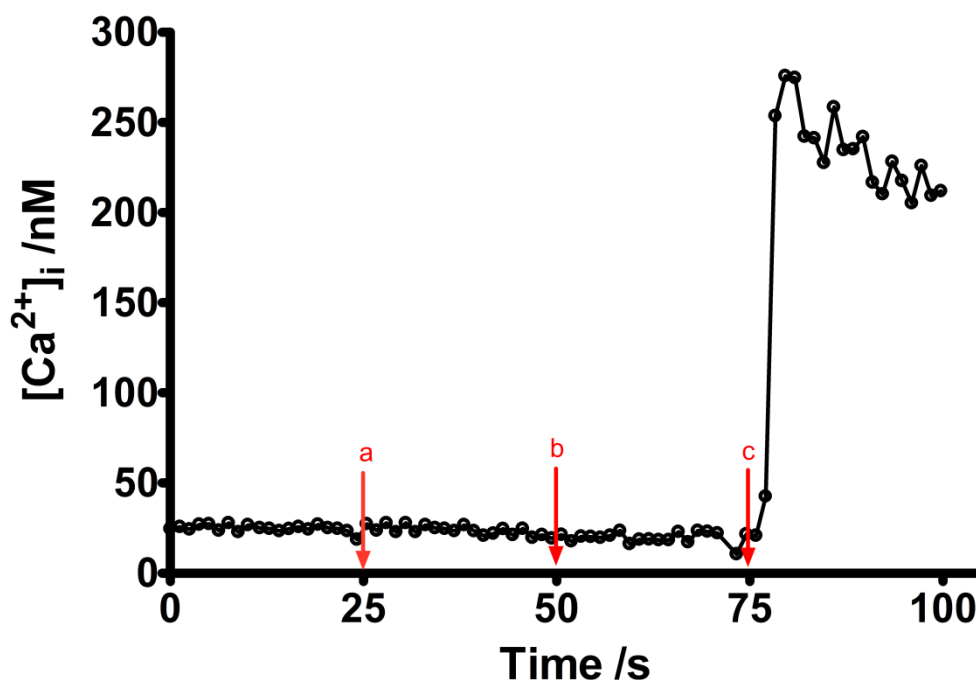


Figure 5.8. An example of data acquired during functional screening of an ERCHO<sub>h</sub>UT monoclonal. Intracellular calcium concentration is shown over a 100 sec period during which (a) buffer (negative control), (b) 10<sup>-6</sup>M U-II (test), and (c) 10<sup>-3</sup>M ATP (positive control) were injected.

Table 5.9. Tabulated data acquired from functional screening of ERCHO<sub>h</sub>UT subclones. ‘✓’ or ‘✗’ indicates whether or not a calcium transient was generated due to injection of buffer, 10<sup>-6</sup>M U-II, or 10<sup>-3</sup>M ATP in vehicle and ponasterone-treated candidates.

Candidate	Non-induced			Induced			Δ[Ca <sup>2+</sup> ] <sub>i</sub>
	Buffer	U-II	ATP	Buffer	U-II	ATP	
4	✗	✗	✓	✗	✗	✓	n/a
5	✗	✗	✓	✗	✗	✓	n/a
7	✗	✗	✓	✗	✗	✓	n/a
10	✗	✓	✓	✗	✓	✓	negligible
15	✗	✗	✓	✗	✗	✓	n/a
20	✗	✗	✓	✗	✗	✓	n/a
23	✗	✗	✓	✗	✗	✓	n/a

### 5.5.2.3 Discussion

The data obtained from both PCR (5.5.1) and functional (5.5.2) screening, indicate that no appropriate subclone was present in this cohort. Based solely on the PCR screen, the most attractive candidate was number 15 (due to the large fold-increase in UT expression following ponasterone treatment). Unfortunately, this subclone failed to produce any U-II-mediated response in the functional assay. This observation may be

explained by the relatively high  $\Delta C_t$  value obtained during PCR screening of this subclone (indicative of a low UT content even in the induced form).

The only subclone within this cohort to produce a U-II-mediated response was number 10. This subclone exhibited a 2-fold increase of UT mRNA on ponasterone treatment, however, no notable increase in calcium mobilisation was observed in the functional assay between the induced and non-induced forms.

*The data presented within this section are produced from a representative batch of 24 subclones. This batch accounts for less than 20% of the total number of subclones produced and screened. Data for all subclones has not been included within this thesis for reasons of brevity. However, the author would like to highlight the considerable time spent during the project at this stage.*

In-line with the above results, none of the subsequent subclones displayed the appropriate characteristics to warrant further characterisation. The main failing of all subclones was a lack of induction of UT expression at a *functional* level.

## 5.6 Troubleshooting

Following the failure to isolate an appropriate ERCHO<sub>h</sub>UT subclone, and in consultation with a representative from Stratagene, a number of potential problems were addressed (Table 5.10).

**Table 5.10. Approaches undertaken to identify the lack of UT induction in ERCHO<sub>h</sub>UT monoclonal lines.**

<b>Possible problem</b>	<b>Method</b>	<b>Outcome</b>
Ponasterone-A lacking efficacy	Second batch of ponasterone-A purchased and tested	No difference in UT induction was noted between the two batches of ponasterone-A
PCR assay not validated to measure changes in expression of an inducible cell line	An existing ecdysone-inducible cell-line (ERCHO <sub>h</sub> NOP) was assayed by PCR with and without ponasterone treatment	Changes in expression of the GOI were readily detectable by PCR. The efficacy of ponasterone was also validated
Hygromycin-B concentration too low during initial selection	A new batch of subclones was produced and selected with 1000µg mL <sup>-1</sup> of hygromycin-B	No appropriate subclones were obtained
ERCHO <sub>h</sub> UT plasmid degraded or contaminated	Plasmid re-sequenced	Sequence unchanged from initial DNA sequencing
Presence of a Kozak initiation sequence and stop codon	DNA sequencing data analysed	Both sequences were present in the DNA sequence
UT protein not compatible with the biology of CHO cells	-	Fully functional stable CHO <sub>h</sub> UT transfects already characterised

After the above potential problems failed to resolve the issue of the lack of UT induction in ERCHO<sub>h</sub>UT monoclonal lines, it was agreed that the most likely problem still remaining pertained to the ERCHO cell-line originally supplied by Stratagene. After considerable time was expended during the troubleshooting procedure, a new batch of ER-CHO cells was supplied and tested against the original batch.

### 5.6.1 *ER-CHO cell-line validation*

#### 5.6.1.1 *Methods*

The two batches of ER-CHO cells were seeded in 6-well plates and grown to near confluence overnight. Media were removed from the monolayers and rinsed with ice-

cold PBS. The cells were then lysed with 1mL of TRI reagent and total RNA was extracted as previously described (2.5.1). RNA was then quantified and 10µg was DNase treated and reverse transcribed as previously described. PCR was performed using primers specific to the ecdysone receptor (normalised to the EC 18s).

In a separate experiment, both batches of cells were seeded in 6-well plates and allowed to establish for 6 hrs. Cells were transfected with the pEGSH-UT vector as previously described (5.3.3) and allowed to recover overnight. The following day, media were removed from the transient transfects and replaced with medium supplemented with 5µM ponasterone-A or equivalent vehicle. After 20 hrs, media were removed and cell monolayers were rinsed with ice-cold PBS and lysed with 1mL of TRI reagent. Total RNA was extracted as previously described (2.5.1). RNA was then quantified and 10µg was DNase treated and reverse transcribed as previously described. PCR was performed to quantify the relative expression of UT (EC 18s).

#### *5.6.1.2 Results*

Data demonstrating the expression of the ecdysone receptor in the two batches of ER-CHO are given in Figure 5.9. The ecdysone nuclear receptor displayed a 3.25-fold higher expression in the new batch of cells when compared to the original batch. Data showing the expression of UT mRNA in transient ERCHOhUT transfects produced from both batches of ER-CHO cells are given in Figure 5.10 in both ponasterone and vehicle-treated forms.

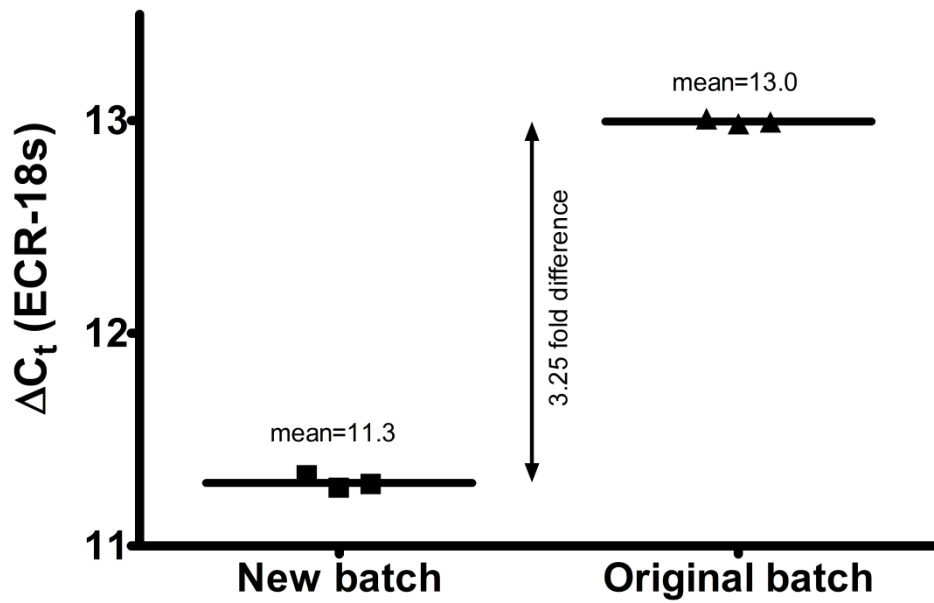


Figure 5.9. Expression of the ecdysone receptor mRNA in the two batches of ER-CHO cells, n=3.

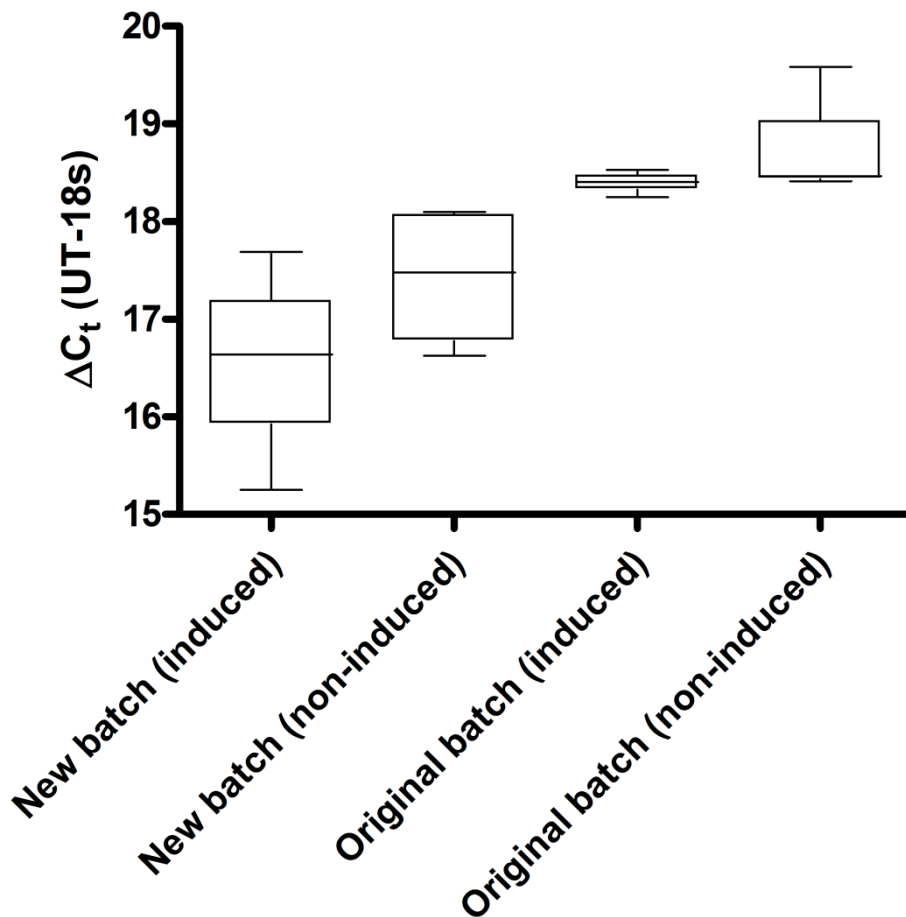


Figure 5.10. Box and whiskers plot of UT mRNA in ERCHOhUT transient transfects produced from both batches of ERCHO cells. Data are shown for both the ponasterone and vehicle-treated forms, n=4.

The original batch of ER-CHO cells had median $\pm$ IQR  $\Delta C_t$  values of 18.41 $\pm$ 0.14 and 18.47 $\pm$ 0.60 for the induced and non-induced forms respectively. The new batch of ER-CHO cells had median $\pm$ IQR  $\Delta C_t$  values of 16.67 $\pm$ 1.27 and 17.48 $\pm$ 1.29 for the induced and non-induced forms respectively.

### *5.6.1.3 Discussion*

These data demonstrate that the two batches of ER-CHO cells possessed different characteristics. Firstly, the expression of the ecdysone nuclear receptor (ECR) mRNA was significantly higher in the new batch of cells ( $P < 0.05$ ), as determined by RT-qPCR. Secondly, transient ERCHO<sub>h</sub>UT transfects produced from the two batches of cells induced UT expression with different characteristics. The median  $\Delta C_t$  values obtained from the induced and non-induced forms of the original batch of cells were virtually identical. Moreover, the distribution of data around the medians was limited for the original batch of cells. In contrast, the median  $\Delta C_t$  values obtained from the induced and non-induced forms of the new batch of cells, suggested a slightly higher expression of UT in the induced form (approximately 1.8-fold). Moreover, the distribution of data around the medians was far greater in the new batch of cells for both the induced and non-induced forms.

These data suggest that the new batch of cells possess a greater capacity to induce UT expression when compared to the original batch. Although the induction of UT expression was small within the new batch of cells, this may be explained by the use of a polyclonal cell-line in this assay. Furthermore, it is anticipated that monoclones carefully selected from such a polyclonal stock should exhibit suitable induction characteristics. The reason for lack of induction of gene expression in the original batch

is unclear but may be due to the reduced expression of ECR when compared to the new batch.

## **5.7 Final production of an ERCHO<sub>h</sub>UT cell-line**

### ***5.7.1 Methods***

6-well plates were seeded with ER-CHO cells and grown to 70% confluence overnight. Fugene HD/pEGSH-UT complexes were formed for 15 min in serum-free medium at the predetermined ratio of 8:2. The complexes were added to cell monolayers and incubated for 24 hours. Selection pressure was applied to the transfects by addition of 500 µg mL<sup>-1</sup> hygromycin-B. Selection pressure was maintained throughout regular media changes.

Monoclones were obtained through two rounds of subcloning by the limiting dilution method, as previously described (5.4.2). Once expanded, 24 monoclones were screened by RT-qPCR as previously described (5.5.1).

### ***5.7.2 Results***

Tabulated data acquired from PCR screening of 24 ERCHO<sub>h</sub>UT monoclones are given in Table 5.11. Of the 24 monoclones screened, 9 fell below the arbitrary threshold of 1.5-fold increase in UT expression and it was not possible to calculate the fold-increase in UT expression in 2 monoclones. Two monoclones were selected from the remaining 13 for functional characterisation, primarily due to time constraints (highlighted entries 2 and 21).

**Table 5.11. Tabulated data acquired from PCR screening of ERCHO<sub>h</sub>UT monoclones.  $\Delta$ CT values (hUT-18s) for each monoclonal are given in the induced state along with the fold change in UT expression after induction with 5 $\mu$ M ponasterone-A. 'n/a' indicates that UT mRNA was unamplified after 60 cycles of PCR in the non-induced form and it was therefore impossible to calculate a fold-change. Highlighted entries are selected candidates for further characterisation.**

<b>Monoclonal</b>	<b><math>\Delta</math>CT (induced)</b>	<b>Fold change in UT expression</b>
1	13.3	2.0
<b>2</b>	<b>11.9</b>	<b>39.4</b>
3	17.2	13.4
4	22.0	2.4
5	16.4	1.1
6	15.5	2.2
7	20.2	0.9
8	18.2	1.0
9	15.5	2.4
10	18.5	0.9
11	17.2	0.9
12	15.2	6.6
13	16.0	4.5
14	19.9	4.4
15	32.0	n/a
16	23.2	0.04
17	15.6	2.0
18	17.1	6.7
19	28.6	n/a
20	16.0	0.9
<b>21</b>	<b>11.8</b>	<b>42.5</b>
22	15.6	2.1
23	15.3	0.6
24	16.3	0.8

## **5.8 Functional screening of ERCHO<sub>h</sub>UT**

### **5.8.1 *Methods***

ERCHO<sub>h</sub>UT candidates 2 and 21 (previously identified from PCR screening) were seeded in T75 tissue culture flasks and grown to 70% confluence overnight. The following day, media were removed from flasks and replaced with medium supplemented with 5 $\mu$ M ponasterone A or equivalent vehicle. Cell cultures were incubated for 20hrs prior to functional characterisation, as per the single cuvette method, as previously described (2.10). Determinations were made on addition of 10<sup>-6</sup>M U-II in both the induced and non-induced forms of the monoclonal candidates.

### 5.8.2 Results

Typical datasets demonstrating functional characterisation of monoclonal candidates 2 and 21 are given in Figure 5.11 and Figure 5.12 respectively.

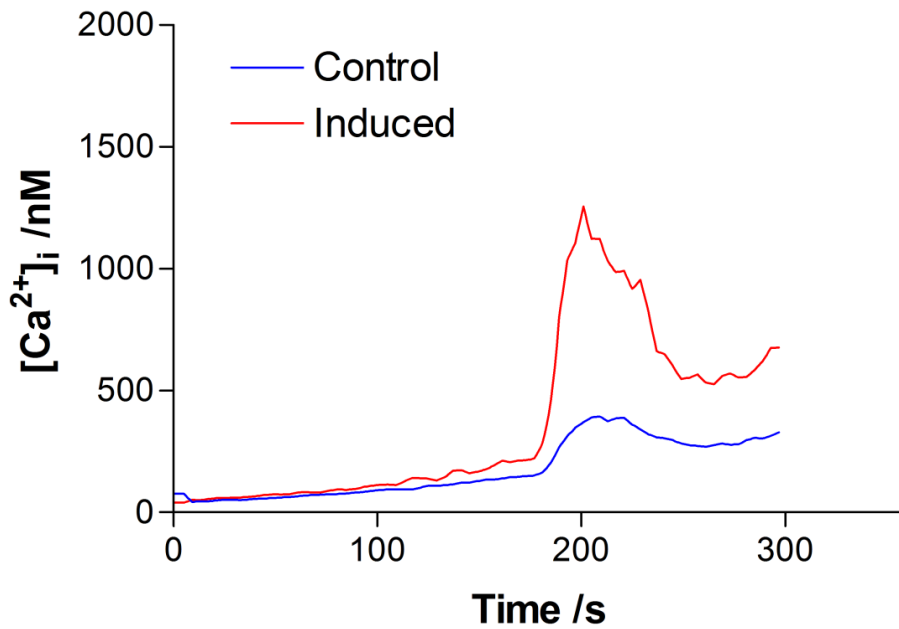


Figure 5.11. A typical dataset demonstrating functional characterisation of monoclonal candidate 2.

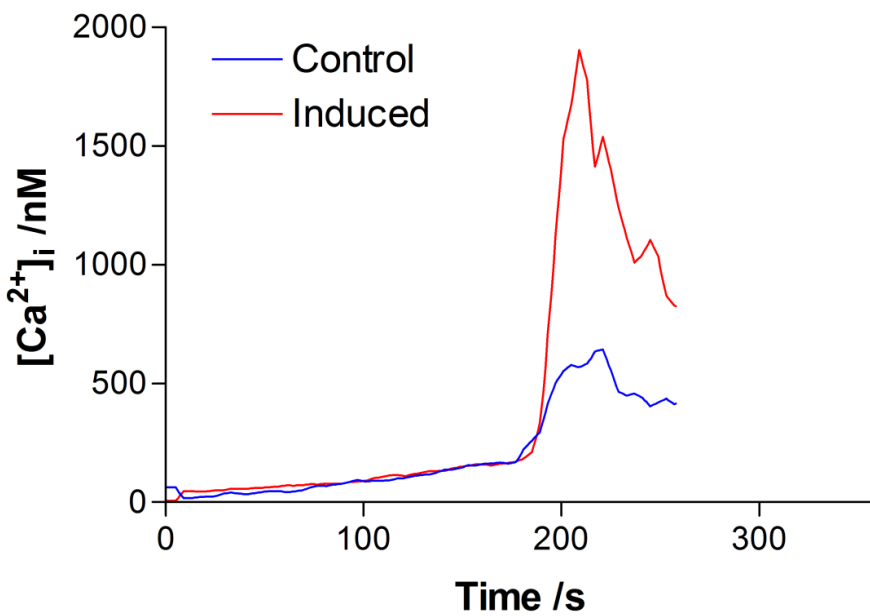


Figure 5.12. A typical dataset demonstrating functional characterisation of monoclonal candidate 21.

Candidates 2 and 21 both displayed an increase in  $[Ca^{2+}]_i$  in response to  $10^{-6}M$  U-II in the vehicle-treated samples (mean  $\pm$  S.E.M peak  $[Ca^{2+}]_i = 388 \pm 7$  and  $646 \pm 2$  respectively,  $n=3$ ). In candidates 2 and 21 which had been treated with  $5\mu M$  ponasterone-A for 20 hrs, the mean peak  $[Ca^{2+}]_i$  were  $1184 \pm 72$  and  $1803 \pm 103$  respectively ( $n=3$ ). The percentage increases in U-II-mediated  $[Ca^{2+}]_i$  between vehicle and ponasterone-treated samples were 205% and 179% for clones 2 and 21 respectively.

### **5.8.3 Discussion**

These data demonstrate that ERCHO<sub>h</sub>UT subclones 2 and 21 increased U-II-mediated  $[Ca^{2+}]_i$  following incubation with  $5\mu M$  ponasterone-A for 20 hrs, suggestive of increased UT expression. Peak U-II-mediated  $[Ca^{2+}]_i$  was lower in clone 2 when compared with clone 21 both in the induced and non-induced samples. Despite this, the percentage increase in U-II-mediated  $[Ca^{2+}]_i$  between vehicle and ponasterone-treated samples was highest in clone 2. Collectively, these findings may suggest that clone 2 has a greater sensitivity to ponasterone-A than clone 21. Moreover, the absolute level of UT 'leak' is also lower in clone 2 making this clone the most attractive identified.

Despite the ability of clones 2 and 21 to induce expression of UT, the level of non-induced expression was considered to be too high. Primarily for this reason and for the considerable length of time expended, no further data were obtained with this model of altering UT expression. Despite this, the above data demonstrate that the pEGSH-UT plasmid had been correctly engineered and that an appropriate ERCHO<sub>h</sub>UT clone might be obtained by use of the new batch of ERCHO cells.

# Chapter Six

## **6. siRNA-mediated RNA interference studies**

Studies were performed in CHO<sub>h</sub>UT, into which siRNAs specific to the UT mRNA were transfected to knockdown expression. Background information pertaining to siRNA-mediated RNA interference (RNAi) is given in 1.10. siRNA transfection was afforded by an RNA-specific transfection reagent (siPORT™ amine transfection reagent (Ambion)) and knockdown was assayed 48 hrs afterwards by RT-qPCR (genomic studies) and with a calcium mobilisation assay (functional studies). Optimisation of the transfection conditions is usually necessary to ensure that maximum knockdown is achieved whilst minimising transfection reagent-mediated cytotoxicity. In this instance however, a transfection protocol had previously been optimised and published by the manufacturer; serving as a starting point in this study (Ambion).

### **6.1 A trial of the supplied transfection protocol**

#### ***6.1.1 Methods***

This experiment served as a ‘proof of concept’ in order to test our theory that the degree of UT knockdown may be experimentally controlled by the concentration of siRNA in the preparation. A pre-validated positive control siRNA was used for this purpose which targeted the ubiquitously expressed GAPDH mRNA.

CHO<sub>h</sub>UT were transfected according to a ‘reverse transfection’ procedure, in which the transfection complexes were formed in wells of a 96-well plate prior to the cell suspension being added to the wells (Ambion). CHO<sub>h</sub>UT cells were trypsinised and adjusted to the required density (6000 cells well<sup>-1</sup> in the final assay) in a sterilin tube, the cell suspension was maintained at 37°C/5%CO<sub>2</sub> while the transfection complexes

were formed. Transfection complexes were allowed to form for 10 min at room temperature (10 $\mu$ L of siRNA + 10 $\mu$ L of diluted transfection reagent in serum-free medium). The CHO<sub>h</sub>UT cell suspension was then added to each of the wells containing a transfection mixture (180 $\mu$ L containing 6000 cells). Cells were incubated at 37°C / 5% CO<sub>2</sub> for a total of 48hrs and the media were replaced with fresh growth medium after 24hrs.

After 48hrs, media were removed and cell monolayers were rinsed three times with ice-cold PBS. cDNA was obtained by use of the cells-to-CT™ gene expression kit (Ambion) as previously described (2.5.3). GAPDH mRNA expression was assayed by TaqMan™ PCR as previously described (2.4.2). GAPDH expression was normalised to the endogenous control 18s. A negative control siRNA (limited sequence similarity to known genes) was included at each of the concentrations used, for the purpose of calculating  $\Delta\Delta C_t$  values (paired wells).

### **6.1.2 Results**

A CRC of GAPDH percentage-knockdown is given in Figure 6.1. The maximum and minimum GAPDH knockdown achieved were 92.9% and 6.8% obtained with 10<sup>-8</sup> and 10<sup>-12</sup>M siRNA respectively. The calculated EC<sub>50</sub> value was 2.98x10<sup>-10</sup>.

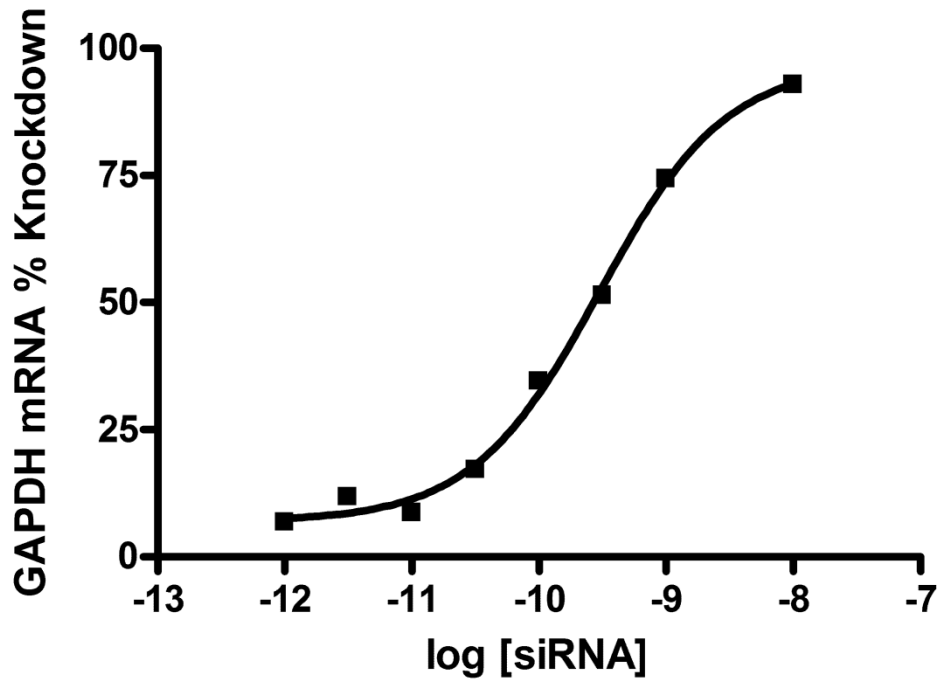


Figure 6.1. A concentration-response curve of GAPDH knockdown in siRNA-transfected CHO<sub>h</sub>UT cell-line (n=1).

### 6.1.3 Discussion

This experiment succeeded as a proof of concept, demonstrating that siRNA-mediated knockdown may be controlled by the concentration of transfected siRNA. Moreover, the range of mRNA knockdown was large and the model possessed appropriate sensitivity to [siRNA]. This experiment utilised the pre-validated protocol provided by the manufacturer (Ambion), which recommended a seeding density of 6000 cells well<sup>-1</sup>. In order to allow [Ca<sup>2+</sup>]<sub>i</sub> measurements to be made following siRNA transfection, it was necessary to increase the cell seeding density to 20,000 cells well<sup>-1</sup> (6.2).

## **6.2 Optimising cell number for siRNA studies**

This experiment compared how the cell seeding density affected the percentage-knockdown of GAPDH mRNA. Two seeding densities were compared: the recommended density of 6000 cells well<sup>-1</sup> (Ambion) and 20,000 cells well<sup>-1</sup>, the density required to make [Ca<sup>2+</sup>]<sub>i</sub> measurements for functional assays.

### **6.2.1 *Methods***

siRNA transfection complexes were formed as previously described (6.1.1) at a fixed final siRNA concentration of 10<sup>-8</sup>M. Following formation of the complexes, 180µL of each of the cell suspensions were added yielding 6000 and 20,000 cells well<sup>-1</sup>. Media were replaced after 24hrs and cDNA was obtained by use of the cells-to-CT™ gene expression kit (Ambion) as previously described (2.5.3). GAPDH mRNA expression was assayed by TaqMan™ PCR as previously described (2.4.2). GAPDH expression was normalised to the endogenous control 18s. ΔC<sub>t</sub> values were normalised to that of the negative control siRNA (10<sup>-8</sup>M).

### **6.2.2 *Results***

Data demonstrating the remaining GAPDH mRNA expression following siRNA-mediated RNA interference is given in Figure 6.2 for wells seeded with 6000 and 20,000 cells well<sup>-1</sup>.

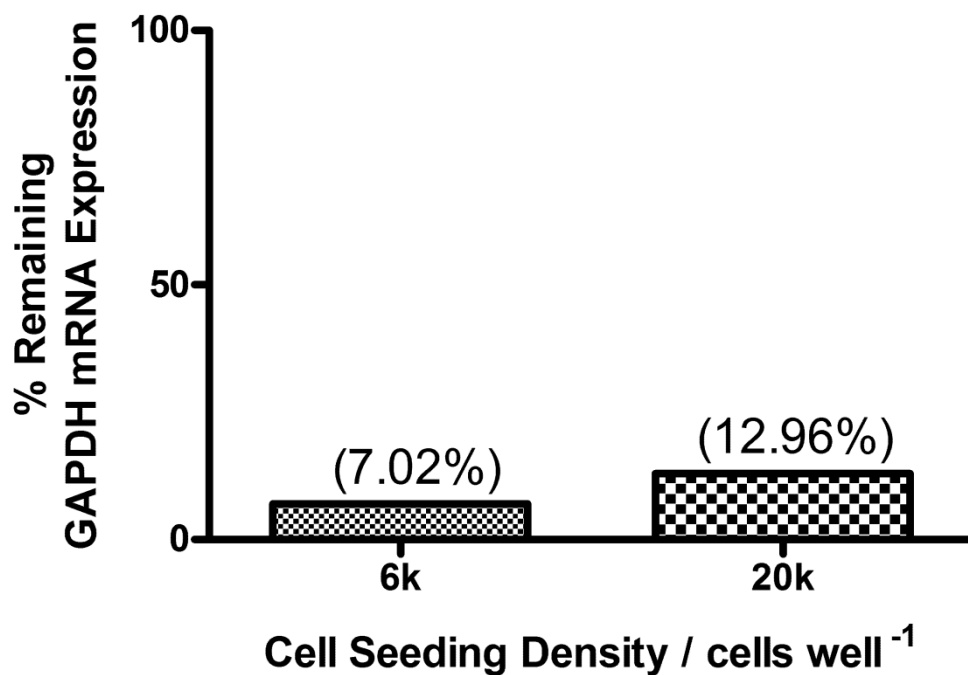


Figure 6.2. Remaining GAPDH mRNA expression following siRNA-mediated knockdown with  $10^{-8}$  M of siRNA in wells seeded with 6000 and 20,000 cells well<sup>-1</sup> (n=1).

### 6.2.3 Discussion

These data demonstrate that the transfection efficiency of siRNA may be reduced when the cell seeding density is increased from 6000 to 20,000 cells well<sup>-1</sup>. Despite this, the reduction in transfection efficiency is small and the increase in seeding density is necessary in order to obtain useful  $[Ca^{2+}]_i$  measurements.

### **6.3 Genomic characterisation of UT-targeting siRNAs**

Two siRNAs (Ambion) which targeted the UT mRNA sequence were characterised, in order to assess their potency and efficacy in CHO<sub>h</sub>UT cell-line.

#### **6.3.1 *Methods***

CHO<sub>h</sub>UT cells were trypsinised and adjusted to the required density in a sterilin tube, the cell suspension was maintained at 37°C/5%CO<sub>2</sub> while the transfection complexes were formed. Transfection complexes were allowed to form for 10 min at room temperature (10µL of siRNA + 10µL of diluted transfection reagent in serum-free medium). The CHO<sub>h</sub>UT cell suspension was then added to each of the wells containing a transfection mixture (180µL containing 20,000 cells). Cells were incubated at 37°C / 5% CO<sub>2</sub> for a total of 48hrs and the media were replaced with fresh growth medium after 24hrs.

After 48hrs, media were removed and cell monolayers were rinsed three times with ice-cold PBS. cDNA was obtained by use of the cells-to-CT™ gene expression kit (Ambion) as previously described (2.5.3). UT mRNA expression was assayed by TaqMan™ PCR as previously described (2.4.2). UT expression was normalised to the endogenous control 18s. A negative control siRNA (limited sequence similarity to known genes) was included at each of the concentrations used, for the purpose of calculating  $\Delta\Delta C_t$  values (paired wells).

### 6.3.2 Results

CRCs demonstrating the percentage-knockdown of UT mRNA in response to the two UT-targeting siRNAs are given in Figure 6.3.

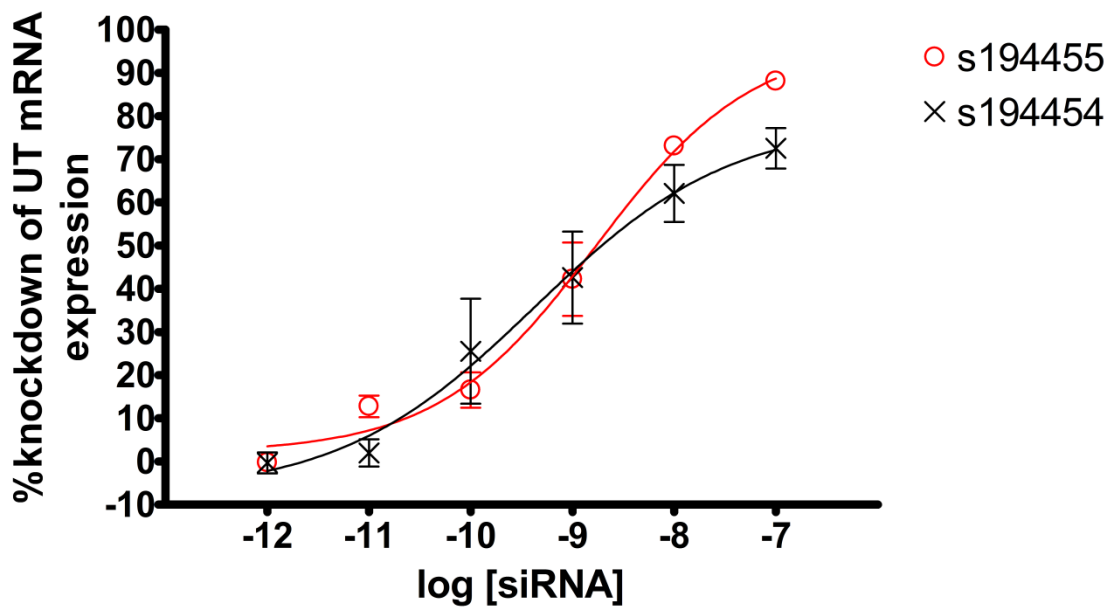


Figure 6.3. Concentration-response curves demonstrating percentage knockdown of UT mRNA expression in response to varying concentrations of siRNAs (siRNA IDs shown). Data are expressed as means  $\pm$  S.E.M, n=3.

Both siRNAs knocked down UT mRNA expression in a concentration-dependent manner in CHO<sub>h</sub>UT. The efficacy for knockdown of s194455 was higher than that of s194454 (93.5 $\pm$ 2.8 and 73.0 $\pm$ 2.5 percentage knockdown respectively, p=0.006). Both s194455 and s194454 knocked down UT mRNA expression with equal potency (pEC<sub>50</sub> values 8.86 $\pm$ 0.19(1.38nM) and 9.35 $\pm$ 0.45(0.45nM) for s194455 and s194454 respectively, p=0.37).

### **6.3.3 Discussion**

Both UT-targeting siRNAs knocked down UT mRNA expression in a concentration-dependent manner with different efficacies and potencies. These data indicate that both of these siRNAs are suitable tools for facilitating efficacy studies with peptide UT ligands at the UT receptor in CHO<sub>h</sub>UT cell-line.

## **6.4 siRNA-mediated efficacy studies at the UT receptor**

Experimental peptide ligands urantide and UFP-803 were functionally characterised in an intracellular calcium mobilisation assay at reduced UT receptor density, afforded by siRNA-mediated RNAi of the UT receptor.

### **6.4.1 Methods**

CHO<sub>h</sub>UT cells were trypsinised and adjusted to the required density in a sterilin tube, the cell suspension was maintained at 37°C/5%CO<sub>2</sub> while the transfection complexes were formed. Transfection complexes were allowed to form for 10 min at room temperature (10µL of siRNA + 10µL of diluted transfection reagent in serum-free medium). The CHO<sub>h</sub>UT cell suspension was then added to each of the wells containing a transfection mixture (180µL containing 20,000 cells). Cells were incubated at 37°C / 5% CO<sub>2</sub> for a total of 48hrs and the media were replaced with fresh growth medium after 24hrs. Cells were transfected with negative control siRNA, s194454, or s194455 (previously characterised) at 10<sup>-7</sup>M.

48-hours after seeding, auto-fluorescence values were obtained and the cells were loaded with fura-2/AM as per the previously described method (2.11). Experimental and

reagent plates were loaded into the NOVOstar plate reader which was set to incubate at 37°C. Fluorometric measurements were made as U-II, urantide, or UFP-803 was injected ( $10^{-6}$ M final concentration).

#### 6.4.2 Results

Intracellular calcium mobilisation traces for U-II, urantide, and UFP-803 are given in Figure 6.4, Figure 6.5, and Figure 6.6 respectively.

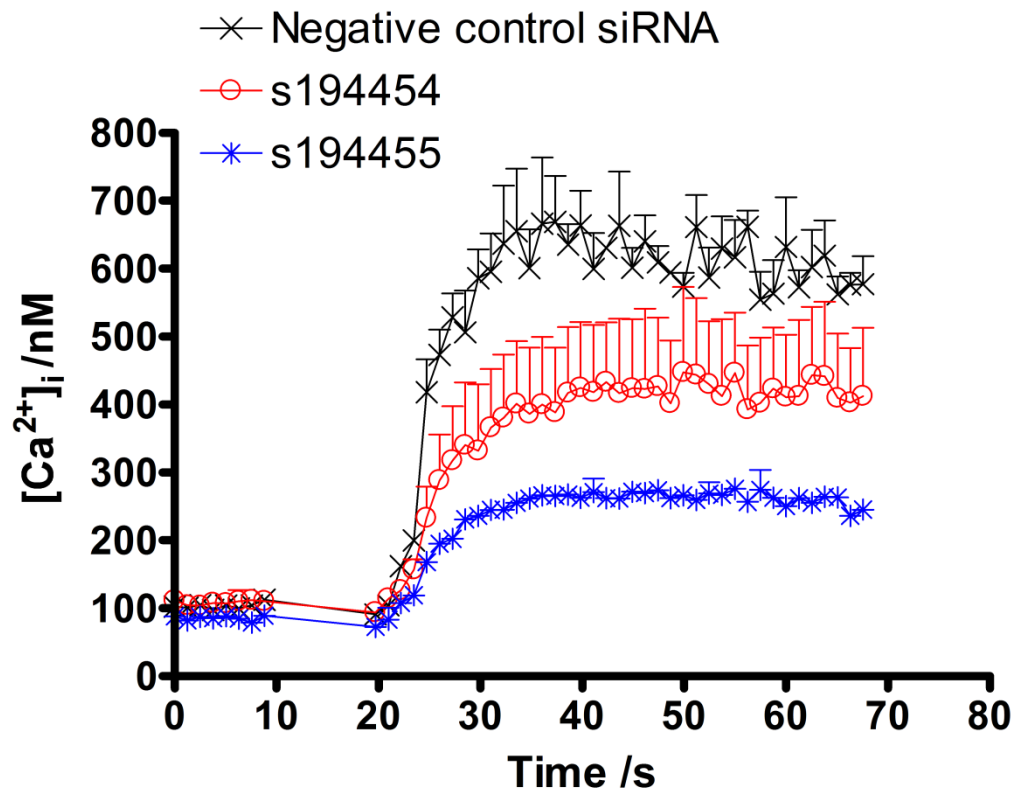


Figure 6.4. Intracellular calcium measurements made on injection of  $10^{-6}$ M U-II following transfection over a 48-hour period with negative control siRNA, s194454, or s194455 ( $10^{-7}$ M final concentration). Data are expressed as means  $\pm$  S.E.M, n=3.

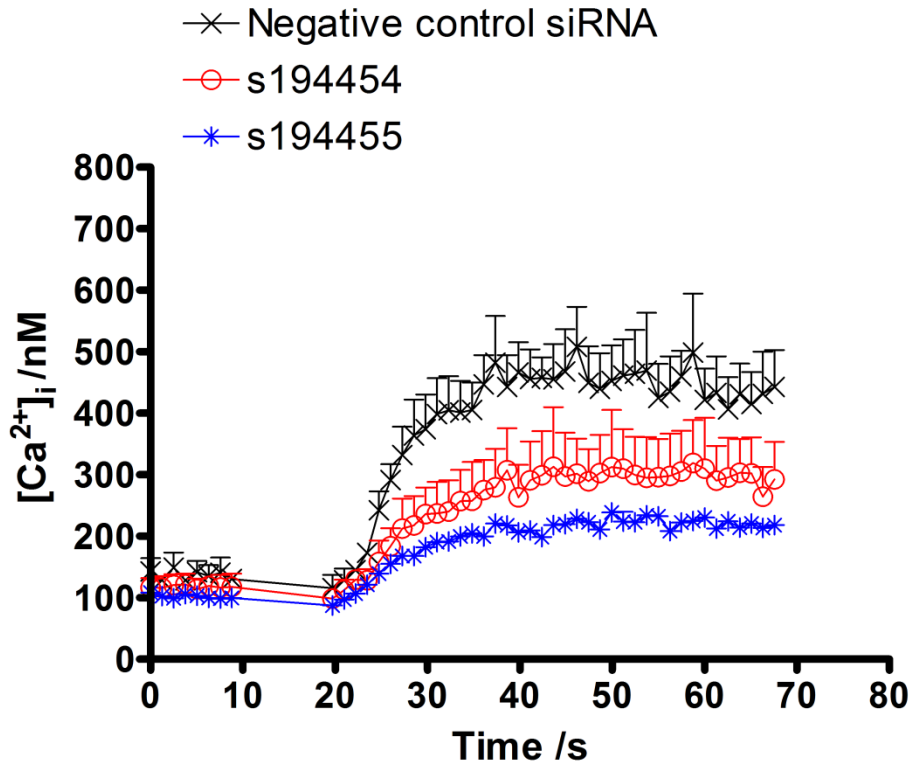


Figure 6.5. Intracellular calcium measurements made on injection of  $10^{-6}$ M urantide following transfection over a 48-hour period with negative control siRNA, s194454, or s194455 ( $10^{-7}$ M final concentration). Data are expressed as means  $\pm$  S.E.M, n=3.

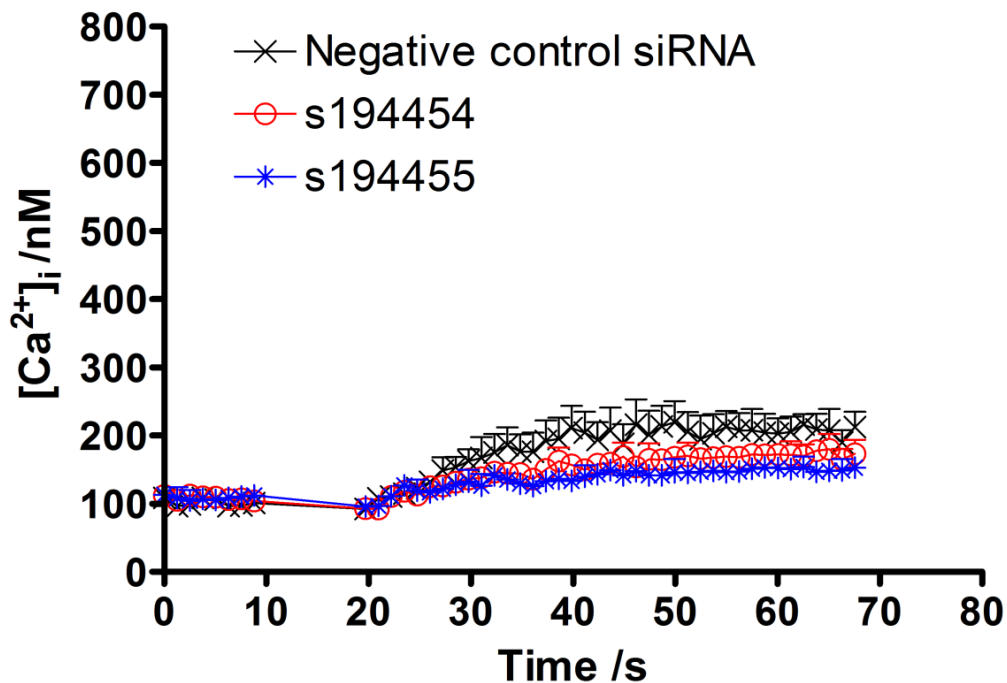


Figure 6.6. Intracellular calcium measurements made on injection of  $10^{-6}$ M UFP-803 following transfection over a 48-hour period with negative control siRNA, s194454, or s194455 ( $10^{-7}$ M final concentration). Data are expressed as means  $\pm$  S.E.M, n=3.

U-II ( $10^{-6}$ M) produced increases in  $[Ca^{2+}]_i$  of  $630\pm 69$ ,  $402\pm 49$ , and  $190\pm 14$ nM (ANOVA  $p=0.002$ ) for negative control siRNA, s194454 ( $p<0.05$  compared to negative), and s194455 ( $p<0.01$  compared to negative)-transfected cells respectively. Urantide ( $10^{-6}$ M) produced increases in  $[Ca^{2+}]_i$  of  $408\pm 55$ ,  $191\pm 40$ , and  $131\pm 10$ nM (ANOVA  $p=0.006$ ) for negative control siRNA, s194454 ( $p<0.05$  compared to negative), and s194455 ( $p<0.01$  compared to negative)-transfected cells respectively. UFP-803 ( $10^{-6}$ M) produced increases in  $[Ca^{2+}]_i$  of  $134\pm 23$ ,  $83\pm 11$ , and  $53\pm 3$ nM (ANOVA  $p=0.02$ ) for negative control siRNA, s194454 (NS compared to negative), and s194455 ( $p<0.05$  compared to negative)-transfected cells respectively. Due to the small size of the responses with UFP-803 it was difficult to assess maximum responses with the active siRNAs. Calculated alpha values for each of the three UT ligands in each of the transfection conditions are given in Figure 6.7.

		Decreasing ligand efficacy →		
		<u>U-II</u>	<u>Urantide</u>	<u>UFP-803</u>
Decreasing UT density ↓	<u>-ve control</u>	1.00	0.65~	0.21~
	<u>s194454</u>	0.64*	0.48~	0.21~
	<u>s194455</u>	0.30*	0.69~	0.28~

\* Relative to full U-II response in negative control siRNA-treated cells.  
~ Relative to full U-II response in cells treated with the same siRNA.

**Figure 6.7.** Calculated alpha values for each of the three UT ligands in cells transfected with each of the three siRNAs.

### 6.4.3 Discussion

Absolute UT ligand-mediated  $\Delta[\text{Ca}^{2+}]_i$  were attenuated in CHO<sub>h</sub>UT cells transfected with either of the UT-targeting siRNAs when compared to cells transfected with the negative control siRNA. In concordance with the genomic characterisation of both of the UT-targeting siRNAs (6.3), the greatest reduction in peptide efficacy was achieved with s194455 for all UT peptides tested.  $\alpha$ -values calculated from U-II-mediated responses in cells transfected with s194454 or s194455 (normalised to the negative control siRNA), indicated reductions in UT functional expression of 40% and 64% respectively  $[100.(1-\alpha)]$ .  $\alpha$ -values calculated from urantide and UFP-803-mediated responses in cells transfected with s194454 or s194455 (normalised to the negative control siRNA), indicated that the *relative* efficacy of urantide and UFP-803 was unchanged as a result of a reduction in UT receptor density.

Considering that UFP-803 does not display residual agonist activity in the rat aorta bioassay [111], it is reasonable to surmise that UT receptor density was still at a supra-physiological level in this assay. However, differences in cellular background and assay design cannot be ignored.

The implications of these findings are considered further in the general discussion (7.2).

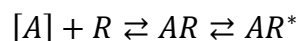
# Chapter Seven

## 7. General discussion

This study aimed to characterise the experimental UT ligands urantide and UFP-803. These ligands have displayed behaviour consistent with partial agonists in classical *in vitro* assays (4.1). However, both of these ligands fail to elicit contractile responses in the isolated rat aorta bioassay [110, 111]. The assay-dependence of the efficacy of these UT ligands is most likely determined by the collective effect of the following two factors [163]:

1. The receptor density of the tissue.
2. Tissue factors (the ability of bound receptor to generate an intracellular response within a given tissue), consisting of:
  - The cellular background
  - coupling efficiency

Considering the first of these factors and with reference to the following simple equation describing receptor activation, it is well-understood that increasing the concentration of agonist 'A' will shift the equilibrium of this equation to the right [163]. Thus, consequentially increasing the proportion of bound receptor and activated receptor producing a tissue response.



*Where 'A' represents agonist binding a receptor 'R' to give 'AR' (inactive) and 'AR\*' (active).*

Although the concept of concentration does not strictly apply to cellular receptors due to their restricted movement within the plane of a plasma membrane, the above

relationship is a simple stoichiometric one nonetheless. Thus, it is also true that increasing the mass of receptors per cell (receptor density) will also shift this equilibrium to the right.

This principle is illustrated by the constitutive (agonist independent) signalling of some 7-TM receptors. Jinsi-Parimoo & Gershengorn demonstrated that the constitutive activity of the G<sub>q</sub>-coupled TRH receptor is directly proportional to its experimentally-controlled density [164]. Although constitutive receptor activity is afforded by a spontaneous switch from the non-active to active receptor states, which is an agonist-independent process, the same principle holds; that increased receptor density will shift the equilibrium to the right, resulting in increased receptor activation and downstream signalling (see equation below).



Typically, the proportion of a population of wildtype receptors in the constitutively active conformation is very low and consequential tissue responses are usually only observable at an amplified downstream vantage point [163, 164]. This phenomenon enables us to visualise how the magnitude of downstream signalling may be affected by an altered receptor density in the presence of a fixed concentration of agonist / receptor occupancy.

Established receptor theory dictates that the relative efficacy of a partial agonist should increase as the receptor density of a given tissue is increased (Figure 7.1).

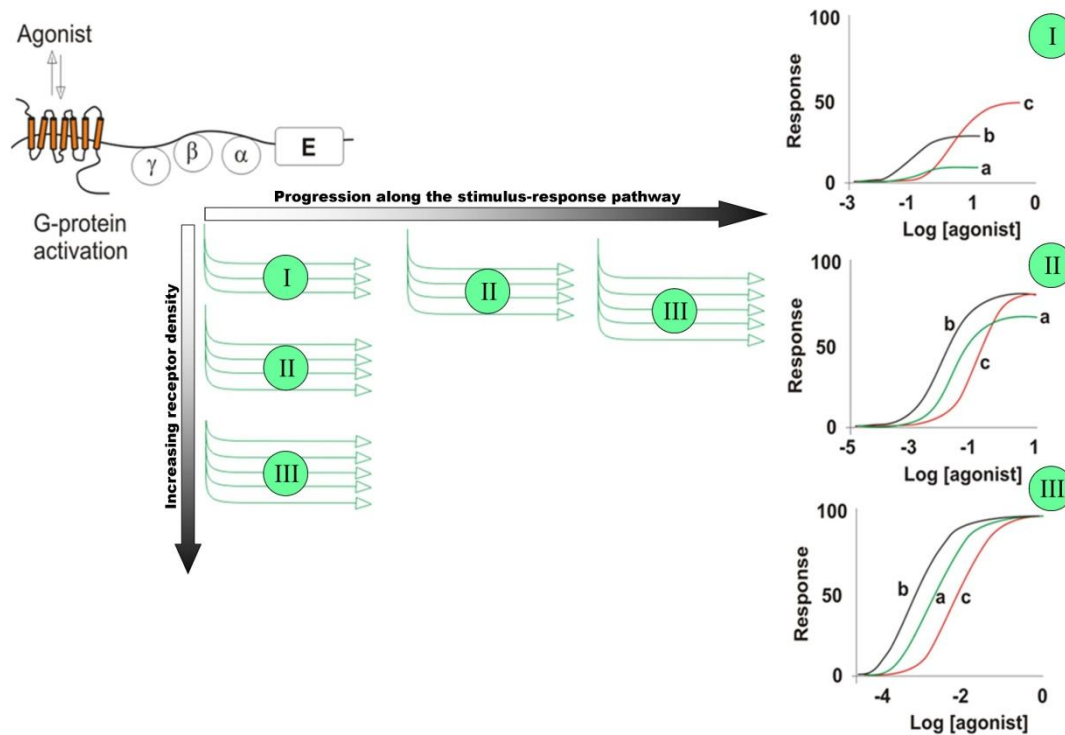


**Figure 7.1.** Amplification of response observed as receptor density increases or as the stimulus progresses along the stimulus-response pathway. The rank order of efficacy is  $c > b > a$ , however the rank order of potency is  $b > a > c$ . In this example, the rank order of potency is maintained as receptor density increases or the stimulus propagates along the pathway. However, the rank order of efficacy is not apparent at high receptor density or at the end organ response. Adapted from [138].

In order to determine the effects of receptor density on the apparent efficacy of experimental UT ligands, two *in vitro* models were produced allowing the density of UT to be controlled in the presence of a fixed cellular background:

1. Ecdysone-inducible CHO cell-line, allowing UT transcription to be induced by a nuclear steroid hormone.
2. UT-targeting siRNAs, allowing UT translation to be inhibited in stable CHO<sub>h</sub>UT transfects.

The data obtained from each of these models is considered in turn below.

## **7.1 Ecdysone-inducible CHO cell-line**

The human UT receptor gene insert was isolated and ligated into pEGSH, located downstream of a minimal heat shock promoter and ecdysone response element (ERE). Uptake of the UT receptor insert was confirmed by endonuclease digestion fragment analysis and DNA sequencing with primers flanking the multi cloning site (MCS). pEGSH-UT was transfected into ER-CHO cell-line and selection pressure was applied to obtain stable transfects. Monoclonal colonies were expanded following two sequential rounds of subcloning and evaluated at the genomic and functional levels by RT-qPCR and a  $[Ca^{2+}]_i$  mobilisation assay respectively, for their ability to induce UT expression on incubation with ponasterone-A. Seven candidates were identified from a preliminary cohort of 24 for their ability to induce UT expression at the mRNA level. Despite this, all seven failed to induce UT expression as evaluated at the functional level. Following this failure, over 100 subclones were produced and screened. Echoing the above results, all of these subclones failed to induce UT expression at a functional level despite many of them exhibiting attractive characteristics at the genomic level. Following extensive troubleshooting, a new batch of ER-CHO cells was provided by the manufacturer (Stratagene).

The two batches of ER-CHO cells were compared and the following observations were made:

1. Expression of the ecdysone receptor (ECR) was over 3-fold higher in the new batch of cells when compared to the original batch.

2. Transient ERCHO<sub>h</sub>UT transfects produced with both batches of ER-CHO cells indicated higher expression of UT in the new batch of cells in both the induced and non-induced forms.

3. The range of UT expression in ERCHO<sub>h</sub>UT transfects produced from the new batch of cells was greater in both the induced and non-induced forms when compared to the original batch.

4. The difference in UT expression between induced and non-induced transfects was greatest for the new batch of cells when compared to the original batch.

Collectively, these observations suggest that the new batch of ER-CHO cells had a greater ability to induce UT expression when compared to the original batch. The reason for lack of induction of gene expression in the original batch is unclear but may be due to the reduced expression of ECR when compared to the new batch. Subsequently, 24 ERCHO<sub>h</sub>UT subclones were produced from the new batch of cells and their ability to induce expression of UT mRNA was evaluated by RT-qPCR. Of these 24 subclones, 13 were shown to induce UT mRNA expression above an arbitrary threshold of 1.5-fold. Two of these were characterised functionally (chosen because they induced the largest fold-increases in UT mRNA expression). Both of the subclones increased functional UT expression (increases in  $[Ca^{2+}]_i$  of 205% and 179% for subclones 2 and 21 respectively), both of these subclones produced U-II-mediated increases in  $[Ca^{2+}]_i$  in the non-induced state. Moreover, the magnitude of these responses (388nM and 646nM for clones 2 and 21 respectively) were just 52% and 20% lower than that of CHO<sub>h</sub>UT [155], but 173% and 355% higher than HEK<sub>h</sub>UT for clones 2 and 21 respectively [165]. In consideration of the sizable UT receptor density in CHO<sub>h</sub>UT [155], these two subclones gave no practical advantage in controlling UT receptor density since U-II-

mediated  $\Delta[\text{Ca}^{2+}]_i$  was only marginally below that of CHO<sub>h</sub>UT in the non-induced form. Despite this, the limited data obtained from ERCHO<sub>h</sub>UT subclones produced from the new batch of ER-CHO cells indicate that control of UT receptor density by this method is possible. Moreover, a review of both the genomic and functional data collected should aid in the identification of candidate subclones in the future (Figure 7.2).

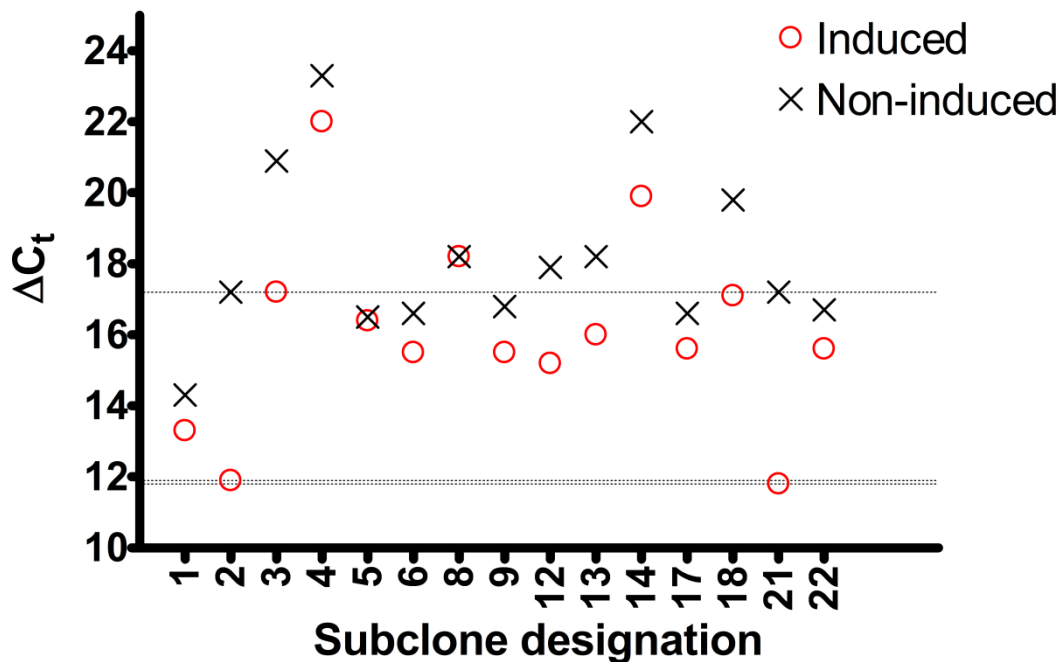


Figure 7.2. Genomic data showing the UT expression of selected subclones (produced from the new batch of ER-CHO cells) in the induced and non-induced state. Dotted lines illustrate genomic range of induction for clones 2 and 21.

Figure 7.2 illustrates the genomic expression of UT in selected subclones previously produced from the new batch of ER-CHO cells. The dotted lines show the expression of UT for clones 2 and 21 in the induced and non-induced states. Considering that clones 2 and 21 gave moderately sized U-II-mediated responses in the non-induced state, and both had UT  $\Delta C_t$  values of 17.2, it may be appropriate to characterise subclones with greater non-induced  $\Delta C_t$  values in the future. Moreover, subclones with induced  $\Delta C_t$  values approximately equal to 17 would be attractive candidates for functional characterisation. For illustrative purposes, subclones 3, 12, 13, and 18 fulfil these

criteria. Note that a relatively low  $\Delta C_t$  value in the non-induced state is indicative of a high level of UT ‘leak’, which is an undesirable characteristic.

Previous studies have successfully employed the ecdysone inducible expression system to control the expression of a 7-TM receptor and study the effects of receptor density on ligand efficacy. McDonald *et al.* placed the nociceptin (NOP) receptor under the control of the ecdysone-inducible system in CHO, which enabled its  $B_{max}$  to be adjusted between 0 and 1100 fmol  $mg^{-1}$  [129]. Figure 7.3 illustrates how agonist-induced cellular responses are nominal even with low concentrations of ponasterone-A.

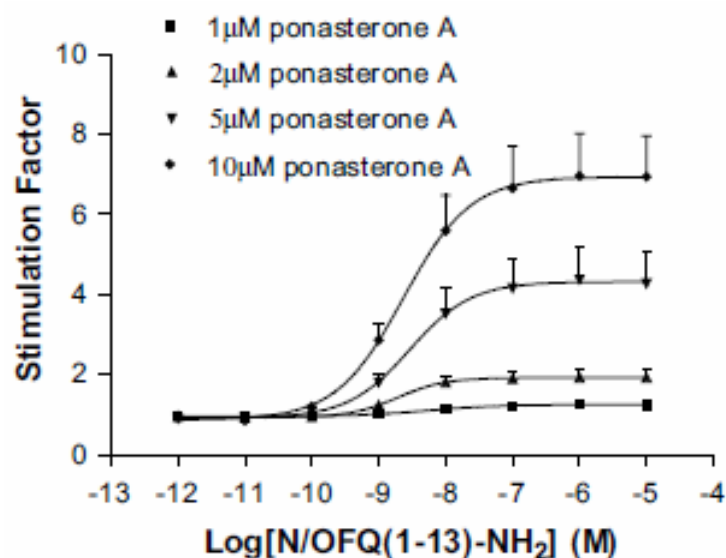


Figure 7.3. Concentration-response curves to a NOP receptor agonist after incubation of an ecdysone-inducible NOP system was incubated with increasing concentrations of ponasterone-A. A higher ponasterone concentration increases NOP receptor density. From [129].

## 7.2 UT-targeting siRNA-mediated RNAi

UT expression was experimentally reduced in CHO<sub>h</sub>UT by transfection with UT-targeting siRNAs. UT knockdown was assayed functionally by means of a  $[Ca^{2+}]_i$  mobilisation assay and at the mRNA level by RT-qPCR. Two UT-targeting siRNAs

were used during this study and their effects were normalised to a negative control siRNA which shared limited sequence similarity to known genes. UT knockdown was greatest when assayed at the mRNA as opposed to the functional level, at a fixed time-point of 48 hrs (post-transfection). This observation is true for both siRNAs used and is consistent with published data (Ambion). This effect may be explained by the length of time taken for mature protein to be recycled from the cell surface after siRNA-mediated translational inhibition. Both of the UT-targeting siRNAs produced reductions in the *absolute* efficacies of U-II, urantide, and UFP-803 (as assessed by  $[Ca^{2+}]_i$  mobilisation). Despite this, the *relative* efficacies of urantide and UFP-803 were unaltered when normalised to the U-II response in cells transfected with the same siRNA. Although the presence of a receptor reserve may explain these findings, this is not supported by the fact that absolute responses to U-II decrease with UT receptor density. Despite this, approaches to reduce UT receptor expression further may yield more useful data, such strategies include:

1. An increased length of incubation following transfection with UT-targeting siRNAs. Theoretically, this would allow the mass of mature receptor to decrease while UT translation is inhibited.

2. Production of a CHO cell-line which places the transcription of UT under the control of a less strong promoter. Such a cell-line would have a lower UT receptor density and subsequent siRNA transfection would reduce it further, possibly abolishing U-II-mediated intracellular responses completely.

Considering that UFP-803 does not exhibit residual agonist activity in the isolated rat aorta bioassay [111], and assuming receptor density to be the principal determinant of

efficacy in this case, it follows that UT density in CHO<sub>h</sub>UT following transfection with siRNA is still higher than that of the rat aorta. In order to confirm this, UT radioligand  $E_{\max}$  determinations would be instructive here. Although the principle of receptor density is well-understood and an attractive one for describing the tissue-dependence of efficacy, the likely effects of an altered cellular background cannot be overlooked. The possibility of different coupling efficiencies between tissues of *in vivo* bioassays and immortalised cell-lines is significant but difficult to quantify and poorly-understood at present [163].

Previous studies have used a similar approach to demonstrate the ligand specificity of a 7-TM receptor. For example, Murakami *et al.* demonstrated that transfection of siRNA specific to the P2Y<sub>10</sub> 7-TM receptor abolishes sphingosine-1-phosphate (S1P)-mediated intracellular responses, thus inferring specificity of S1P for the P2Y<sub>10</sub> receptor [166]. Such studies optimise transfection conditions to afford maximum translational inhibition of the target and complete abolishment of related intracellular responses. However, the uniqueness of this study lies in the fact that the degree of target knockdown has been controlled by the concentration of siRNA. Although only a small number of receptor densities were tested in the present study, it is conceivable that an adapted protocol could achieve a complete range to be tested in the future (previously discussed). If true, then such an adapted protocol would theoretically allow UT receptor density to be controlled between 0 and  $1,110 \pm 70$  fmol mg protein<sup>-1</sup> [155].

### 7.3 Conclusions

Two models were produced to experimentally control UT receptor expression in CHO, allowing the effects of UT receptor density on the efficacy of UT ligands to be determined. To date, one other study has evaluated the effects of UT receptor density on the intrinsic activity of peptidic UT ligands [167]. Behm *et al.* experimentally controlled UT receptor expression in HEK-293 cells by transfecting them with a modified baculovirus encoding UT. By transfecting HEK cells with various viral titres, the UT receptor density was controlled. Behm *et al.* demonstrated that both the absolute and relative efficacies of peptidic ligands urantide and GSK248451 were “augmented in UT-HEK as a result of increased receptor expression”, [167]. The present study found that absolute but not relative efficacies of UT peptidic ligands were decreased in-line with decreasing UT receptor density (6.4). It is unclear why reductions in UT receptor density should produce reductions in the relative intrinsic activity of peptidic UT ligands in one study [167] but not another (6.4). Differences in the cellular background between the two cell types, possibly resulting in different UT receptor coupling/transduction efficiencies cannot be overlooked. It is also possible that each study conducted experiments with ranges of receptor densities which were completely separate from each other. However, it is not possible to confirm this due to the lack of radioligand binding data for the present study.

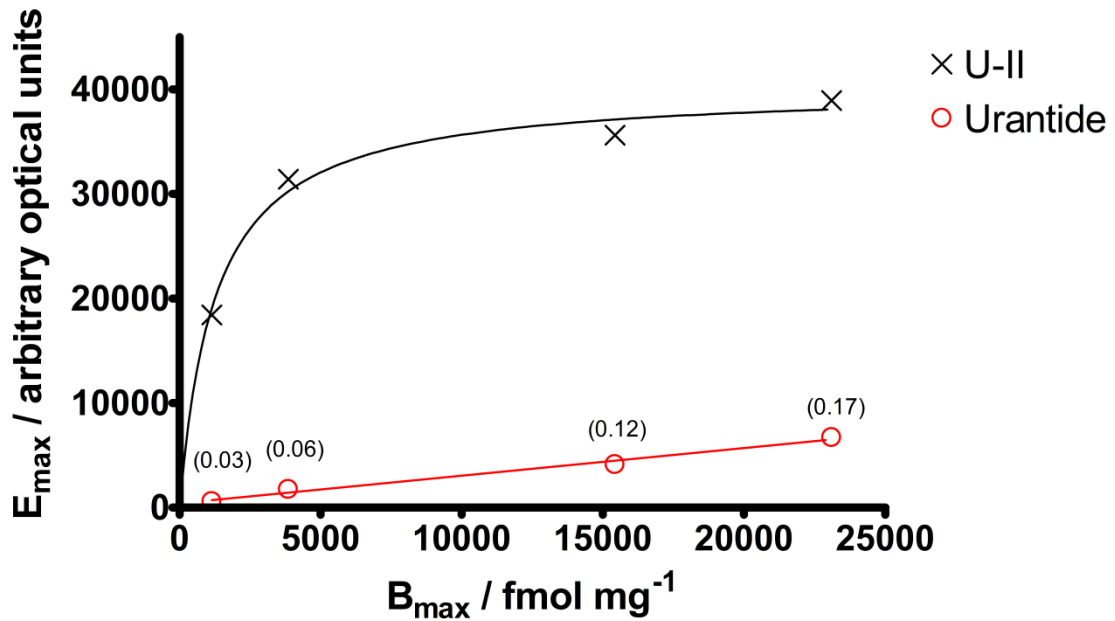


Figure 7.4. A graph of  $E_{max}$  over  $B_{max}$  for U-II and urantide challenges in UT-HEK. Alpha values are given in parentheses. Produced from Behm *et al.*[167].

Figure 7.4 (above) was produced from data presented by Behm *et al.* and helps to illustrate why the relative intrinsic activity of a peptidic UT ligand (urantide) is dependent upon the UT receptor density in this instance. The maximal response ( $E_{max}$ ) to urantide is directly proportional to the  $B_{max}$  of the cell-line ( $m=0.26\pm 0.02$ ,  $r^2=0.99$ ). This is an expected observation as the total number of ligand-receptor complexes should dictate the total tissue response and the receptor density should not influence the cellular response generated per unit ligand-receptor complex. In contrast to these observations, the maximal response ( $E_{max}$ ) to U-II shares a hyperbolic relationship with  $B_{max}$  ( $R^2=0.98$ ) and may be explained by the presence of some saturating factor such as a receptor reserve being reached. When viewed collectively, these observations account for receptor density-mediated changes in ligand relative intrinsic activity. As receptor density is increased, the maximal response obtained from urantide increases in a linear fashion. However, the maximal response obtained from U-II quickly saturates over the same range of receptor densities. Consequentially, resulting in increasing relative

intrinsic activity of urantide with increasing receptor density. Importantly, the effect of increasing relative intrinsic activity of urantide is caused by the U-II response ceiling and not by any change to the cellular response generated per unit urantide-receptor complex.

Given the above observations, it is reasonable to assume that the maximal response to U-II does not saturate over the range of receptor densities used in the present study. Moreover, this implies that a UT receptor reserve is not reached or exceeded over the range of densities used within the present study. These assumptions make it possible to explain how the absolute but not the relative efficacies of UT peptidic ligands change in-line with the UT receptor density. These assertions require vigorous experimental validation and the inclusion of  $B_{\max}$  determinations in future related studies.

#### **7.4 Future work**

Despite considerable research into the UT receptor system, there are still many unanswered questions: what are the non-pathological roles of U-II? What are the principal sites of U-II production and secretion into the circulation? What are the stimuli and mechanisms for changes in U-II/UT expression in pathology and do these changes in expression exacerbate conditions or serve as a protective mechanism?

The solution to answering some of these questions may lie in the production and characterisation of pure and selective UT receptor antagonists. Such tools would allow the (patho)physiological roles of UT to be fully probed and understood.

The present study aimed to characterise a number of experimental UT ligands at various UT receptor densities in order that the effect of density and receptor coupling on ligand efficacy may be understood. Despite difficulties experienced during this project (concerning production of an ecdysone inducible expression system for UT) the polyclonal cell-line produced and the methodologies developed represent a sound base for future work in this area to continue. Moreover, PCR screening data collected during this project should allow suitable monoclonal antibodies to be identified with greater ease in the future.

Although the siRNA study yielded useful data, which highlighted the effect of UT receptor density on ligand efficacy, the methods developed here can easily facilitate further study (not previously possible due to limitations of time). An obvious starting point would be to produce full concentration-response-curves to each of the experimental UT ligands at each of the UT receptor densities. Secondly, it would be interesting to observe the antagonist interactions of the experimental UT ligands concurrently with UT at varying UT density. Finally, it may be possible to increase the level of UT knockdown achieved at the *functional* level by increasing the length of transfection to 72 hours (Ambion). If true then changes in relative UT ligand efficacy may be observable.

## **8. Appendix I**

### **8.1 Harvest buffer (X5)**

- 45g NaCl
- 11.9g HEPES
- 2.5g EDTA
- Made to 1L with dH<sub>2</sub>O
- Adjust to pH 7.4

### **8.2 Krebs-HEPES buffer**

- 8.38g NaCl
- 2.1g glucose
- 2.38g HEPES
- 0.35g KCl
- 0.16g KH<sub>2</sub>PO<sub>4</sub>
- 0.29g MgSO<sub>4</sub>·7H<sub>2</sub>O
- 0.38g CaCl<sub>2</sub>·2H<sub>2</sub>O
- Made to 1L with dH<sub>2</sub>O
- Adjust to pH 7.4

### **8.3 SOC medium**

1. Add the following to 900ml of distilled H<sub>2</sub>O
  - 20g Bacto Tryptone
  - 5g Bacto Yeast Extract
  - 2ml of 5M NaCl.
  - 2.5ml of 1M KCl.
  - 10ml of 1M MgCl<sub>2</sub>
  - 10ml of 1M MgSO<sub>4</sub>
  - 20ml of 1M glucose
2. Adjust to 1L with distilled H<sub>2</sub>O
3. Sterilize by autoclaving

## **8.4 LB agar**

1. Add the following to 800ml H<sub>2</sub>O
  - 10g Bacto-tryptone
  - 5g yeast extract
  - 10g NaCl
2. Adjust pH to 7.5 with NaOH
3. Add 15g agar
4. Melt agar into solution in the microwave
5. Adjust volume to 1L with dH<sub>2</sub>O
6. Sterilize by autoclaving

## **8.5 Phosphate buffered saline**

1. Dissolve the following in 800ml distilled H<sub>2</sub>O.
  - 8g of NaCl
  - 0.2g of KCl
  - 1.44g of Na<sub>2</sub>HPO<sub>4</sub>
  - 0.24g of KH<sub>2</sub>PO<sub>4</sub>
2. Adjust pH to 7.4.
3. Adjust volume to 1L with additional distilled H<sub>2</sub>O.
4. Sterilize by autoclaving

## **8.6 Tissue culture media**

### **8.6.1 *CHO<sub>h</sub>UT growth medium***

D-MEM/F-12 (1X) liquid 1:1 (Invitrogen). supplemented with 10% foetal calf serum, penicillin (100 IU/ml) streptomycin (100 µg/ml) and fungizone (2.5 µg/ml). Stock cultures were further supplemented with geneticin (G418; 800 µg/ml).

### **8.6.2 *ER-CHO growth medium***

Dulbecco's Modified Eagle Medium (D-MEM) (1X), liquid (High Glucose), (Invitrogen) supplemented with 10% foetal calf serum, penicillin (100 IU/ml) streptomycin (100 µg/ml) and fungizone (2.5 µg/ml). Stock cultures were further supplemented with geneticin (G418; 800 µg/ml).

## 9. Appendix II

### 9.1 QIAquick PCR purification kit manufacturer's protocol

#### QIAquick PCR Purification Kit Protocol

##### using a microcentrifuge

This protocol is designed to purify single- or double-stranded DNA fragments from PCR and other enzymatic reactions (see page 8). For cleanup of other enzymatic reactions, follow the protocol as described for PCR samples or use the MinElute Reaction Cleanup Kit. Fragments ranging from 100 bp to 10 kb are purified from primers, nucleotides, polymerases, and salts using QIAquick spin columns in a microcentrifuge.

##### Important points before starting

- Add ethanol (96–100%) to Buffer PE before use (see bottle label for volume).
- All centrifugation steps are carried out at 17,900 x g (13,000 rpm) in a conventional tabletop microcentrifuge at room temperature.
- Add 1:250 volume pH indicator I to Buffer PB (i.e., add 120 µl pH indicator I to 30 ml Buffer PB or add 600 µl pH indicator I to 150 ml Buffer PB). The yellow color of Buffer PB with pH indicator I indicates a pH of  $\leq 7.5$ .
- Add pH indicator I to entire buffer contents. Do not add pH indicator I to buffer aliquots.
- If the purified PCR product is to be used in sensitive microarray applications, it may be beneficial to use Buffer PB without the addition of pH indicator I.

##### Procedure

1. **Add 5 volumes of Buffer PB to 1 volume of the PCR sample and mix. It is not necessary to remove mineral oil or kerosene.**  
For example, add 500 µl of Buffer PB to 100 µl PCR sample (not including oil).
2. **If pH indicator I has been added to Buffer PB, check that the color of the mixture is yellow.**  
If the color of the mixture is orange or violet, add 10 µl of 3 M sodium acetate, pH 5.0, and mix. The color of the mixture will turn to yellow.
3. **Place a QIAquick spin column in a provided 2 ml collection tube.**
4. **To bind DNA, apply the sample to the QIAquick column and centrifuge for 30–60 s.**
5. **Discard flow-through. Place the QIAquick column back into the same tube.**  
Collection tubes are re-used to reduce plastic waste.
6. **To wash, add 0.75 ml Buffer PE to the QIAquick column and centrifuge for 30–60 s.**
7. **Discard flow-through and place the QIAquick column back in the same tube. Centrifuge the column for an additional 1 min.**  
**IMPORTANT:** Residual ethanol from Buffer PE will not be completely removed unless the flow-through is discarded before this additional centrifugation.

8. Place QIAquick column in a clean 1.5 ml microcentrifuge tube.
9. To elute DNA, add 50  $\mu$ l Buffer EB (10 mM Tris-Cl, pH 8.5) or water (pH 7.0–8.5) to the center of the QIAquick membrane and centrifuge the column for 1 min. Alternatively, for increased DNA concentration, add 30  $\mu$ l elution buffer to the center of the QIAquick membrane, let the column stand for 1 min, and then centrifuge.

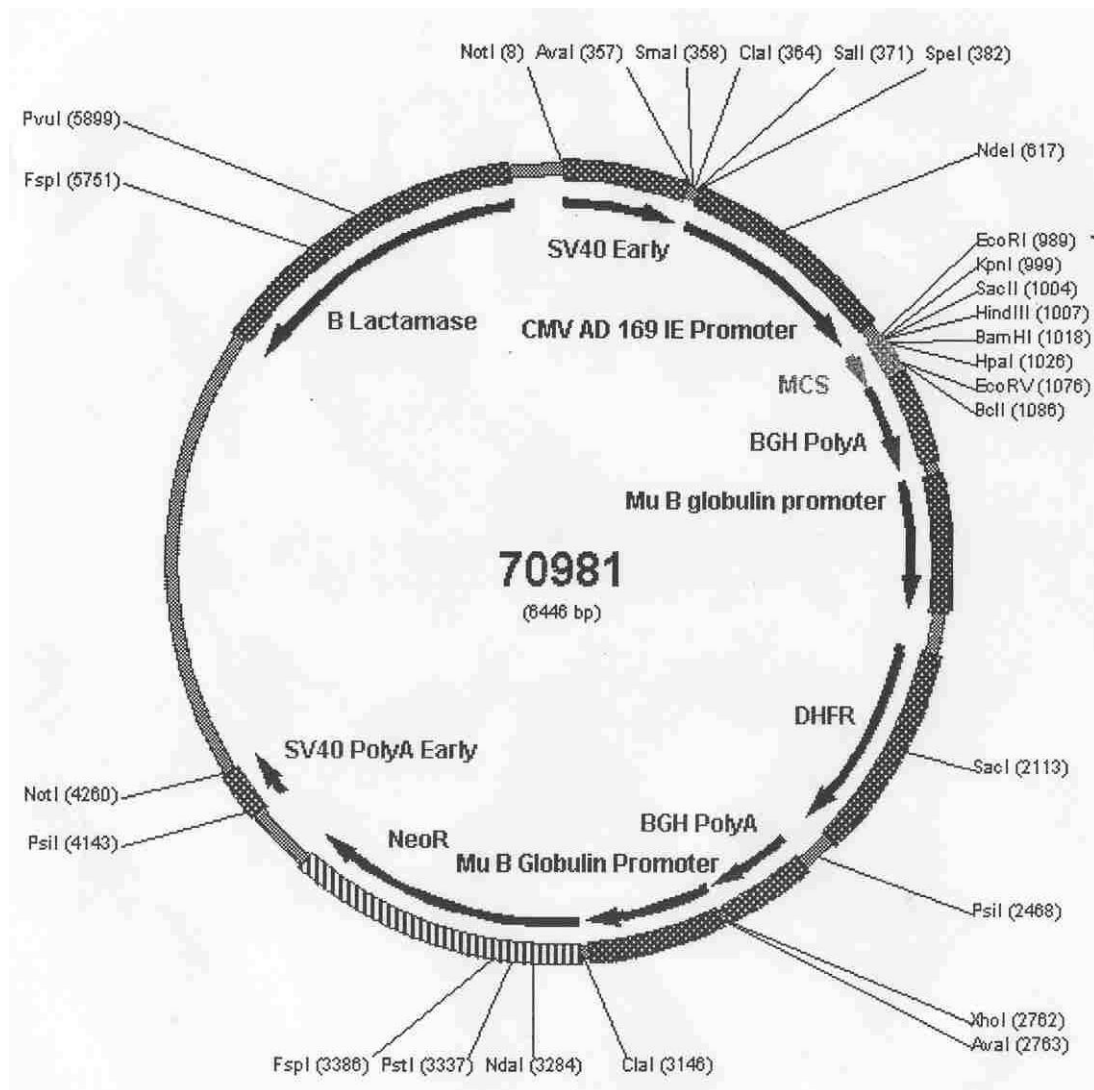
**IMPORTANT:** Ensure that the elution buffer is dispensed directly onto the QIAquick membrane for complete elution of bound DNA. The average eluate volume is 48  $\mu$ l from 50  $\mu$ l elution buffer volume, and 28  $\mu$ l from 30  $\mu$ l elution buffer.

Elution efficiency is dependent on pH. The maximum elution efficiency is achieved between pH 7.0 and 8.5. When using water, make sure that the pH value is within this range, and store DNA at  $-20^{\circ}\text{C}$  as DNA may degrade in the absence of a buffering agent. The purified DNA can also be eluted in TE buffer (10 mM Tris-Cl, 1 mM EDTA, pH 8.0), but the EDTA may inhibit subsequent enzymatic reactions.

10. **If the purified DNA is to be analyzed on a gel, add 1 volume of Loading Dye to 5 volumes of purified DNA. Mix the solution by pipetting up and down before loading the gel.**

Loading dye contains 3 marker dyes (bromophenol blue, xylene cyanol, and orange G) that facilitate estimation of DNA migration distance and optimization of agarose gel run time. Refer to Table 2 (page 15) to identify the dyes according to migration distance and agarose gel percentage and type.

## 9.2 70981 restriction map



### 9.3 UT receptor cDNA insert sequence

#### Human GPR14 (UT)

##### Cloning Vector: 70981

**Insert:** The enzymes used to cut the plasmid for insertion of human UT fragment were **EcoRI** and **EcoRV**.

There is a double stop codon.

(ATG to stop inclusive of tags):

```
GAATCCCAC CATGGCGCTG ACCCCGAGT CCCCAGCAG CTCCCTGGG CTGGCCGCCA CCGGCAGCTC
TGTGCCGGAG CCGCTGGCG GCCCAACGC AACCTCAAC AGTCCTGGG CCAGCCGAC CGAGCCCAGC
TCCCTGGAGG ACCTGGTGGC CACGGGCACC ATTGGGACTC TGCTGTCGGC CATGGGCGTG GTGGGCGTGG
TGGGCAACGC CTACACGCTG GTGGTCACCT GCCGCTCCCT GCGTGCGGTG GCCTCCATGT ACGTCTACGT
GGTCAACCTG GCGCTGGCCG ACCTGCTGTA CCTGCTCAGC ATCCCCTTCA TCGTGCCAC CTACGTCACC
AAGGAGTGGC ACTTCGGGGA CGTGGGCTGC CGCGTGCTCT TCGGCCTGGA CTTCCTGACC ATGCACGCCA
GCATCTTAC GCTGACCGTC ATGAGCAGCG AGCGTACGC TCGGTGCTG CGGCCGCTGG ACACCGTGCA
GCGCCCCAAG GGCTACCGCA AGCTGCTGGC GCTGGGCACC TGGGTGCTGG CGCTGCTGCT GACGCTGCCC
GTGATGCTGG CCATGCGGCT GGTGCGCCGG GGTCCAAGA GCCTGTGCCT GCCCGCTGG GGCCCGCGCG
CCCACCGCGC CTACCTGACG CTGCTCTTCG CCACCAGCAT CGCGGGGCC GGGCTGCTCA TCGGGCTGCT
CTACGCGCGC CTGGCCCGCG CCTACCGCCG CTCGACGCGC GCCTCCTTCA AGCGGGCCCG GCGGCCGGGG
GCGCGCGCGC TGCCTGCTGGT GCTGGGCATC GTGCTGCTCT TCTGGCCTG CTCTGCCC TTCTGGCTGT
GGCAGTGTCT CGCCAGTAC CACCAGGCC CGCTGGCGCC GCGGACGGCG CGCATCGTCA ACTACCTGAC
CACCTGCCTC ACCTACGGCA ACAGCTGCGC CAACCCCTC CTCTACACGC TGCTACCAAG GAACTACCGC
GACCACCTGC GCGGCCGCGT GCGGGGCCCG GGCAGCGGGG GAGGCCGGGG GCCCGTTCCC TCCCTGCAGC
CCCAGCCCCG CTTCCAGCGC TGTTCCGGGC GCTCCCTGTC TTCCTGCAGC CCACAGCCCA CTGACAGCCT
CGTGCTGGCC CCAGCGGCC CGGCCGACC TGCGCCGAG GGTCCAGGG CCCCAGCGTG ATAAGGTTGA TATC
```

##### Protein Sequence:

```
MALTPESPSS FPGLAATGSS VPEPPGGPNA TLNSSWASPT EPSSLEDLVA TGTIGTLLSA MGVVGVVGNV YTLVVTCRSL
RAVASMYVYV VNLALADLLY LLSIPFIVAT YVTKEWHFGD VGCRVLFGLD FLTMHASIFT LTMSSERYA
AVLRPLDTVQ RPKGYRKLLA LGTWLLALLL TLPVMLAMRL VRRGPKSLCL PAWGPRAHRA YLTLFATSI
AGPGLLIGLL YARLARAYRR SQRASFKRAR RPARALRLV LGIVLLFWAC FLPFWLWQLL AQYHQAPLAP
RTARIVNYLT TCLTYGNSCA NPFLYTLTR NYRDHLRGRV RGPSSGGGRG PVPSLQPRAR FQRCSGRSL SCSQPQTDLSL
VLAPAARPA APEGPRAPA
```

## 9.4 pEGSH-UT consensus sequencing data

		Section 1					
		(1)	1	10	20	30	43
clone 9 forward	(1)	CAGAAGAGCAATTGGTACCGGATCCGATCCCACC					ATGGCGCTG
cpr 14 clone 9 reverse	(1)	-----					-----
gpr14(human)	(1)	-----					ATGGCGCTG
Consensus	(1)						ATGGCGCTG
		Section 2					
		(44)	44	50	60	70	86
clone 9 forward	(44)	ACCCCCGAGTCCCCGAGCAGCTTCCCTGGGCTGGCCGCCACCG					
cpr 14 clone 9 reverse	(1)	-----					-----
gpr14(human)	(10)	ACCCCCGAGTCCCCGAGCAGCTTCCCTGGGCTGGCCGCCACCG					
Consensus	(44)	ACCCCCGAGTCCCCGAGCAGCTTCCCTGGGCTGGCCGCCACCG					
		Section 3					
		(87)	87	100	110		129
clone 9 forward	(87)	GCAGCTCTGTGCCGGAGCCGCCTGGCGGCCCAACGCAACCCT					
cpr 14 clone 9 reverse	(1)	-----					-----
gpr14(human)	(53)	GCAGCTCTGTGCCGGAGCCGCCTGGCGGCCCAACGCAACCCT					
Consensus	(87)	GCAGCTCTGTGCCGGAGCCGCCTGGCGGCCCAACGCAACCCT					
		Section 4					
		(130)	130	140	150	160	172
clone 9 forward	(130)	CAACAGCTCCTGGGCCAGCCGACCGAGCCAGCTCCCTGGAG					
cpr 14 clone 9 reverse	(1)	-----					-----
gpr14(human)	(96)	CAACAGCTCCTGGGCCAGCCGACCGAGCCAGCTCCCTGGAG					
Consensus	(130)	CAACAGCTCCTGGGCCAGCCGACCGAGCCAGCTCCCTGGAG					
		Section 5					
		(173)	173	180	190	200	215
clone 9 forward	(173)	GACCTGGTGGCCACGGGCACCATTTGGGACTCTGCTGTCTGGCCA					
cpr 14 clone 9 reverse	(1)	-----					-----
gpr14(human)	(139)	GACCTGGTGGCCACGGGCACCATTTGGGACTCTGCTGTCTGGCCA					
Consensus	(173)	GACCTGGTGGCCACGGGCACCATTTGGGACTCTGCTGTCTGGCCA					
		Section 6					
		(216)	216	230	240		258
clone 9 forward	(216)	TGGGCGTGGTGGGCGTGGTGGGCAACGCCTACACGCTGGTGGT					
cpr 14 clone 9 reverse	(1)	-----					-----
gpr14(human)	(182)	TGGGCGTGGTGGGCGTGGTGGGCAACGCCTACACGCTGGTGGT					
Consensus	(216)	TGGGCGTGGTGGGCGTGGTGGGCAACGCCTACACGCTGGTGGT					
		Section 7					
		(259)	259	270	280	290	301
clone 9 forward	(259)	CACCTGCCGCTCCCTGCGTGCGGTGGCCTCCATGTACGTCTAC					
cpr 14 clone 9 reverse	(1)	-----					-----
gpr14(human)	(225)	CACCTGCCGCTCCCTGCGTGCGGTGGCCTCCATGTACGTCTAC					
Consensus	(259)	CACCTGCCGCTCCCTGCGTGCGGTGGCCTCCATGTACGTCTAC					

						Section 8
	(302)	302	310	320	330	344
clone 9 forward	(302)	GTGGTCAACCTGGCGCTGGCCGACCTGCTGTACCTGCTCAGCA				
cpr 14 clone 9 reverse	(1)	-----				
gpr14(human)	(268)	GTGGTCAACCTGGCGCTGGCCGACCTGCTGTACCTGCTCAGCA				
Consensus	(302)	GTGGTCAACCTGGCGCTGGCCGACCTGCTGTACCTGCTCAGCA				
						Section 9
	(345)	345	350	360	370	387
clone 9 forward	(345)	TCCCCTTCATCGTGGCCACCTACGTCACCAAGGAGTGGCACTT				
cpr 14 clone 9 reverse	(1)	-----CTACGTCACCAAGGAGTGGCACTT				
gpr14(human)	(311)	TCCCCTTCATCGTGGCCACCTACGTCACCAAGGAGTGGCACTT				
Consensus	(345)	TCCCCTTCATCGTGGCCACCTACGTCACCAAGGAGTGGCACTT				
						Section 10
	(388)	388	400	410	420	430
clone 9 forward	(388)	CGGGGACGTGGGCTGCGCGTGCTCTTCGGCCTGGACTTCCTG				
cpr 14 clone 9 reverse	(25)	CGGGGACGTGGGNTGCGCGTGCTNTTCGGCCTGGACTTCCTG				
gpr14(human)	(354)	CGGGGACGTGGGCTGCGCGTGCTCTTCGGCCTGGACTTCCTG				
Consensus	(388)	CGGGGACGTGGGCTGCGCGTGCTCTTCGGCCTGGACTTCCTG				
						Section 11
	(431)	431	440	450	460	473
clone 9 forward	(431)	ACCATGCACGCCAGCATCTTCACGCTGACCGTCATGAGCAGCG				
cpr 14 clone 9 reverse	(68)	ACCATGCACGCCAGCATNTTCACGCTGACCGTCATGAGCAGCG				
gpr14(human)	(397)	ACCATGCACGCCAGCATCTTCACGCTGACCGTCATGAGCAGCG				
Consensus	(431)	ACCATGCACGCCAGCATCTTCACGCTGACCGTCATGAGCAGCG				
						Section 12
	(474)	474	480	490	500	516
clone 9 forward	(474)	AGCGCTACGCTGCGGTGCTGCGGCCGCTGGACACCGTGCAGCG				
cpr 14 clone 9 reverse	(111)	AGCGNTACGNTGCGGTGCTGCGGCCGCTGGACACCGTGCAGCG				
gpr14(human)	(440)	AGCGCTACGCTGCGGTGCTGCGGCCGCTGGACACCGTGCAGCG				
Consensus	(474)	AGCGCTACGCTGCGGTGCTGCGGCCGCTGGACACCGTGCAGCG				
						Section 13
	(517)	517	530	540		559
clone 9 forward	(517)	CCCCAAGGGCTACCGCAAGCTGCTGGCGCTGGGCACCTGGCTG				
cpr 14 clone 9 reverse	(154)	CCCCAAGGGCTACCGCAAGCTGCTGGCGCTGGGCACCTGGCTG				
gpr14(human)	(483)	CCCCAAGGGCTACCGCAAGCTGCTGGCGCTGGGCACCTGGCTG				
Consensus	(517)	CCCCAAGGGCTACCGCAAGCTGCTGGCGCTGGGCACCTGGCTG				
						Section 14
	(560)	560	570	580	590	602
clone 9 forward	(560)	CTGGCGCTGCTGCTGACGCTGCCCGTGATGCTGGCCATGCGGC				
cpr 14 clone 9 reverse	(197)	CTGGCGCTGCTGCTGACGCTGCCCGTGATGCTGGCCATGCGGC				
gpr14(human)	(526)	CTGGCGCTGCTGCTGACGCTGCCCGTGATGCTGGCCATGCGGC				
Consensus	(560)	CTGGCGCTGCTGCTGACGCTGCCCGTGATGCTGGCCATGCGGC				

		Section 15				
		(603) 603	610	620	630	645
clone 9 forward	(603)	TGGTGCGCCGGGGTCCCAAGAGCCTGTGCCTGCCCGCCTGGGG				
cpr 14 clone 9 reverse	(240)	TGGTGCGCCGGGGTCCCAAGAGCCTGTGCCTGCCCGCCTGGGG				
gpr14(human)	(569)	TGGTGCGCCGGGGTCCCAAGAGCCTGTGCCTGCCCGCCTGGGG				
Consensus	(603)	TGGTGCGCCGGGGTCCCAAGAGCCTGTGCCTGCCCGCCTGGGG				
		Section 16				
		(646) 646	660	670		688
clone 9 forward	(646)	CCCGCGCGCCACCAGCGCCTACCTGACGCTGCTCTTCGCCACC				
cpr 14 clone 9 reverse	(283)	CCCGCGCGCCACCAGCGCCTACCTGACGCTGCTCTTCGCCACC				
gpr14(human)	(612)	CCCGCGCGCCACCAGCGCCTACCTGACGCTGCTCTTCGCCACC				
Consensus	(646)	CCCGCGCGCCACCAGCGCCTACCTGACGCTGCTCTTCGCCACC				
		Section 17				
		(689) 689	700	710	720	731
clone 9 forward	(689)	ANNATCGCGGGGGCCCGGGCTGCTCATCGGGCTGCTCTACGCGC				
cpr 14 clone 9 reverse	(326)	AGCATCGCGGGGGCCCGGGCTGCTCATCGGGCTGCTCTACGCGC				
gpr14(human)	(655)	AGCATCGCGGGGGCCCGGGCTGCTCATCGGGCTGCTCTACGCGC				
Consensus	(689)	AGCATCGCGGGGGCCCGGGCTGCTCATCGGGCTGCTCTACGCGC				
		Section 18				
		(732) 732	740	750	760	774
clone 9 forward	(732)	GCCTGGCCCGCGCCTACCGCCGCTCGCAGCGCGCCTCCTTCAA				
cpr 14 clone 9 reverse	(369)	GCCTGGCCCGCGCCTACCGCCGCTCGCAGCGCGCCTCCTTCAA				
gpr14(human)	(698)	GCCTGGCCCGCGCCTACCGCCGCTCGCAGCGCGCCTCCTTCAA				
Consensus	(732)	GCCTGGCCCGCGCCTACCGCCGCTCGCAGCGCGCCTCCTTCAA				
		Section 19				
		(775) 775	780	790	800	817
clone 9 forward	(775)	GCGGGCCCGCGCGCCGGGGGCGCGCGCGCTGCGCCTGGTGCTG				
cpr 14 clone 9 reverse	(412)	GCGGGCCCGCGCGCCGGGGGCGCGCGCGCTGCGCCTGGTGCTG				
gpr14(human)	(741)	GCGGGCCCGCGCGCCGGGGGCGCGCGCGCTGCGCCTGGTGCTG				
Consensus	(775)	GCGGGCCCGCGCGCCGGGGGCGCGCGCGCTGCGCCTGGTGCTG				
		Section 20				
		(818) 818	830	840	850	860
clone 9 forward	(818)	GGCATCGTGCTGCTCTTCTGGGCCTGCTTCCTGCCCTTCTGGC				
cpr 14 clone 9 reverse	(455)	GGCATCGTGCTGCTCTTCTGGGCCTGCTTCCTGCCCTTCTGGC				
gpr14(human)	(784)	GGCATCGTGCTGCTCTTCTGGGCCTGCTTCCTGCCCTTCTGGC				
Consensus	(818)	GGCATCGTGCTGCTCTTCTGGGCCTGCTTCCTGCCCTTCTGGC				
		Section 21				
		(861) 861	870	880	890	903
clone 9 forward	(861)	TGTGGCAGCTGCTCGCCCAGTACACNNNNNCCCCGCTGGCGCC				
cpr 14 clone 9 reverse	(498)	TGTGGCAGCTGCTCGCCCAGTACCACCAGGCCCCGCTGGCGCC				
gpr14(human)	(827)	TGTGGCAGCTGCTCGCCCAGTACCACCAGGCCCCGCTGGCGCC				
Consensus	(861)	TGTGGCAGCTGCTCGCCCAGTACCACCAGGCCCCGCTGGCGCC				

		Section 22					
		(904)	904	910	920	930	946
clone 9 forward	(904)	GCGGANGGCGCGCATCGTCAACTACCTGACNACCTGCCTCANC					
cpr 14 clone 9 reverse	(541)	GCGGACGGCGCGCATCGTCAACTACCTGACCACCTGCCTCACC					
gpr14(human)	(870)	GCGGACGGCGCGCATCGTCAACTACCTGACCACCTGCCTCACC					
Consensus	(904)	GCGGACGGCGCGCATCGTCAACTACCTGACCACCTGCCTCACC					
		Section 23					
		(947)	947	960	970	989	
clone 9 forward	(947)	TACGGCAACAGCTGCGCCAACCCCTTC-NCTACACGCTGCTC-					
cpr 14 clone 9 reverse	(584)	TACGGCAACAGCTGCGCCAACCCCTTCCTCTACACGCTGCTCA					
gpr14(human)	(913)	TACGGCAACAGCTGCGCCAACCCCTTCCTCTACACGCTGCTCA					
Consensus	(947)	TACGGCAACAGCTGCGCCAACCCCTTCCTCTACACGCTGCTCA					
		Section 24					
		(990)	990	1000	1010	1020	1032
clone 9 forward	(988)	-----					
cpr 14 clone 9 reverse	(627)	CCAGGAACTACCGCGACCACCTGCGCGGCCGCGTGCGGGGCC					
gpr14(human)	(956)	CCAGGAACTACCGCGACCACCTGCGCGGCCGCGTGCGGGGCC					
Consensus	(990)	CCAGGAACTACCGCGACCACCTGCGCGGCCGCGTGCGGGGCC					
		Section 25					
		(1033)	1033	1040	1050	1060	1075
clone 9 forward	(988)	-----					
cpr 14 clone 9 reverse	(670)	GGGCAGCGGGGGAGGCCGGGGGCCCGTTCCCTCCCTGCAGCC					
gpr14(human)	(999)	GGGCAGCGGGGGAGGCCGGGGGCCCGTTCCCTCCCTGCAGCC					
Consensus	(1033)	GGGCAGCGGGGGAGGCCGGGGGCCCGTTCCCTCCCTGCAGCC					
		Section 26					
		(1076)	1076	1090	1100	1118	
clone 9 forward	(988)	-----					
cpr 14 clone 9 reverse	(713)	CGCGCCCGCTTCCAGCGCTGTTTCGGGCCGCTCCCTGTCTTCCT					
gpr14(human)	(1042)	CGCGCCCGCTTCCAGCGCTGTTTCGGGCCGCTCCCTGTCTTCCT					
Consensus	(1076)	CGCGCCCGCTTCCAGCGCTGTTTCGGGCCGCTCCCTGTCTTCCT					
		Section 27					
		(1119)	1119	1130	1140	1150	1161
clone 9 forward	(988)	-----					
cpr 14 clone 9 reverse	(756)	GCAGCCACAGCCCACTGACAGCCTCGTGCTGGCCCCAGCGGC					
gpr14(human)	(1085)	GCAGCCACAGCCCACTGACAGCCTCGTGCTGGCCCCAGCGGC					
Consensus	(1119)	GCAGCCACAGCCCACTGACAGCCTCGTGCTGGCCCCAGCGGC					
		Section 28					
		(1162)	1162	1170	1180	1190	1204
clone 9 forward	(988)	-----					
cpr 14 clone 9 reverse	(799)	CCCGGCCCGACCTGCGCCCGAGGGTCCCAGGGCCCCGGCGTGA					
gpr14(human)	(1128)	CCCGGCCCGACCTGCGCCCGAGGGTCCCAGGGCCCCGGCGTGA					
Consensus	(1162)	CCCGGCCCGACCTGCGCCCGAGGGTCCCAGGGCCCCGGCGTGA					

## 10. Appendix III

Effects of the putative UT receptor antagonists [Pen<sup>5</sup>, DTrp<sup>7</sup>, Orn<sup>8</sup>] U-II (4-11) and [Pen<sup>5</sup>, DTrp<sup>7</sup>, Dab<sup>8</sup>] U-II (4-11) on [<sup>3</sup>H] inositol phosphate turnover at recombinant UT receptors

BD Hunt<sup>\*</sup>, J McDonald<sup>\*</sup>, R Guerrini<sup>\*</sup>, LL Ng<sup>\*</sup>, G Calo<sup>\*</sup>, DG Lambert

*Department of Cardiovascular Sciences, Division of Anaesthesia, Critical Care and Pain Management, University of Leicester, Leicester Royal Infirmary, Leicester, LE1 5WW*

Urotensin II (U-II) is a cyclic undecapeptide which activates the G<sub>q/11</sub> protein-coupled UT receptor<sup>1</sup>. Changes in the levels of expression of U-II and UT have been observed in a range of pathological conditions, including but not limited to those which may be observed in the intensive care setting<sup>2</sup>. Pharmacological characterisation of the action of U-II in health and disease is hampered by the relative lack of UT ligands, particularly antagonists<sup>2</sup>. In this study we characterise the actions of the putative UT receptor antagonists [Pen<sup>5</sup>, DTrp<sup>7</sup>, Orn<sup>8</sup>] U-II (4-11), (Urantide) and [Pen<sup>5</sup>, DTrp<sup>7</sup>, Dab<sup>8</sup>] U-II (4-11), (UFP-803)<sup>3</sup> in Chinese Hamster Ovary cells stably expressing 1.11 pmol mg protein<sup>-1</sup> of the recombinant human UT receptor (CHO<sub>hUT</sub>)<sup>4</sup>.

CHO<sub>hUT</sub> cells were cultured for 48hrs in medium supplemented with 1μCi ml<sup>-1</sup> [<sup>3</sup>H] myo-inositol<sup>5</sup>. Loaded cells were harvested, resuspended in Krebs-HEPES buffer containing 10μM lithium chloride and equally divided between test tubes. Dilution series of U-II, urantide and UFP-803 were prepared and added to the suspensions for production of full concentration response curves. In antagonism studies urantide (1μM) or UFP-803 (1μM) was added concurrently with U-II. Following 15min incubation at 37°C, cells were lysed and [<sup>3</sup>H] inositol phosphates ([<sup>3</sup>H]IP<sub>x</sub>) were extracted using gravity-fed ion exchange chromatography. Samples were mixed with scintillation fluid and radioactivity quantified in a scintillation counter. Data are presented as mean ± SEM, (n=3 as single data points or in duplicate).

Urantide and UFP-803 stimulated [<sup>3</sup>H]IP<sub>x</sub> turnover in CHO<sub>hUT</sub> cells; the relative intrinsic activities, expressed as the maximal response (E<sub>max</sub>) relative to that of the full agonist U-II, were 0.44±0.01 and 0.18±0.02 respectively. In antagonism studies urantide (1μM) and UFP-803 (1μM) both produced parallel rightward shifts in the concentration response curve to U-II on an elevated baseline in accordance with their residual agonist activity. Application of the Gaddum-Schild equation yields pK<sub>B</sub> values of 7.45±0.08 and 6.93±0.19 respectively.

In this upstream [<sup>3</sup>H]IP<sub>x</sub> assay at high levels of receptor expression, both urantide and UFP-803 behaved as partial agonists. Substitution of ornithine in position 8 of urantide with diaminobutyric acid in UFP-803 markedly reduced residual agonist activity of this peptide. Simple competitive antagonism at lower levels of receptor expression such as might be encountered *in vivo* is to be anticipated.

*References:* 1. McDonald J, Batuwangala M, Lambert DG. *J Anesth* 2007; 21: 378-89; 2. Carotenuto A, Grieco P, Rovero P, Novellino E. *Curr Med Chem* 2006; 13: 267-75; 3. Camarda V, Spagnol M, Song W, et al. *British journal of pharmacology* 2006; 147: 92-100; 4. Song W, McDonald J, Camarda V, et al. *Naunyn Schmiedebergs Arch Pharm.* 2006; 373: 148-57; 5. Challiss R. (Ed.) *Receptor Signal Transduction Protocols: Humana Press, 1997*

*Acknowledgement:* BD Hunt is funded by a British Heart Foundation studentship.

Presented orally at the winter scientific meeting of the Anaesthetic Research Society, in January 2008. (**Br. J. Anaesth., April 2008; 100: 574-590**).

## EFFECTS OF THE PUTATIVE UT RECEPTOR ANTAGONIST, UFP-803: PRE-INCUBATION OR CONCURRENT ADDITION?

**B. D. HUNT<sup>1\*</sup>, L. L. NG<sup>1</sup>, G. CALO<sup>2</sup>, R. GUERRINI<sup>3</sup> & D. G. LAMBERT<sup>1</sup>**

<sup>1</sup>University Department of Cardiovascular Sciences; Division of Anaesthesia, Critical Care and Pain Management; University of Leicester; Leicester Royal Infirmary; LE1 5WW.

Departments of <sup>2</sup>Experimental and Clinical Medicine, <sup>3</sup>Pharmaceutical Sciences and Biotechnology Centre; University of Ferrara; Ferrara; Italy.

\***B. D. Hunt is funded by a British Heart Foundation studentship.**

Urotensin II (U-II) is a cyclic undecapeptide which activates the G<sub>q/11</sub> protein-coupled UT receptor<sup>1</sup>. UFP-803 is a putative UT receptor antagonist, which possesses residual agonist activity in CHO cells expressing the human UT receptor (CHO<sub>hUT</sub>)<sup>2</sup>. Estimation of antagonist potency generally requires pre-incubation to allow the ligand(s) to reach equilibrium<sup>3</sup>. Here we characterise UFP-803 with specific emphasis given to the effects of antagonist pre-incubation.

CHO<sub>hUT</sub> cells were cultured for 48hrs in medium supplemented with 1μCi ml<sup>-1</sup> [<sup>3</sup>H] myo-inositol<sup>4</sup>. Loaded cells were resuspended in Krebs-HEPES buffer containing 10mM LiCl and divided between test tubes. Serially diluted U-II or UFP-803 was added to the cell suspensions to produce full concentration response curves (CRC). In antagonism studies UFP-803 was included at a fixed concentration of 1μM, administered either 15 min prior to or concurrently with U-II. Following 15min incubation, cells were lysed, [<sup>3</sup>H] inositol phosphates ([<sup>3</sup>H]IP<sub>x</sub>) were extracted by ion exchange chromatography and radioactivity was quantified.

U-II and UFP-803 produced concentration dependent increases in [<sup>3</sup>H]IP<sub>x</sub> formation. pEC<sub>50</sub>/E<sub>max</sub> values were 8.91±0.10/ 2074±116DPM and 7.68±0.14/ 367±6DPM respectively (mean±SEM, n=3); thus UFP-803 behaved as a low efficacy partial agonist (α = 0.18). When added either 15 min prior to or concurrently with U-II, UFP-803 produced a parallel rightward shift in the CRC to U-II. Mean E<sub>max</sub> values for control, pre-incubation and concurrent groups were 2074±116; 2759±45 and 2014±119 DPM respectively. E<sub>max</sub> was significantly higher than control in the pre-incubation (p=0.043) but not concurrent addition group. pK<sub>b</sub> values for the pre-incubation and concurrent addition groups were 7.17±0.17 & 6.94±0.19 respectively.

As expected for a partial agonist, UFP-803 displays antagonist activity in CHO<sub>hUT</sub>. These data show that E<sub>max</sub> is overestimated as a consequence of combined inositol-1-phosphatase blockade and antagonist pre-incubation. The use of a partial agonist at a supra-physiological receptor density, in this assay, is likely to have exacerbated this effect to significance. This response can be abolished by adopting a concurrent addition method.

1. McDonald J, *J. Anesth.* 2007; 21: 378-89; 2. Camarda V, *Br. J. Pharma.* 2006; 147: 92-100; 3. Kenakin T. *Elsevier Health Sciences*, 2006; 4. Challiss RE. *Humana Press*, 1997.

Presented as a poster presentation at the joint meeting of the European Opioid Conference and European Neuropeptide Club, in June 2008. (Published online at the European Opioid Conference's

## **11. REFERENCES**

1. Bern, H.A. and K. Lederis, *A reference preparation for the study of active substances in the caudal neurosecretory system of teleosts*. J Endocrinol, 1969. **45**(1): p. Suppl:xi-xii.
2. Bern, H.A., Lederis, K., *Neurosecretion and Neuroendocrine Activity: Evolution, Structure and Function*, W. Bargmann, Oksche, A., Polenov, A. & Scharrer, B. , Editor. 1978, Springer, Berlin. p. 341-349.
3. Gibson, A., et al., *Neuropeptide-induced contraction and relaxation of the mouse anococcygeus muscle*. Proc Natl Acad Sci U S A, 1984. **81**(2): p. 625-9.
4. Itoh, H., et al., *Contraction of major artery segments of rat by fish neuropeptide urotensin II*. Am J Physiol, 1987. **252**(2 Pt 2): p. R361-6.
5. Coulouarn, Y., et al., *Cloning of the cDNA encoding the urotensin II precursor in frog and human reveals intense expression of the urotensin II gene in motoneurons of the spinal cord*. Proc Natl Acad Sci U S A, 1998. **95**(26): p. 15803-8.
6. Itoh, H., D. McMaster, and K. Lederis, *Functional receptors for fish neuropeptide urotensin II in major rat arteries*. Eur J Pharmacol, 1988. **149**(1-2): p. 61-6.
7. Ames, R.S., et al., *Human urotensin-II is a potent vasoconstrictor and agonist for the orphan receptor GPR14*. Nature, 1999. **401**(6750): p. 282-6.
8. Marchese, A., et al., *Cloning and chromosomal mapping of three novel genes, GPR9, GPR10, and GPR14, encoding receptors related to interleukin 8, neuropeptide Y, and somatostatin receptors*. Genomics, 1995. **29**(2): p. 335-44.
9. Liu, Q., et al., *Identification of urotensin II as the endogenous ligand for the orphan G-protein-coupled receptor GPR14*. Biochem Biophys Res Commun, 1999. **266**(1): p. 174-8.
10. Mori, M., et al., *Urotensin II is the endogenous ligand of a G-protein-coupled orphan receptor, SENR (GPR14)*. Biochem Biophys Res Commun, 1999. **265**(1): p. 123-9.
11. Nothacker, H.P., et al., *Identification of the natural ligand of an orphan G-protein-coupled receptor involved in the regulation of vasoconstriction*. Nat Cell Biol, 1999. **1**(6): p. 383-5.
12. Hill, S.J., *G-protein-coupled receptors: past, present and future*. Br J Pharmacol, 2006. **147 Suppl 1**: p. S27-37.
13. Fredriksson, R. and H.B. Schioth, *The repertoire of G-protein-coupled receptors in fully sequenced genomes*. Mol Pharmacol, 2005. **67**(5): p. 1414-25.
14. Fredriksson, R., et al., *The G-protein-coupled receptors in the human genome form five main families. Phylogenetic analysis, paralogon groups, and fingerprints*. Mol Pharmacol, 2003. **63**(6): p. 1256-72.
15. Pierce, K.L., R.T. Premont, and R.J. Lefkowitz, *Seven-transmembrane receptors*. Nat Rev Mol Cell Biol, 2002. **3**(9): p. 639-50.
16. Lescot, E., et al., *Three-dimensional model of the human urotensin-II receptor: Docking of human urotensin-II and nonpeptide antagonists in the binding site and comparison with an antagonist pharmacophore model*. Proteins, 2008. **73**(1): p. 173-184.

17. Wess, J., *Molecular basis of receptor/G-protein-coupling selectivity*. Pharmacol Ther, 1998. **80**(3): p. 231-64.
18. McIntire, W.E., *Structural determinants involved in the formation and activation of G protein betagamma dimers*. Neurosignals, 2009. **17**(1): p. 82-99.
19. Rens-Domiano, S. and H.E. Hamm, *Structural and functional relationships of heterotrimeric G-proteins*. Faseb J, 1995. **9**(11): p. 1059-66.
20. Milligan, G. and E. Kostenis, *Heterotrimeric G-proteins: a short history*. Br J Pharmacol, 2006. **147 Suppl 1**: p. S46-55.
21. Birnbaumer, L., et al., *Molecular diversity and function of G proteins and calcium channels*. Biol Reprod, 1991. **44**(2): p. 207-24.
22. Hubbard, K.B. and J.R. Hepler, *Cell signalling diversity of the Gqalpha family of heterotrimeric G proteins*. Cell Signal, 2006. **18**(2): p. 135-50.
23. Pattni, K. and G. Banting, *Ins(1,4,5)P3 metabolism and the family of IP3-3Kinases*. Cell Signal, 2004. **16**(6): p. 643-54.
24. Berridge, M.J., *Unlocking the secrets of cell signaling*. Annu Rev Physiol, 2005. **67**: p. 1-21.
25. Rang, H.P., Dale, M. M., Ritter, J. M. & Moore P. K. , *Pharmacology*. Fifth ed. 2003: Churchill Livingstone. 797.
26. Lee, M.W. and D.L. Severson, *Signal transduction in vascular smooth muscle: diacylglycerol second messengers and PKC action*. Am J Physiol, 1994. **267**(3 Pt 1): p. C659-78.
27. Williamson, J.R. and J.R. Monck, *Signal transduction mechanisms involved in hormonal Ca<sup>2+</sup> fluxes*. Environ Health Perspect, 1990. **84**: p. 121-36.
28. Ohsako, S., et al., *Cloning and sequence analysis of cDNAs encoding precursors of urotensin II-alpha and -gamma*. J Neurosci, 1986. **6**(9): p. 2730-5.
29. Kumar, S. and S.B. Hedges, *A molecular timescale for vertebrate evolution*. Nature, 1998. **392**(6679): p. 917-20.
30. Sugo, T., et al., *Identification of urotensin II-related peptide as the urotensin II-immunoreactive molecule in the rat brain*. Biochem Biophys Res Commun, 2003. **310**(3): p. 860-8.
31. Nothacker, H.P. and S. Clark, *From heart to mind. The urotensin II system and its evolving neurophysiological role*. Febs J, 2005. **272**(22): p. 5694-702.
32. Protopopov, A., et al., *Assignment of the GPR14 gene coding for the G-protein-coupled receptor 14 to human chromosome 17q25.3 by fluorescent in situ hybridization*. Cytogenet Cell Genet, 2000. **88**(3-4): p. 312-3.
33. Saetrum Opgaard, O., et al., *Human urotensin II mediates vasoconstriction via an increase in inositol phosphates*. Eur J Pharmacol, 2000. **406**(2): p. 265-71.
34. Suzuki, S., et al., *Genetic variations at urotensin II and urotensin II receptor genes and risk of type 2 diabetes mellitus in Japanese*. Peptides, 2004. **25**(10): p. 1803-8.
35. Wenyi, Z., et al., *Role of urotensin II gene in genetic susceptibility to Type 2 diabetes mellitus in Japanese subjects*. Diabetologia, 2003. **46**(7): p. 972-6.
36. Yi, L., et al., *Association of ACE, ACE2 and UTS2 polymorphisms with essential hypertension in Han and Dongxiang populations from north-western China*. J Int Med Res, 2006. **34**(3): p. 272-83.
37. Russell, F.D., et al., *Elevated plasma levels of human urotensin-II immunoreactivity in congestive heart failure*. Am J Physiol Heart Circ Physiol, 2003. **285**(4): p. H1576-81.

38. Nakayama, K., *Furin: a mammalian subtilisin/Kex2p-like endoprotease involved in processing of a wide variety of precursor proteins*. *Biochem J*, 1997. **327** ( Pt 3): p. 625-35.
39. Russell, F.D., et al., *Urotensin-II-converting enzyme activity of furin and trypsin in human cells in vitro*. *J Pharmacol Exp Ther*, 2004. **310**(1): p. 209-14.
40. Russell, F.D., *Emerging roles of urotensin-II in cardiovascular disease*. *Pharmacol Ther*, 2004. **103**(3): p. 223-43.
41. Conlon, J.M., D. Arnold-Reed, and R.J. Balment, *Post-translational processing of prepro-urotensin II*. *FEBS Lett*, 1990. **266**(1-2): p. 37-40.
42. Rossowski, W.J., et al., *Human urotensin II-induced aorta ring contractions are mediated by protein kinase C, tyrosine kinases and Rho-kinase: inhibition by somatostatin receptor antagonists*. *Eur J Pharmacol*, 2002. **438**(3): p. 159-70.
43. Ziltener, P., et al., *Urotensin II mediates ERK1/2 phosphorylation and proliferation in GPR14-transfected cell lines*. *J Recept Signal Transduct Res*, 2002. **22**(1-4): p. 155-68.
44. Tamura, K., et al., *Urotensin II-induced activation of extracellular signal-regulated kinase in cultured vascular smooth muscle cells: involvement of cell adhesion-mediated integrin signaling*. *Life Sci*, 2003. **72**(9): p. 1049-60.
45. Totsune, K., et al., *Increased plasma urotensin II levels in patients with diabetes mellitus*. *Clin Sci (Lond)*, 2003. **104**(1): p. 1-5.
46. Maguire, J.J., R.E. Kuc, and A.P. Davenport, *Orphan-receptor ligand human urotensin II: receptor localization in human tissues and comparison of vasoconstrictor responses with endothelin-1*. *Br J Pharmacol*, 2000. **131**(3): p. 441-6.
47. Douglas, S.A., et al., *Congestive heart failure and expression of myocardial urotensin II*. *Lancet*, 2002. **359**(9322): p. 1990-7.
48. Coulouarn, Y., et al., *Cloning, sequence analysis and tissue distribution of the mouse and rat urotensin II precursors*. *FEBS Lett*, 1999. **457**(1): p. 28-32.
49. Thompson, J.P., et al., *A comparison of cerebrospinal fluid and plasma urotensin II concentrations in normotensive and hypertensive patients undergoing urological surgery during spinal anesthesia: a pilot study*. *Anesth Analg*, 2003. **97**(5): p. 1501-3.
50. Matsushita, M., et al., *Co-expression of urotensin II and its receptor (GPR14) in human cardiovascular and renal tissues*. *J Hypertens*, 2001. **19**(12): p. 2185-90.
51. Aiyar, N., et al., *Differential levels of "urotensin-II-like" activity determined by radio-receptor and radioimmuno-assays*. *Peptides*, 2004. **25**(8): p. 1339-47.
52. Charles, C.J., et al., *Urotensin II: evidence for cardiac, hepatic and renal production*. *Peptides*, 2005. **26**(11): p. 2211-4.
53. Mosenkis, A., et al., *Human Urotensin II in the plasma of anephric subjects*. *Nephrol Dial Transplant*, 2006.
54. Gartlon, J., et al., *Central effects of urotensin-II following ICV administration in rats*. *Psychopharmacology (Berl)*, 2001. **155**(4): p. 426-33.
55. Clark, S.D., et al., *The urotensin II receptor is expressed in the cholinergic mesopontine tegmentum of the rat*. *Brain Res*, 2001. **923**(1-2): p. 120-7.
56. Elshourbagy, N.A., et al., *Molecular and pharmacological characterization of genes encoding urotensin-II peptides and their cognate G-protein-coupled receptors from the mouse and monkey*. *Br J Pharmacol*, 2002. **136**(1): p. 9-22.
57. Totsune, K., et al., *Role of urotensin II in patients on dialysis*. *Lancet*, 2001. **358**(9284): p. 810-1.

58. Tal, M., et al., *A novel putative neuropeptide receptor expressed in neural tissue, including sensory epithelia*. *Biochem Biophys Res Commun*, 1995. **209**(2): p. 752-9.
59. Chartrel, N., et al., *Urotensin II in the central nervous system of the frog *Rana ridibunda**. *Biochemical characterization and immunohistochemical localization*. *Ann N Y Acad Sci*, 1998. **839**: p. 506-7.
60. Dun, S.L., et al., *Urotensin II-immunoreactivity in the brainstem and spinal cord of the rat*. *Neurosci Lett*, 2001. **305**(1): p. 9-12.
61. Dschietzig, T., et al., *Plasma levels and cardiovascular gene expression of urotensin-II in human heart failure*. *Regul Pept*, 2002. **110**(1): p. 33-8.
62. Gardiner, S.M., et al., *Depressor and regionally-selective vasodilator effects of human and rat urotensin II in conscious rats*. *Br J Pharmacol*, 2001. **132**(8): p. 1625-9.
63. Zhu, Y.Z., et al., *Urotensin II causes fatal circulatory collapse in anesthetized monkeys in vivo: a "vasoconstrictor" with a unique hemodynamic profile*. *Am J Physiol Heart Circ Physiol*, 2004. **286**(3): p. H830-6.
64. Bohm, F. and J. Pernow, *Urotensin II evokes potent vasoconstriction in humans in vivo*. *Br J Pharmacol*, 2002. **135**(1): p. 25-7.
65. Wilkinson, I.B., et al., *High plasma concentrations of human urotensin II do not alter local or systemic hemodynamics in man*. *Cardiovasc Res*, 2002. **53**(2): p. 341-7.
66. Affolter, J.T., et al., *No effect on central or peripheral blood pressure of systemic urotensin II infusion in humans*. *Br J Clin Pharmacol*, 2002. **54**(6): p. 617-21.
67. Behm, D.J., et al., *Deletion of the UT receptor gene results in the selective loss of urotensin-II contractile activity in aortae isolated from UT receptor knockout mice*. *Br J Pharmacol*, 2003. **139**(2): p. 464-72.
68. Douglas, S.A., et al., *Differential vasoconstrictor activity of human urotensin-II in vascular tissue isolated from the rat, mouse, dog, pig, marmoset and cynomolgus monkey*. *Br J Pharmacol*, 2000. **131**(7): p. 1262-74.
69. Bottrill, F.E., et al., *Human urotensin-II is an endothelium-dependent vasodilator in rat small arteries*. *Br J Pharmacol*, 2000. **130**(8): p. 1865-70.
70. Douglas, S.A., *Human urotensin-II as a novel cardiovascular target: 'heart' of the matter or simply a fishy 'tail'?* *Curr Opin Pharmacol*, 2003. **3**(2): p. 159-67.
71. Russell, F.D., P. Molenaar, and D.M. O'Brien, *Cardiostimulant effects of urotensin-II in human heart in vitro*. *Br J Pharmacol*, 2001. **132**(1): p. 5-9.
72. Camarda, V., et al., *Effects of human urotensin II in isolated vessels of various species; comparison with other vasoactive agents*. *Naunyn Schmiedebergs Arch Pharmacol*, 2002. **365**(2): p. 141-9.
73. MacLean, M.R., et al., *Contractile responses to human urotensin-II in rat and human pulmonary arteries: effect of endothelial factors and chronic hypoxia in the rat*. *Br J Pharmacol*, 2000. **130**(2): p. 201-4.
74. Hillier, C., et al., *Effects of urotensin II in human arteries and veins of varying caliber*. *Circulation*, 2001. **103**(10): p. 1378-81.
75. Paysant, J., et al., *Comparison of the contractile responses of human coronary bypass grafts and monkey arteries to human urotensin-II*. *Fundam Clin Pharmacol*, 2001. **15**(4): p. 227-31.
76. Zou, Y., R. Nagai, and T. Yamazaki, *Urotensin II induces hypertrophic responses in cultured cardiomyocytes from neonatal rats*. *FEBS Lett*, 2001. **508**(1): p. 57-60.

77. Johns, D.G., et al., *Urotensin-II-mediated cardiomyocyte hypertrophy: effect of receptor antagonism and role of inflammatory mediators*. Naunyn Schmiedebergs Arch Pharmacol, 2004. **370**(4): p. 238-50.
78. Onan, D., et al., *Urotensin II promotes hypertrophy of cardiac myocytes via mitogen-activated protein kinases*. Mol Endocrinol, 2004. **18**(9): p. 2344-54.
79. Zhang, Y.G., et al., *Urotensin II accelerates cardiac fibrosis and hypertrophy of rats induced by isoproterenol*. Acta Pharmacol Sin, 2007. **28**(1): p. 36-43.
80. Douglas, S.A. and E.H. Ohlstein, *Human urotensin-II, the most potent mammalian vasoconstrictor identified to date, as a therapeutic target for the management of cardiovascular disease*. Trends Cardiovasc Med, 2000. **10**(6): p. 229-37.
81. Ng, L.L., et al., *Plasma urotensin in human systolic heart failure*. Circulation, 2002. **106**(23): p. 2877-80.
82. Richards, A.M., et al., *Plasma urotensin II in heart failure*. Lancet, 2002. **360**(9332): p. 545-6.
83. Lim, M., et al., *Differential effect of urotensin II on vascular tone in normal subjects and patients with chronic heart failure*. Circulation, 2004. **109**(10): p. 1212-4.
84. Nakayama, T., et al., *Increased gene expression of urotensin II-related peptide in the hearts of rats with congestive heart failure*. Peptides, 2008.
85. Cheung, B.M., et al., *Plasma concentration of urotensin II is raised in hypertension*. J Hypertens, 2004. **22**(7): p. 1341-4.
86. Sondermeijer, B., et al., *Effect of exogenous urotensin-II on vascular tone in skin microcirculation of patients with essential hypertension*. Am J Hypertens, 2005. **18**(9 Pt 1): p. 1195-9.
87. Bousette, N., et al., *Increased expression of urotensin II and its cognate receptor GPR14 in atherosclerotic lesions of the human aorta*. Atherosclerosis, 2004. **176**(1): p. 117-23.
88. Maguire, J.J., et al., *Cellular distribution of immunoreactive urotensin-II in human tissues with evidence of increased expression in atherosclerosis and a greater constrictor response of small compared to large coronary arteries*. Peptides, 2004. **25**(10): p. 1767-74.
89. Watanabe, T., et al., *Human urotensin II accelerates foam cell formation in human monocyte-derived macrophages*. Hypertension, 2005. **46**(4): p. 738-44.
90. Qi, J., et al., *The upregulation of endothelial nitric oxide synthase and urotensin-II is associated with pulmonary hypertension and vascular diseases in rats produced by aortocaval shunting*. Heart Vessels, 2004. **19**(2): p. 81-8.
91. Deuchar, G.A., et al., *The in vivo effects of human urotensin II in the rabbit and rat pulmonary circulation: effects of experimental pulmonary hypertension*. Eur J Pharmacol, 2006. **537**(1-3): p. 135-42.
92. Ong, K.L., L.Y. Wong, and B.M. Cheung, *The role of urotensin II in the metabolic syndrome*. Peptides, 2007.
93. Ong, K.L., et al., *Haplotypes in the urotensin II gene and urotensin II receptor gene are associated with insulin resistance and impaired glucose tolerance*. Peptides, 2006. **27**(7): p. 1659-67.
94. Hood, S.G., A.M. Watson, and C.N. May, *Cardiac actions of central but not peripheral urotensin II are prevented by beta-adrenoceptor blockade*. Peptides, 2005. **26**(7): p. 1248-56.

95. Watson, A.M., et al., *Urotensin II acts centrally to increase epinephrine and ACTH release and cause potent inotropic and chronotropic actions*. Hypertension, 2003. **42**(3): p. 373-9.
96. Do-Rego, J.C., et al., *Behavioral effects of urotensin-II centrally administered in mice*. Psychopharmacology (Berl), 2005. **183**(1): p. 103-17.
97. Totsune, K., et al., *Elevated plasma levels of immunoreactive urotensin II and its increased urinary excretion in patients with Type 2 diabetes mellitus: association with progress of diabetic nephropathy*. Peptides, 2004. **25**(10): p. 1809-14.
98. Sidharta, P.N., et al., *Pharmacodynamics and pharmacokinetics of the urotensin II receptor antagonist palosuran in macroalbuminuric, diabetic patients*. Clin Pharmacol Ther, 2006. **80**(3): p. 246-56.
99. Heller, J., et al., *Increased urotensin II plasma levels in patients with cirrhosis and portal hypertension*. J Hepatol, 2002. **37**(6): p. 767-72.
100. Kemp, W., et al., *Urotensin II in chronic liver disease: In vivo effect on vascular tone*. Scand J Gastroenterol, 2007: p. 1-7.
101. Sauzeau, V., et al., *Human urotensin II-induced contraction and arterial smooth muscle cell proliferation are mediated by RhoA and Rho-kinase*. Circ Res, 2001. **88**(11): p. 1102-4.
102. Takahashi, K., et al., *Three vasoactive peptides, endothelin-1, adrenomedullin and urotensin-II, in human tumour cell lines of different origin: expression and effects on proliferation*. Clin Sci (Lond), 2002. **103 Suppl 48**: p. 35S-38S.
103. Spinazzi, R., et al., *Urotensin-II and its receptor (UT-R) are expressed in rat brain endothelial cells, and urotensin-II via UT-R stimulates angiogenesis in vivo and in vitro*. Int J Mol Med, 2006. **18**(6): p. 1107-12.
104. Ribatti, D., M.T. Conconi, and G.G. Nussdorfer, *Nonclassic endogenous novel [corrected] regulators of angiogenesis*. Pharmacol Rev, 2007. **59**(2): p. 185-205.
105. Takahashi, K., et al., *Expression of urotensin II and urotensin II receptor mRNAs in various human tumor cell lines and secretion of urotensin II-like immunoreactivity by SW-13 adrenocortical carcinoma cells*. Peptides, 2001. **22**(7): p. 1175-9.
106. Morimoto, R., et al., *Immunolocalization of urotensin II and its receptor in human adrenal tumors and attached non-neoplastic adrenal tissues*. Peptides, 2007.
107. Flohr, S., et al., *Identification of nonpeptidic urotensin II receptor antagonists by virtual screening based on a pharmacophore model derived from structure-activity relationships and nuclear magnetic resonance studies on urotensin II*. J Med Chem, 2002. **45**(9): p. 1799-805.
108. Guerrini, R., et al., *Structure-activity relationship study on human urotensin II*. J Pept Sci, 2005. **11**(2): p. 85-90.
109. Camarda, V., et al., *A new ligand for the urotensin II receptor*. Br J Pharmacol, 2002. **137**(3): p. 311-4.
110. Patacchini, R., et al., *Urantide: an ultrapotent urotensin II antagonist peptide in the rat aorta*. Br J Pharmacol, 2003. **140**(7): p. 1155-8.
111. Camarda, V., et al., *In vitro and in vivo pharmacological characterization of the novel UT receptor ligand [Pen<sup>5</sup>,DTrp<sup>7</sup>,Dab<sup>8</sup>]urotensin II(4-11) (UFP-803)*. Br J Pharmacol, 2006. **147**(1): p. 92-100.

112. Camarda, V., et al., *Urantide mimics urotensin-II induced calcium release in cells expressing recombinant UT receptors*. Eur J Pharmacol, 2004. **498**(1-3): p. 83-6.
113. Clozel, M., et al., *Pharmacology of the urotensin-II receptor antagonist palosuran (ACT-058362; 1-[2-(4-benzyl-4-hydroxy-piperidin-1-yl)-ethyl]-3-(2-methyl-quinolin-4-yl) -urea sulfate salt): first demonstration of a pathophysiological role of the urotensin System*. J Pharmacol Exp Ther, 2004. **311**(1): p. 204-12.
114. Behm, D.J., et al., *Palosuran inhibits binding to primate UT receptors in cell membranes but demonstrates differential activity in intact cells and vascular tissues*. Br J Pharmacol, 2008.
115. Malagon, M.M., et al., *Urotensin II and urotensin II-related peptide activate somatostatin receptor subtypes 2 and 5*. Peptides, 2008.
116. Douglas, S.A., et al., *Nonpeptidic urotensin-II receptor antagonists I: in vitro pharmacological characterization of SB-706375*. Br J Pharmacol, 2005. **145**(5): p. 620-35.
117. Herold, C.L., et al., *The neuromedin B receptor antagonist, BIM-23127, is a potent antagonist at human and rat urotensin-II receptors*. Br J Pharmacol, 2003. **139**(2): p. 203-7.
118. No, D., T.P. Yao, and R.M. Evans, *Ecdysone-inducible gene expression in mammalian cells and transgenic mice*. Proc Natl Acad Sci U S A, 1996. **93**(8): p. 3346-51.
119. Yao, T.P., et al., *Functional ecdysone receptor is the product of EcR and Ultraspiracle genes*. Nature, 1993. **366**(6454): p. 476-9.
120. Yao, T.P., et al., *Drosophila ultraspiracle modulates ecdysone receptor function via heterodimer formation*. Cell, 1992. **71**(1): p. 63-72.
121. Chen, J.D., K. Umesono, and R.M. Evans, *SMRT isoforms mediate repression and anti-repression of nuclear receptor heterodimers*. Proc Natl Acad Sci U S A, 1996. **93**(15): p. 7567-71.
122. Saez, E., et al., *Identification of ligands and coligands for the ecdysone-regulated gene switch*. Proc Natl Acad Sci U S A, 2000. **97**(26): p. 14512-7.
123. Ryding, A.D., M.G. Sharp, and J.J. Mullins, *Conditional transgenic technologies*. J Endocrinol, 2001. **171**(1): p. 1-14.
124. Oehme, I., S. Bossler, and M. Zornig, *Agonists of an ecdysone-inducible mammalian expression system inhibit Fas Ligand- and TRAIL-induced apoptosis in the human colon carcinoma cell line RKO*. Cell Death Differ, 2006. **13**(2): p. 189-201.
125. Constantino, S., et al., *The ecdysone inducible gene expression system: unexpected effects of muristerone A and ponasterone A on cytokine signaling in mammalian cells*. Eur Cytokine Netw, 2001. **12**(2): p. 365-7.
126. Van Craenenbroeck, K., et al., *Evaluation of the tetracycline- and ecdysone-inducible systems for expression of neurotransmitter receptors in mammalian cells*. Eur J Neurosci, 2001. **14**(6): p. 968-76.
127. Law, P.Y., et al., *Deltorphin II-induced rapid desensitization of delta-opioid receptor requires both phosphorylation and internalization of the receptor*. J Biol Chem, 2000. **275**(41): p. 32057-65.
128. Cole, S.L., et al., *Titration of the expression of a Gi protein-coupled receptor using an ecdysone-inducible system in CHO-K1 cells*. Receptors Channels, 2001. **7**(4): p. 289-302.

129. McDonald, J., et al., *Partial agonist behaviour depends upon the level of nociceptin/orphanin FQ receptor expression: studies using the ecdysone-inducible mammalian expression system*. British Journal of Pharmacology, 2003. **140**(1): p. 61-70.
130. Fire, A., et al., *Potent and specific genetic interference by double-stranded RNA in *Caenorhabditis elegans**. Nature, 1998. **391**(6669): p. 806-11.
131. Gantier, M.P. and B.R. Williams, *The response of mammalian cells to double-stranded RNA*. Cytokine Growth Factor Rev, 2007. **18**(5-6): p. 363-71.
132. Elbashir, S.M., et al., *Duplexes of 21-nucleotide RNAs mediate RNA interference in cultured mammalian cells*. Nature, 2001. **411**(6836): p. 494-8.
133. Tijsterman, M., R.F. Ketting, and R.H. Plasterk, *The genetics of RNA silencing*. Annu Rev Genet, 2002. **36**: p. 489-519.
134. Amarzguioui, M., J.J. Rossi, and D. Kim, *Approaches for chemically synthesized siRNA and vector-mediated RNAi*. FEBS Lett, 2005. **579**(26): p. 5974-81.
135. Agrawal, N., et al., *RNA interference: biology, mechanism, and applications*. Microbiol Mol Biol Rev, 2003. **67**(4): p. 657-85.
136. Aigner, A., *Delivery Systems for the Direct Application of siRNAs to Induce RNA Interference (RNAi) In Vivo*. J Biomed Biotechnol, 2006. **2006**(4): p. 71659.
137. Behlke, M.A., *Progress towards in vivo use of siRNAs*. Mol Ther, 2006. **13**(4): p. 644-70.
138. Kenakin, T., *A Pharmacology Primer*. 3 ed. 2004: Elsevier
139. Puck, T.T., S.J. Cieciura, and A. Robinson, *Genetics of somatic mammalian cells. III. Long-term cultivation of euploid cells from human and animal subjects*. J Exp Med, 1958. **108**(6): p. 945-56.
140. Freshney, I.R., *Culture of animal cells: a manual of basic technique*. fifth ed. 2005: John Wiley & Sons, Inc.
141. Rutledge, R.G. and C. Cote, *Mathematics of quantitative kinetic PCR and the application of standard curves*. Nucleic Acids Res, 2003. **31**(16): p. e93.
142. Schneeberger, C., et al., *Quantitative detection of reverse transcriptase-PCR products by means of a novel and sensitive DNA stain*. PCR Methods Appl, 1995. **4**(4): p. 234-8.
143. Gudnason, H., et al., *Comparison of multiple DNA dyes for real-time PCR: effects of dye concentration and sequence composition on DNA amplification and melting temperature*. Nucleic Acids Res, 2007. **35**(19): p. e127.
144. Wittwer, C.T., et al., *Continuous fluorescence monitoring of rapid cycle DNA amplification*. Biotechniques, 1997. **22**(1): p. 130-1, 134-8.
145. Lutfalla, G. and G. Uze, *Performing quantitative reverse-transcribed polymerase chain reaction experiments*. Methods Enzymol, 2006. **410**: p. 386-400.
146. Heid, C.A., et al., *Real time quantitative PCR*. Genome Res, 1996. **6**(10): p. 986-94.
147. Chomczynski, P. and N. Sacchi, *Single-step method of RNA isolation by acid guanidinium thiocyanate-phenol-chloroform extraction*. Anal Biochem, 1987. **162**(1): p. 156-9.
148. Somlyo, A.P., *Excitation-contraction coupling and the ultrastructure of smooth muscle*. Circ Res, 1985. **57**(4): p. 497-507.
149. Bito, H., *The role of calcium in activity-dependent neuronal gene regulation*. Cell Calcium, 1998. **23**(2-3): p. 143-50.

150. MacLennan, D.H., *Ca<sup>2+</sup> signalling and muscle disease*. Eur J Biochem, 2000. **267**(17): p. 5291-7.
151. Hirst, R., Harrison, C., Hirota, K., & Lambert, D., *Measurement of [Ca<sup>2+</sup>]<sub>i</sub> in whole cell suspensions using fura-2*, in *Methods in molecular biology: calcium signalling protocols*, D.G. Lambert, Editor. 2006, Humana press.
152. Robinson, J.A., et al., *Ratiometric and nonratiometric Ca<sup>2+</sup> indicators for the assessment of intracellular free Ca<sup>2+</sup> in a breast cancer cell line using a fluorescence microplate reader*. J Biochem Biophys Methods, 2004. **58**(3): p. 227-37.
153. Hurteau, G.J. and S.D. Spivack, *mRNA-specific reverse transcription-polymerase chain reaction from human tissue extracts*. Anal Biochem, 2002. **307**(2): p. 304-15.
154. Bustin, S.A., et al., *The MIQE guidelines: minimum information for publication of quantitative real-time PCR experiments*. Clin Chem, 2009. **55**(4): p. 611-22.
155. Song, W., et al., *Cell and tissue responses of a range of Urotensin II analogs at cloned and native urotensin II receptors. Evidence for coupling promiscuity*. Naunyn Schmiedebergs Arch Pharmacol, 2006. **373**(2): p. 148-57.
156. Ranjan, V., et al., *Fluid shear stress induction of the transcriptional activator c-fos in human and bovine endothelial cells, HeLa, and Chinese hamster ovary cells*. Biotechnol Bioeng, 1996. **49**(4): p. 383-90.
157. Yin, H., et al., *Influence of hydrodynamic conditions on quantitative cellular assays in microfluidic systems*. Anal Chem, 2007. **79**(18): p. 7139-44.
158. Skippen, A., Swigart, P. and Cockcroft, S., *Measurement of phospholipase C by monitoring inositol phosphates using [<sup>3</sup>H]inositol-labelling protocols in permeabilized cells*, in *Methods in molecular biology: calcium signalling protocols*, D.G. Lambert, Editor. 2006, Humana Press.
159. Berridge, M.J., C.P. Downes, and M.R. Hanley, *Lithium amplifies agonist-dependent phosphatidylinositol responses in brain and salivary glands*. Biochem J, 1982. **206**(3): p. 587-95.
160. Ellis, R.B., T. Galliard, and J.N. Hawthorne, *Phosphoinositides. 5. The inositol lipids of ox brain*. Biochem J, 1963. **88**(1): p. 125-31.
161. Lehman, I.R., *DNA ligase: structure, mechanism, and function*. Science, 1974. **186**(4166): p. 790-7.
162. Yoshida, N. and M. Sato, *Plasmid uptake by bacteria: a comparison of methods and efficiencies*. Appl Microbiol Biotechnol, 2009. **83**(5): p. 791-8.
163. Foreman, J.C., Johansen, T., *Textbook of Receptor Pharmacology*. Second ed. 2003: CRC Press.
164. Jinsi-Parimoo, A. and M.C. Gershengorn, *Constitutive activity of native thyrotropin-releasing hormone receptors revealed using a protein kinase C-responsive reporter gene*. Endocrinology, 1997. **138**(4): p. 1471-5.
165. Batuwangala, M.S., et al., *Desensitisation of native and recombinant human urotensin-II receptors*. Naunyn Schmiedebergs Arch Pharmacol, 2009. **380**(5): p. 451-7.
166. Murakami, M., et al., *Identification of the orphan GPCR, P2Y(10) receptor as the sphingosine-1-phosphate and lysophosphatidic acid receptor*. Biochem Biophys Res Commun, 2008. **371**(4): p. 707-12.
167. Behm, D.J., et al., *The peptidic urotensin-II receptor ligand GSK248451 possesses less intrinsic activity than the low-efficacy partial agonists SB-710411 and urantide in native mammalian tissues and recombinant cell systems*. Br J Pharmacol, 2006. **148**(2): p. 173-90.

